2023 Fall

"Phase Transformation *in* Materials"

10. 16. 2023

Eun Soo Park

Office: 33-313
Telephone: 880-7221
Email: espark@snu.ac.kr
Office hours: by an appointment

Contents for previous class

Chapter 3 Crystal Interfaces and Microstructure

1) Interfacial Free Energy
2) Solid/Vapor Interfaces
3) Solid/Liquid Interfaces
4) **Boundaries in Single-Phase Solids**
5) Interphase Interfaces in Solid (α/β)
6) Interface migration

Contents for previous class

3) Boundaries in Single-Phase Solids

(a) Low-Angle and High-Angle Boundaries

Θ < 15° : total energy of the dislocations within unit area of boundary

Θ > 15° : impossible to physically identify the individual dislocations → strain field overlap → cancel out

Broken Bonds → high angle $\gamma_{g.b.} \approx 1/3\ \gamma_{S/V.}$

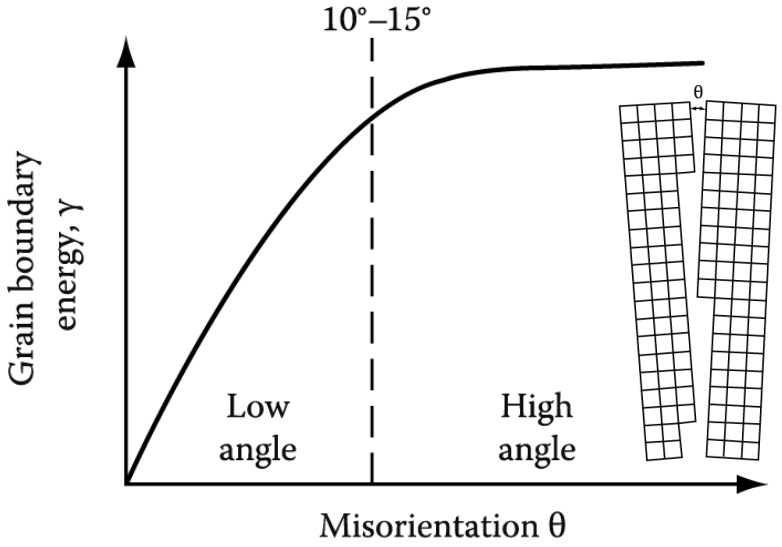

(b) Special High-Angle Grain Boundaries

: high angle boundary but with low $\gamma_{g.b.}$

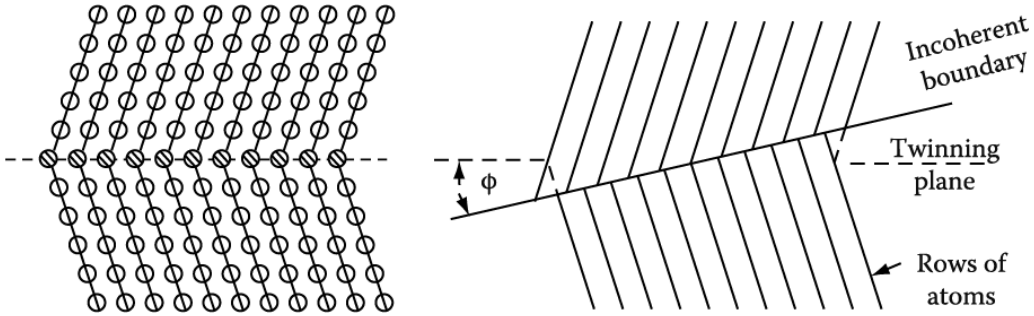

→ twin boundary

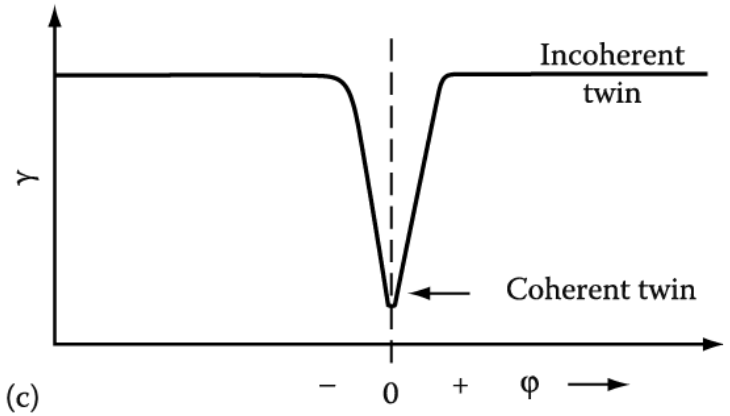

Atoms in the boundary are essentially in undistorted positions ~relatively little free volume

3.4.4 Grain boundary energy of dilute binary alloys

Solute tends to segregate to the boundary to reduce the overall free energy of the system

① $$X_S^b \approx \frac{X_S^\alpha exp\{-\Delta G_b/RT\}}{1 + X_S^\alpha exp\{-\Delta G_b/RT\}}$$

Here, ΔG_b=Gibbs energy of segregation
~usually negative (In regular solution, strong A-S bonding in the GB, week A-S bonding in the α phase, In real solution, increasing size misfit btw solute and matrix; varies with temp. and atomic structure (misorientation btw the grains and the orientation of the GB plane)

② **GB energy for binary alloys** $\gamma = \gamma_0 - \frac{\delta RT}{V_m^b} \ln \{1 + X_S^\alpha \exp(-\Delta G_b/RT)\}$ **(3.25)**

Since ln (1+x) → x as x→ 0, for very dilute solutions, i.e., metals containing impurities
The rate of change of GB energy with increasing X_S^α is given by

$$\frac{\partial \gamma}{\partial X_S^\alpha} = -\frac{\delta RT}{V_m^b} \exp(-\Delta G_b/RT)\} \quad \textbf{(3.26)}$$

- **The stronger the tendency for solute or impurities to segregate to the grain boundary, the greater is the reduction in the GB energy.** Note that, in the case of impurity contents, is essential the same as the total impurity content in the alloy.

For example, Putting δ=0.75 nm, V_m^b=7 cm³, R =8.314 J/mol·K and T =773 K (500 ℃) gives X_S^α = 1,650 J/m² for ΔG_b= -50 kJ/mol, which is a strong free energy of segregation.

In such a case, an addition of just 0.0001 mole fraction (0.01 atomic %) would reduce the GB energy by 165 mJ/m², which is an appreciable effect considering that random high-angle GB energies are typically of the order of 1,000 mJ/m².

Q: Grain boundary (α/ α interfaces)

= Boundaries in Single-Phase Solids

(a) Low-Angle and High-Angle Boundaries

(b) Special High-Angle Grain Boundaries

(c) Equilibrium in Polycrystalline Materials

① GB intersection: Balance of 1) boundary E & 2) surface tension

GBs in a polycrystal can adjust themselves during annealing to produce "a metastable equilibrium at the GB intersections".

(c) 3.4.5 Equilibrium in Polycrystalline Materials

Microstructure → determined by how the different GBs join together in space

⇨ Examine how the possibility of different GB energies affects the microstructure of a poly crystalline material

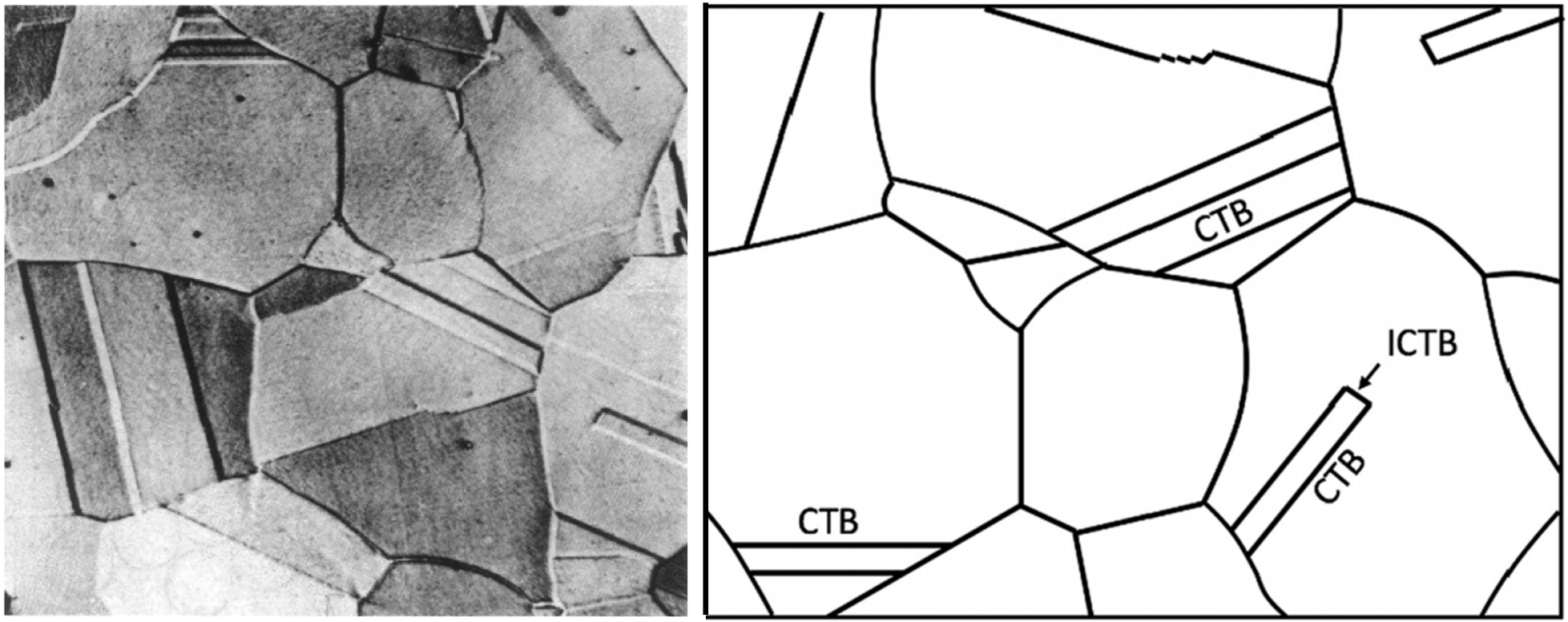

FIGURE 3.23 Grain boundaries in annealed austenitic stainless steel. Some CTBs and incoherent twin boundaries (ICTB) are indicated.

: contains high-/low-angle GBs as well as (in-)coherent twin Bs with different GB energies

Poly grain material: consider the factors that control the grain shapes!

Two grains: a plane (GB), three grains: a line (grain edge), four grains: at a point (grain corner)

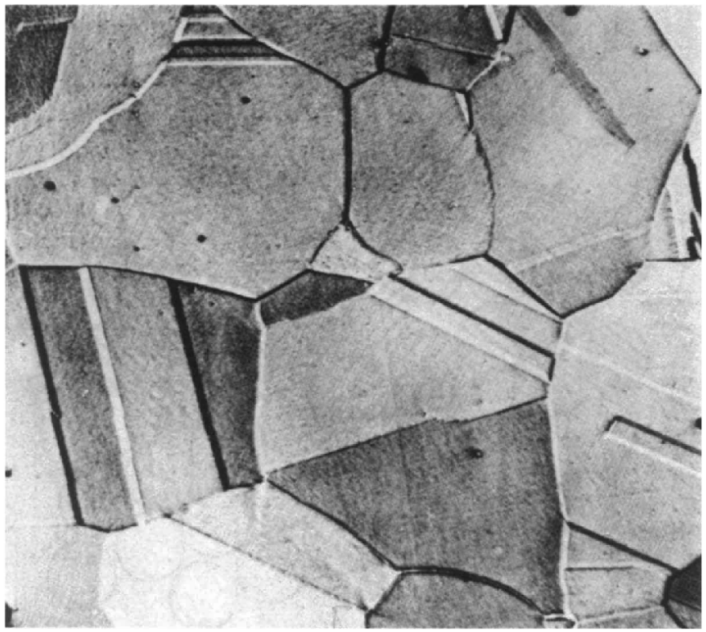

1) Why GBs exist at all in annealed materials?

Equilibrium ~ Mater. with no GB

∵ G.B.=high-E regions → G ↑

: never a true equilibrium structure

→ **GBs in a polycrystal can adjust themselves during annealing to produce a metastable equilibrium at the GB intersections and inverse relationship between relative GB E and relative GB area.**

2) Conditions for equilibrium at a GB junction

by considering the forces that each B exerts on the junction

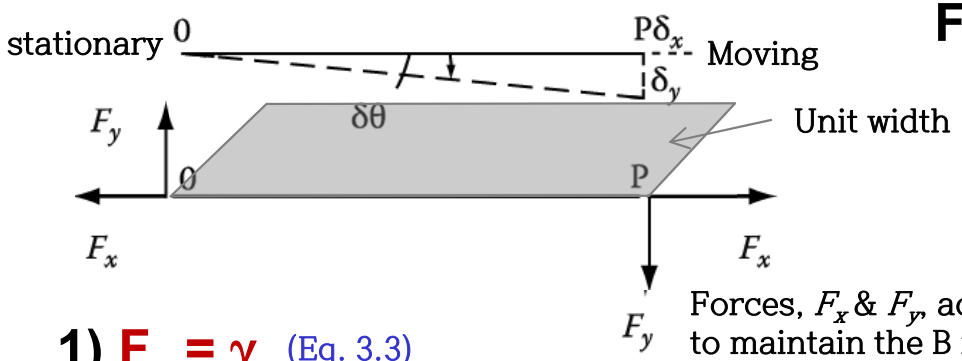

Fig. 3.24

1) $F_x = \gamma$ (Eq. 3.3)

2) F_y ?

P is moved at a small distance (δ_y)

A. work done by : $F_y \delta_y$

B. increase boundary energy caused by the change in orientation $\delta\theta$ ~ $l\,(d\gamma/d\theta)\,\delta\theta$

$F_y \delta_y = l\,(d\gamma/d\theta)\,\delta\theta$ ($\because \delta_y \sim l\,d\theta$)

→ $F_y = d\gamma/d\theta$ **torque force**

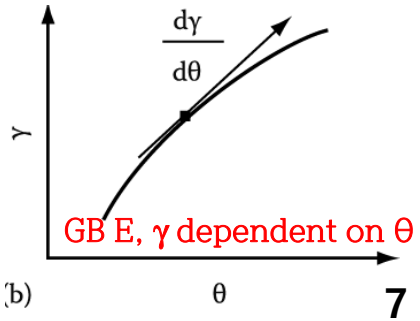

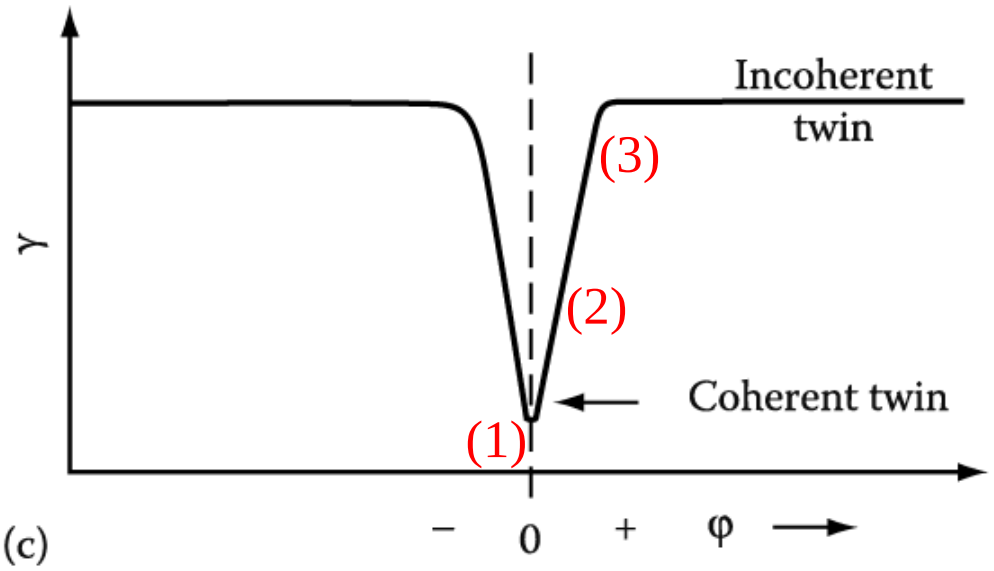

(1)

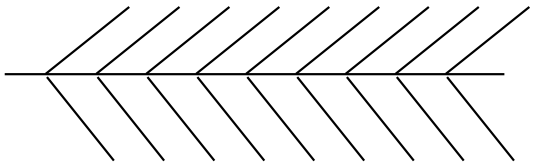

(2)

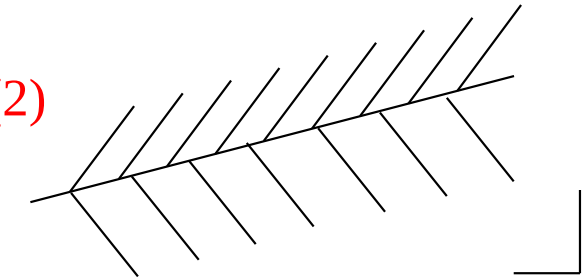

$F_y = d\gamma/d\theta$

Minimum γ ~ torque = 0 No rotation!

$F_y = d\gamma/d\theta$ ~ torque > 0

If the GB E is dependent on the orientation of the B, a force dγ/dθ (>0) must be applied to the ends of the boundary to prevent it rotating into a lower energy orientation.

입계 E가 입계 방위에 의존한다면, 회전하지 않고 유지하기 위해 입계에 cusp까지 끌어당기는 힘에 대응하는 힘 작용

(3)

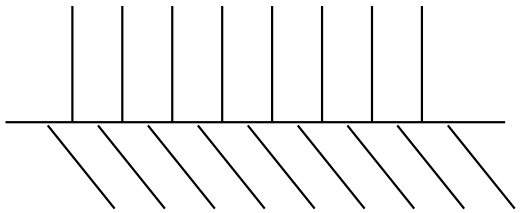

torque = 0

→ There is little effect of orientation

If Pulling force, $F_y > (d\gamma/d\theta)_{cusp}$ → Rotating

⇨ How metastable equilibrium? → force (torque)

If the boundary E is independent of orientation,

* General high angle boundary : $d\gamma/d\theta \approx 0$ (GB behaves like a soap film)

→ Under these conditions the requirements for metastable equilibrium at junction between three grains is that the boundary tensions $\gamma_{13}, \gamma_{23}, \gamma_{12}$ must balance.

3) The balance of GB tensions for a GB intersection in metastable equilibrium

Fig. 3.25

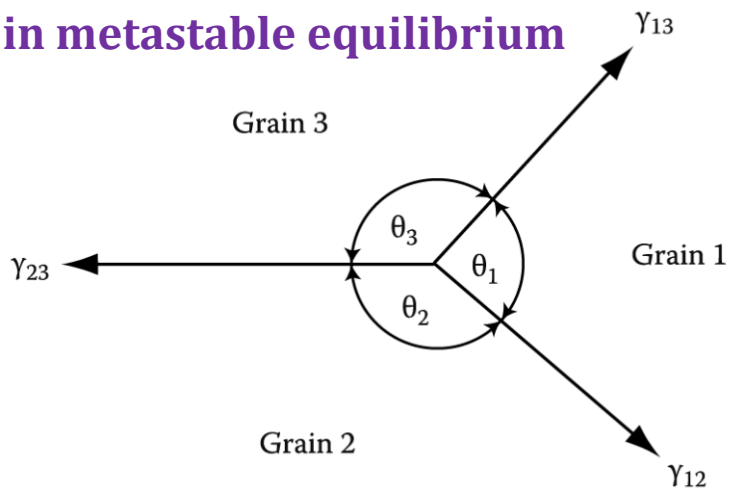

$$\frac{\gamma_{23}}{\sin\theta_1} = \frac{\gamma_{31}}{\sin\theta_2} = \frac{\gamma_{12}}{\sin\theta_3} \quad \text{(Eq. 3.28)}$$

→ **θ = 120°**

Eq. 3.28 applies to any three boundaries
i.e. grain 1~ different phase to grain 2 & 3.

Ex) If the solid-vapor energy ($\gamma_{S/V}$) is the same for both grains,

$$2\gamma_{SV}\cos\frac{\theta}{2} = \gamma_b \quad \text{(Eq. 3.29)}$$

(Here, presence of any torque terms ~ neglected)

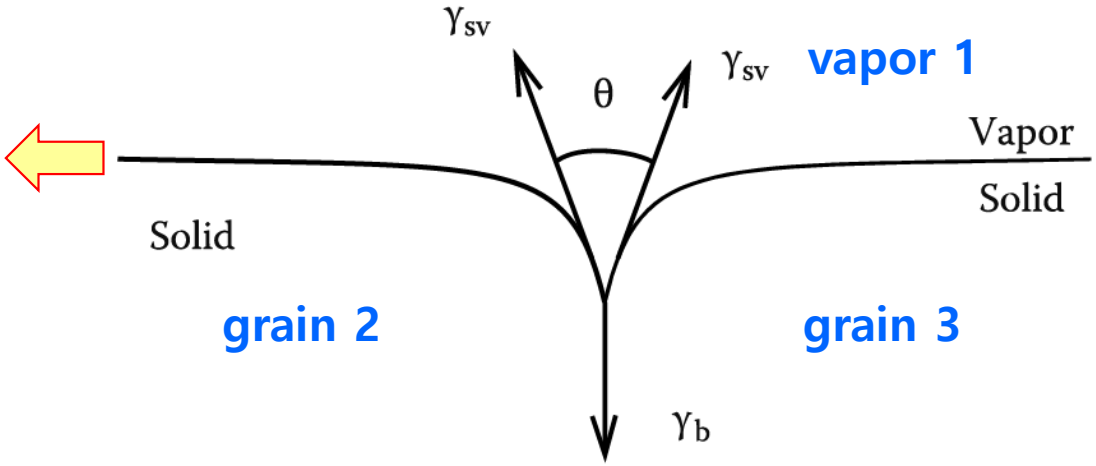

Fig. 3.26 The balance of surface and grain boundary tensions at the intersection of a grain boundary with a free surface.

One method of measuring GB energy:

: anneal a specimen at a high temp. and then measure the angle at the intersection of the surface with B.

* Junction between coherent and incoherent twin boundary segments showing the importance of torque effects

: the orientation dependence of twin boundary E

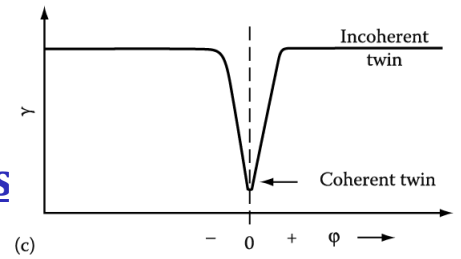

→ It is energetically favorable for twin boundaries **to align themselves parallel to the twinning plane**.

→ **If the boundary is constrained to follow a macroscopic plane that is near but not exactly parallel to the twining plane**, the boundary will usually develop **a stepped appearance** with **large coherent low-E facets** and **small incoherent high-E risers**.

→ **does not minimize the total twin boundary E but minimize the total free E**

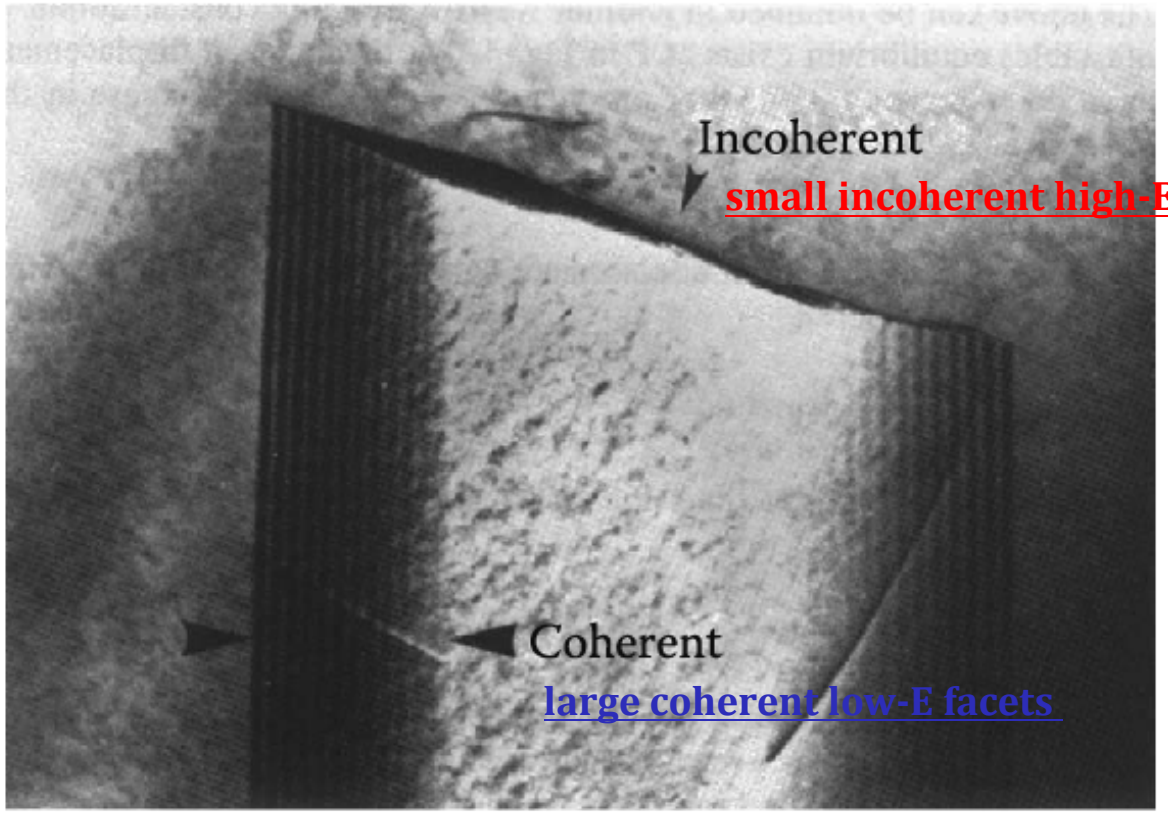

(a) twin boundary in a thin foil specimen as imaged in the TEM

* Junction between coherent and incoherent twin boundary segments showing the importance of torque effects

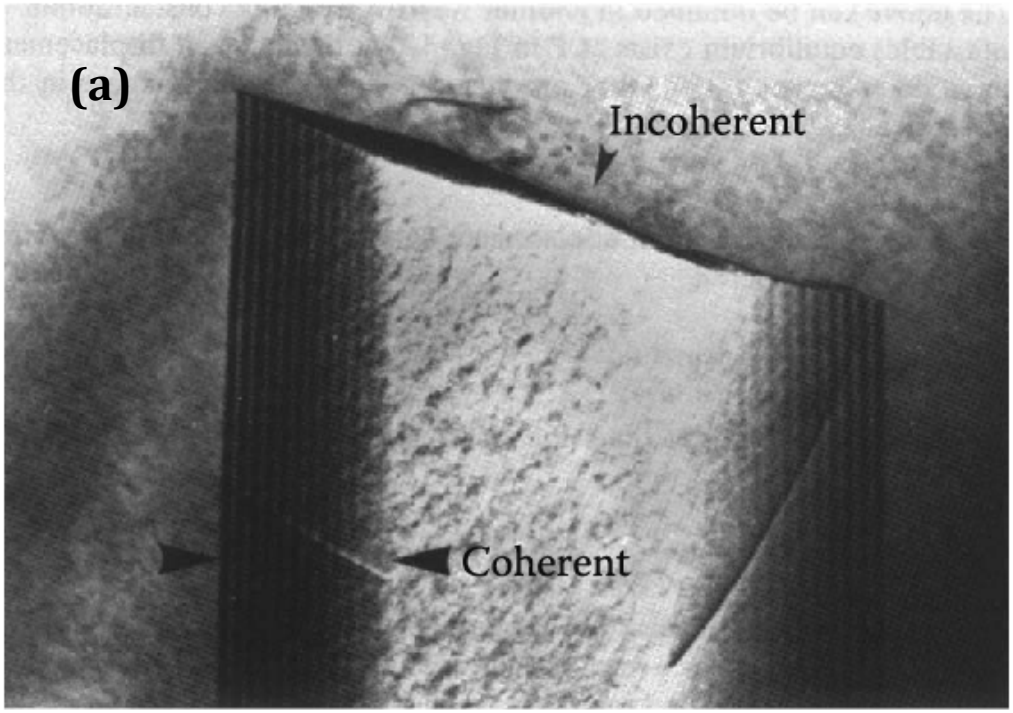

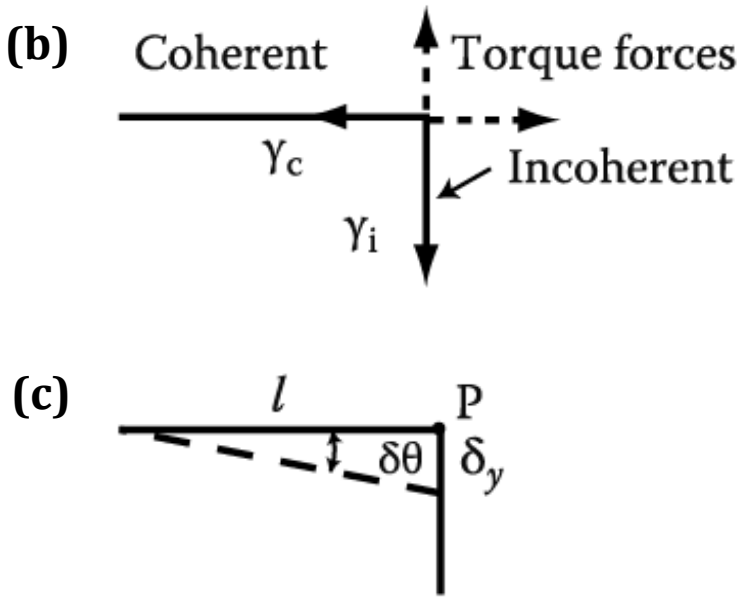

Fig. 3.27

(a) twin B in a thin foil specimen as imaged in the TEM, (b) & (c), the coherent and incoherent segments of the twin B.

At the coherent/incoherent twin junction as shown in (b),

incoherent twin B tension, γ_i must balanced by a torque term

$$\gamma_i \leq d\gamma_c/d\theta \quad \text{(Eq. 3.30)}$$

Likewise, coherent twin B tension, γ_c must balanced by a torque term

$$\gamma_c \leq d\gamma_i/d\theta \quad \text{(Eq. 3.31)}$$

However, since γ_c is usually very small, the incoherent interface need only lie in a rather shallow energy cusp.

From energy consideration,
if (metastable) equilibrium exists at P in Fig. (c), then a small displacement such as that shown should either produce no change or an increase in the total free energy of the system, i.e. $dG > 0$
considering unit depth a small displacement $\delta\gamma$ at P will increase the total free E by an amount

$$dG = l\,(d\gamma_c/d\theta)\,\delta\theta - \gamma_i\,\delta y > 0 \quad (\because \delta y \sim l\,\delta\theta) \Rightarrow \gamma_i \leq d\gamma_c/d\theta$$

Q: Grain boundary (α/ α interfaces)

= Boundaries in Single-Phase Solids

(a) Low-Angle and High-Angle Boundaries

(b) Special High-Angle Grain Boundaries

(c) Equilibrium in Polycrystalline Materials

② 3.4.6. Thermally Activated Migration of Grain Boundaries

: Grain coarsening at high T, annealing due to metastable equilibrium of GB

Considering factors of G.B. growth

(a) Pinning particle

(b) 2nd phases

(c) Anisotropic σ, M

(d) Impurity (solute) drag

(e) Strain energy

(f) Free surface

3.4.6. Thermally Activated Migration of Grain Boundaries

If the boundary is curved in the shape of cylinder, Fig. 3.28a, it is acted on by a force of magnitude γ/r towards its center of curvature.

Therefore, the only way the boundary tension forces can balance in three dimensions is if the boundary is planar (r = ∞) or if it is curved with equal radii in opposite directions, Fig. 3.28b and c.

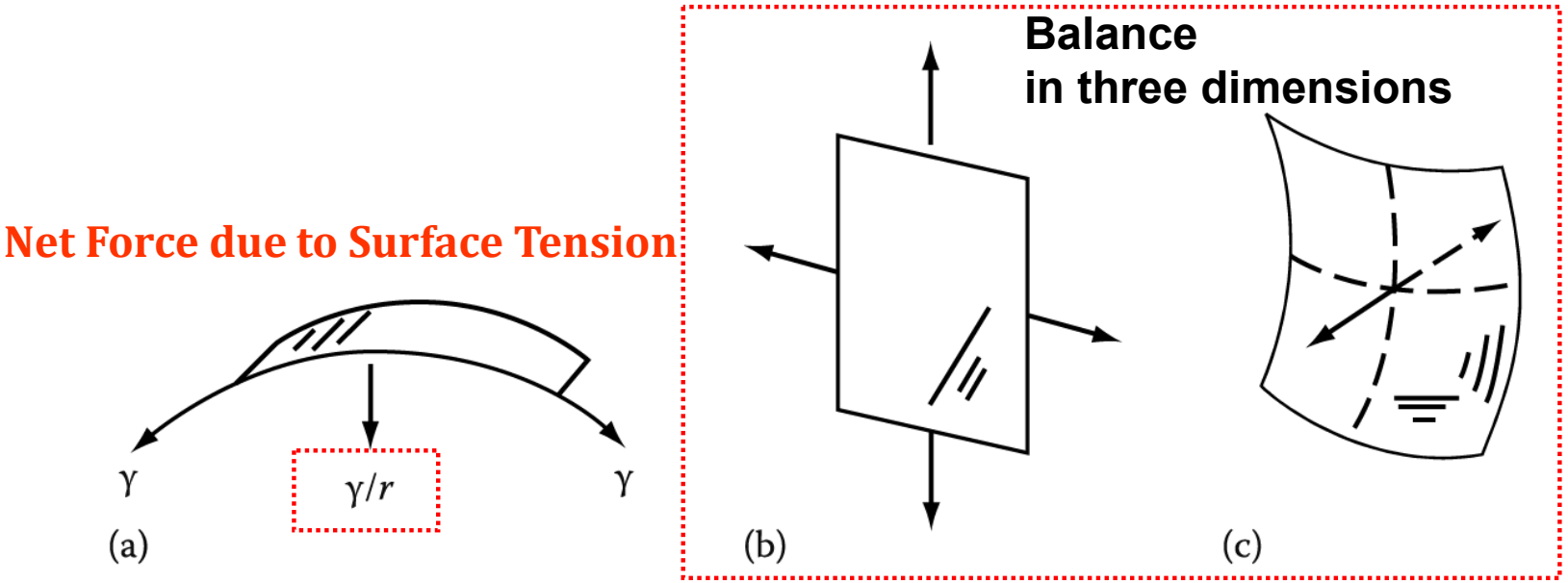

Fig. 3.28 (a) A cylindrical boundary with a radius of curvature r is acted on by a force γ/r. (b) A planar boundary with no net force. (c) A doubly curved boundary with no net force.

A random grain structure is inherently unstable and, on annealing at high temperatures, the unbalanced forces will cause the boundaries to migrate towards their centers of curvature.

a) Direction of Grain Boundary Migration during Grain Growth

For isotropic grain boundary energy in two dimensions,

Equilibrium angle at each boundary junction? → **120°** 3 boundaries intersections

Equilibrium angle at each boundary junction in 3D? → **109°28'** A corner formed by 4 grains

Morphology of metastable equilibrium state → **Migration during annealing**

Effect of different boundary curvatures in two dimensions

Boundaries around Grain < 6

; grain shrink, disappear

Boundaries around Grain = 6

; equilibrium

Boundaries around Grain > 6

; grain growth

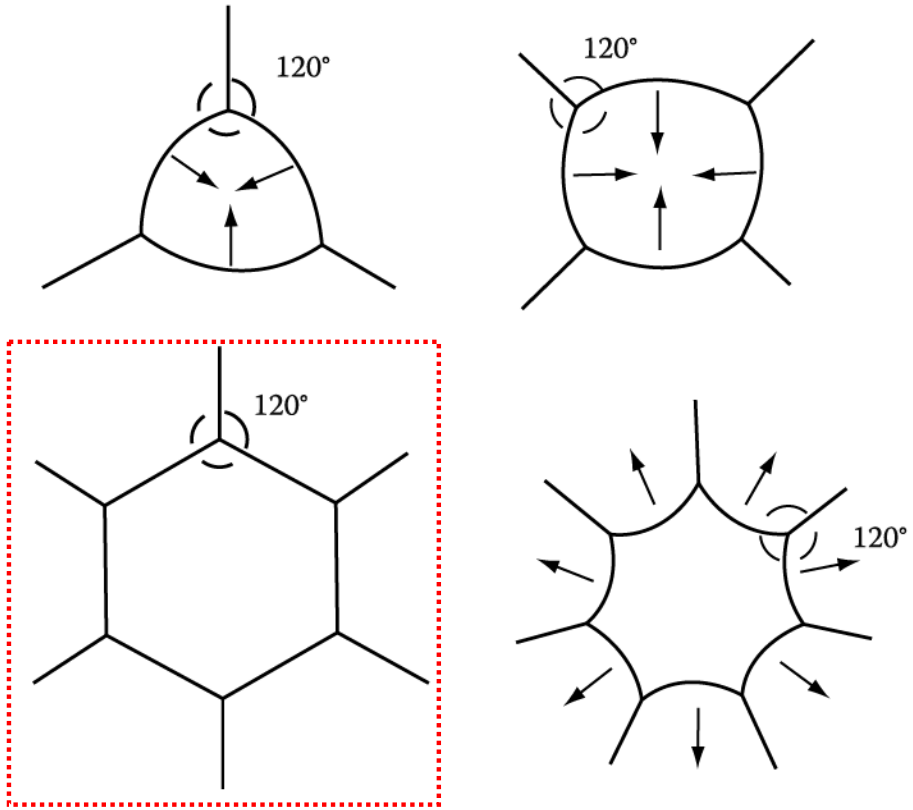

Fig. 3.29 Two-dimensional GB configurations, The arrows indicate the directions boundaries will migrate during grain growth.

⇨ **Reduce the # of grains, increase the mean grain size, reducing the total G.B. energy called grain growth (or grain coarsening): at high temperature above about 0.5 T_m**

Grain Growth (Soap Bubble Model)

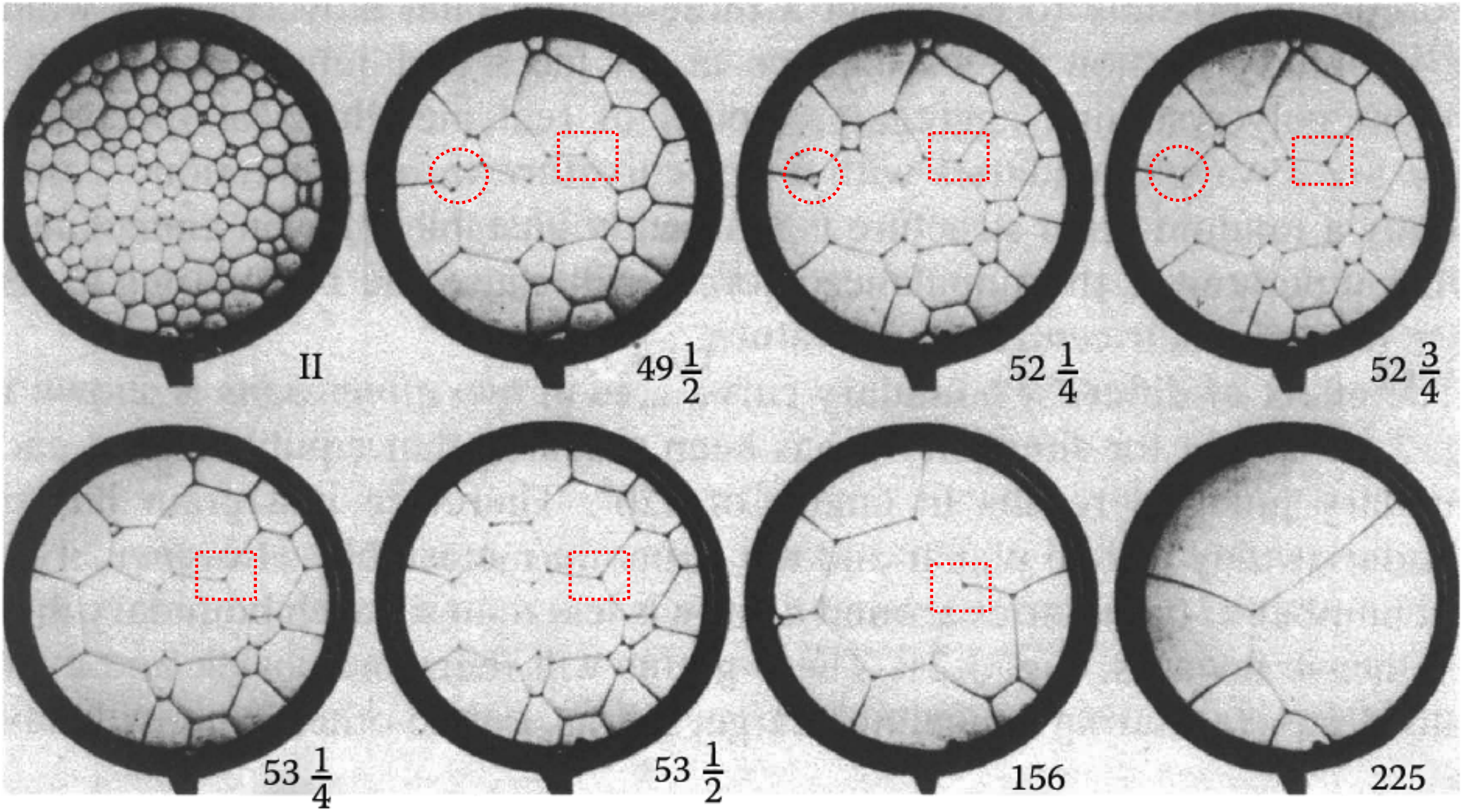

Fig. 3.30 Two-dimensional cells of a soap solution illustration the process of grain growth. Numbers are time in minutes.

Example of Grain Growth simulation in 3D

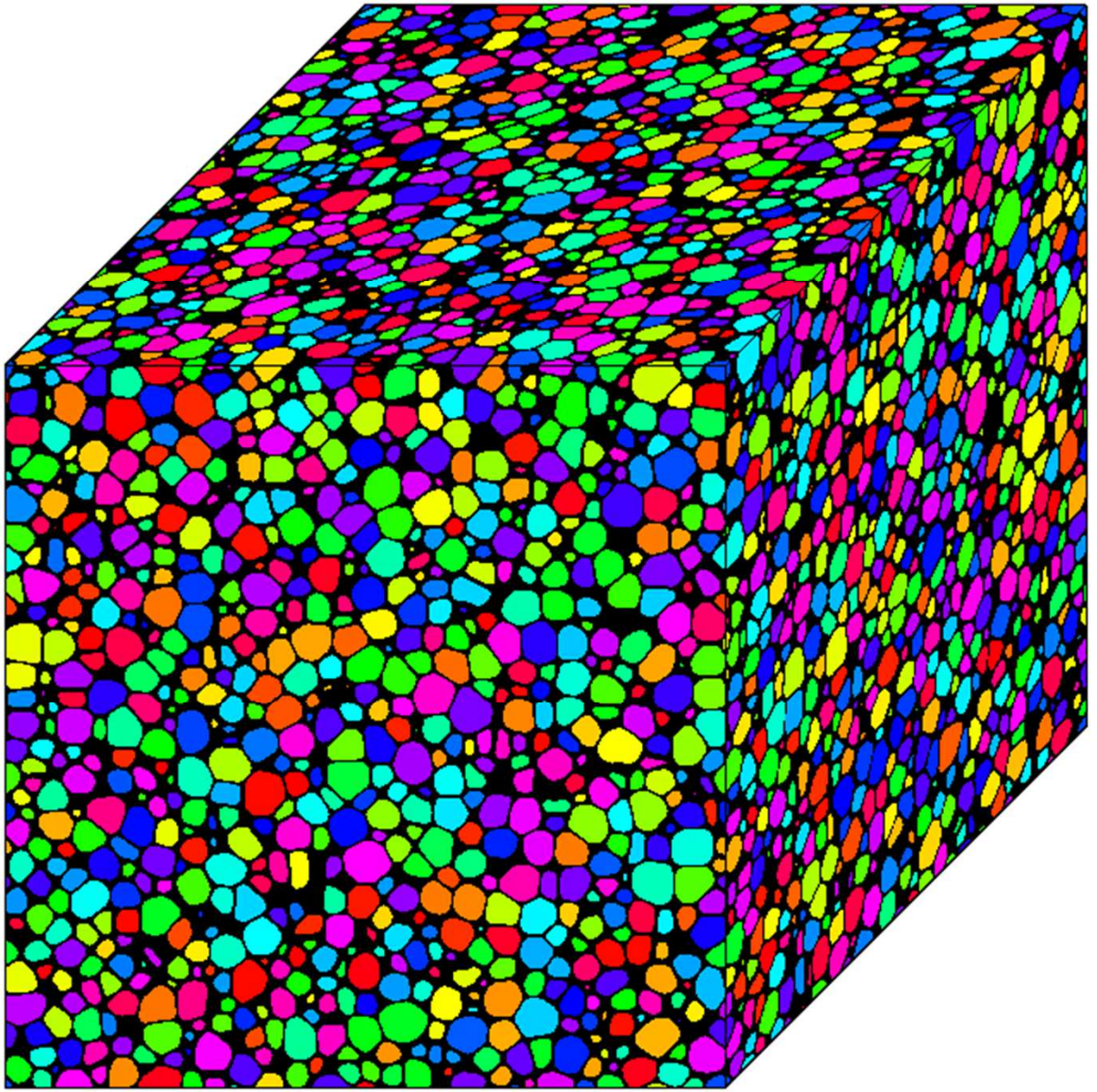

b) Grain Coarsening at High Temp. annealing (above about 0.5 T_m):

The atoms in the shrinking grain detach themselves from the lattice on the high pressure side of the boundary and relocate themselves on a lattice site of the growing grain.

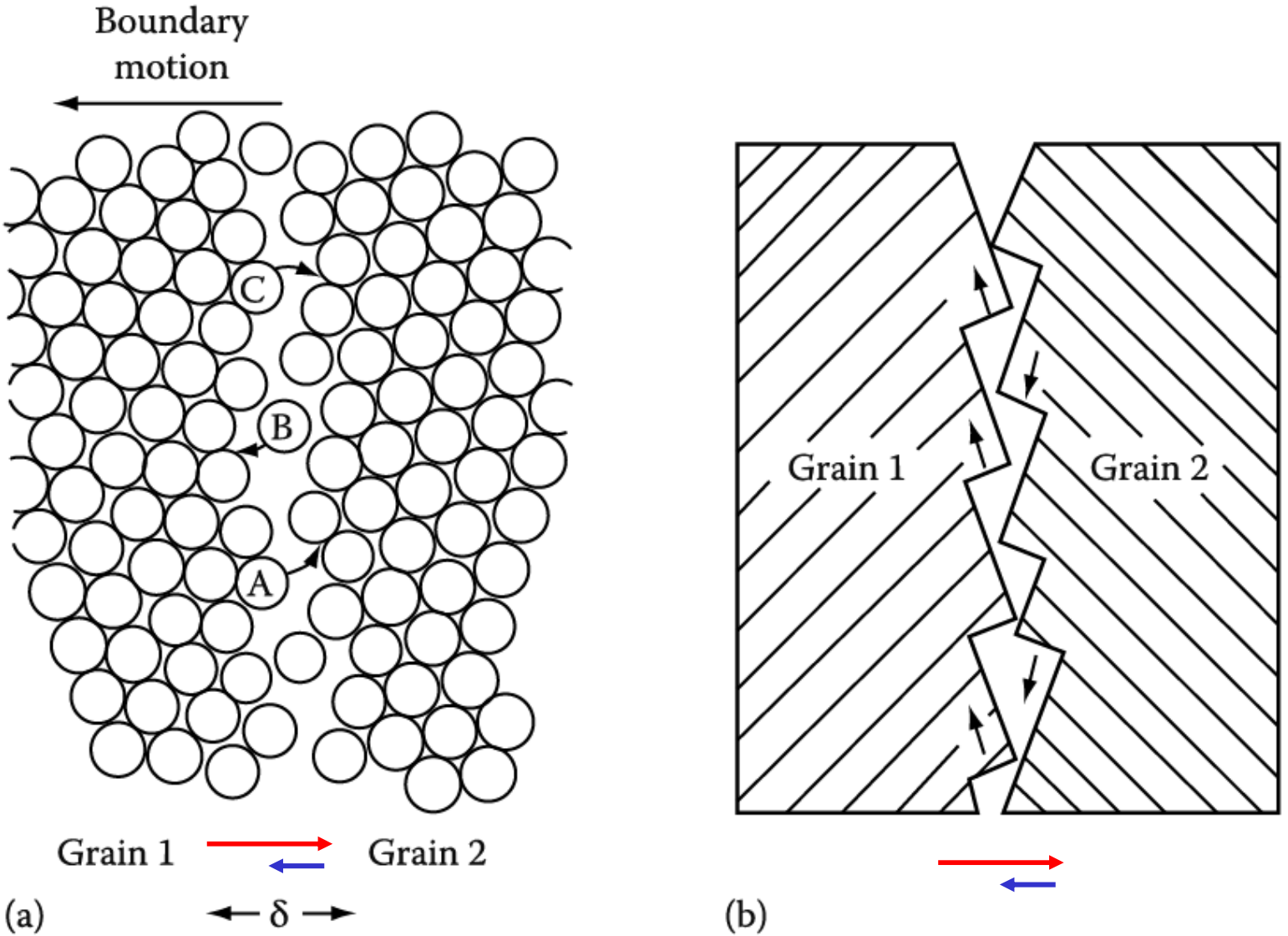

Fig. 3. 31 (a) The atomic mechanism of boundary migration. The boundary migrates to the left if the jump rate from grain 1 → 2 is greater than 2 → 1. Note that the free volume within the boundary has been exaggerated for clarity. (b) Step-like structure (돌출맥 구조) where close-packed planes protrude into the boundary.

* Grain coarsening at high T annealing

→ metastable equilibrium state

: # ↓ , size ↑

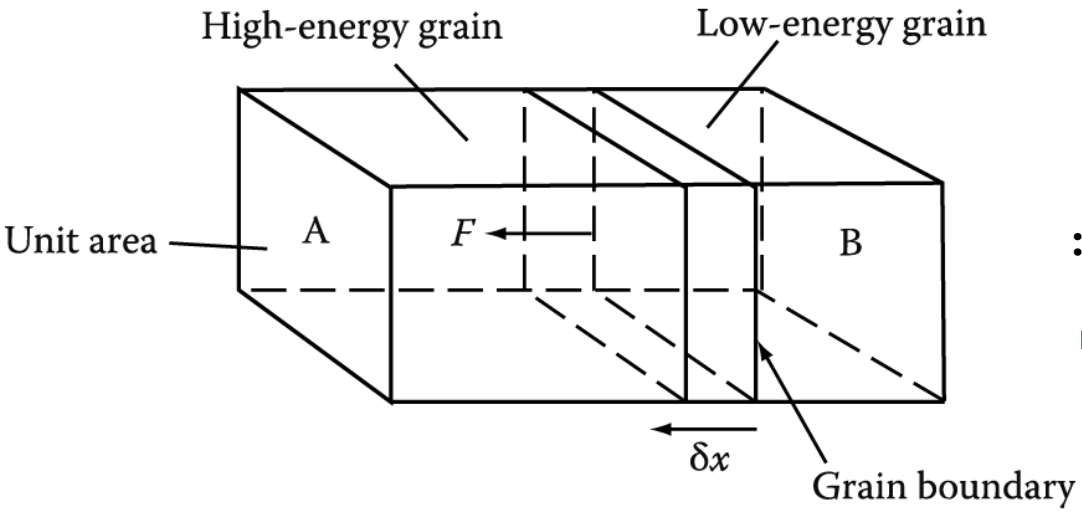

Fig. 3.33 A boundary separating grains with different free energies is subjected to a pulling force F.

curvature ~ $\Delta P \sim \Delta\mu$

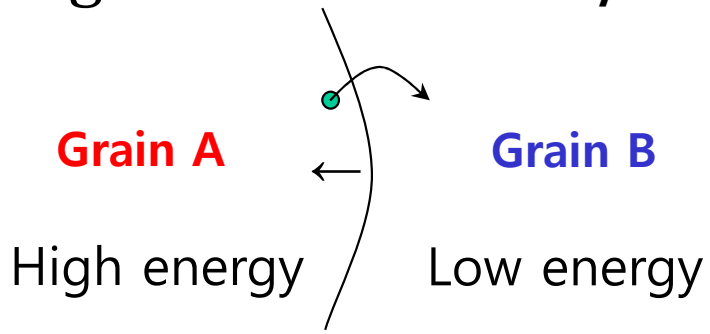

$\Delta G = 2\gamma V_m/r \sim \Delta\mu$ (Eq. 3.32) **Gibbs-Thomson Eq.**

: effect of pressure difference by curved boundary

→ Driving force for grain growth : F

If unit area of GB advances a distance δx, # of moles of material that enter grain B

$\delta x \cdot (1/V_m)$

Work : $F\,dx = (2\gamma V_m/r)(\delta x/V_m)$

→ $F = 2\gamma/r = \Delta G/V_m$ **(by curvature)**

1) Pulling force per unit area of boundary :

$$F = \frac{\Delta G}{V_m} \quad (N\,m^{-2}) \qquad \text{(Eq. 3.33)}$$

Free energy difference per unit volume

Applies equally to any boundary whose migration causes a decrease in free energy, i.e. during recrystallization, the boundaries btw the new strain-free grains and the original deformed grains

Q: Grain boundary (α/ α interfaces)

(a) Low-Angle and High-Angle Boundaries

(b) Special High-Angle Grain Boundaries

(c) Equilibrium in Polycrystalline Materials

③ Kinetics of grain growth

- Grain boundary migration (v) by thermally activated atomic jump

Boundary velocity $$v = \frac{A_2 n_1 v_1 V_m^{\,2}}{N_a RT} \exp\left(-\frac{\Delta G^a}{RT}\right) \frac{\Delta G}{V_m}$$

$v \sim \Delta G/V_m$ driving force

→ $F = \Delta G/V_m$

M : mobility = velocity under unit driving force ~ exp (-1/T)

rate of grain growth $dD/dt \sim 1/D$, exponentially increase with T

→ $D = k't^n$ (Experimental: n << 1/2, ½ at pure metals or high Temp.)

- Mobility of GB~ affected by both type of boundaries and GB segregation or 2nd phase precipitation

i.e Normal grain growth ⟺ Abnormal grain growth

2) How fast boundary moves? : Grain Growth Kinetics

Effect of the driving force on the kinetics of boundary migration

Grain boundary migration by thermally activated atomic jump

*** (1) → (2) : Flux**

(1) atoms in probable site : n_1

Vibration frequency : ν_1

A_2 : probability of being accommodated in grain (2)

$$\rightarrow A_2 n_1 \nu_1 \exp(-\Delta G^a/RT) \ \text{atom/m}^2\text{s} = J_{1\rightarrow 2}$$

*** (2) →(1) : Flux**

$$\rightarrow A_1 n_2 \nu_2 \exp[-(\Delta G^a + \Delta G)/RT] = J_{2\rightarrow 1}$$

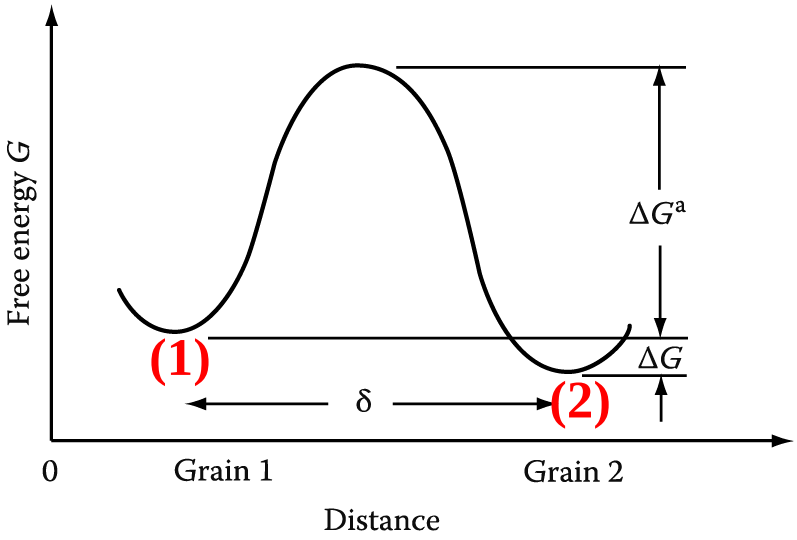

Fig. 3.32 The free energy of an atom during the process of jumping from one grain to the other.

When **ΔG=0**, there is no net boundary movement.

$$A_2 n_1 \nu_1 \approx A_1 n_2 \nu_2 = An\nu$$

When **ΔG >0**, there will be a net flux from grain 1 to 2. **(For a high-angle GB, $A_1 \approx A_2 \approx 1$)**

($A_2 n_1 \nu_1 \approx A_1 n_2 \nu_2 = An\nu$)

$$J_{net} = J_{1\rightarrow 2} - J_{2\rightarrow 1} = An\nu \exp(-\Delta G^a/RT)\,[1 - \exp(-\Delta G/RT)] \quad \text{(Eq. 3.33)}$$

$J_{1\to2} - J_{2\to1} = An\,\nu\exp(-\Delta G^a/RT)\,[1-\exp(-\Delta G/RT)]$

- **If the boundary is moving with a velocity v, the above flux must also be equal to**
  순표류속도

$$J = v \cdot c_B \rightarrow v/(V_m/N_a) \quad (V_m/N_a : \text{atomic volume})$$

Diffusion flux

If ΔG is small [ΔG << RT] → **Apply Tayler expansion to exp (- ΔG/RT) term**

$$J_{net} = A_2 n_1 \nu_1 \exp(-\Delta G^a/RT)\,[\Delta G/RT] \ (\text{atom/m}^2\text{s}) = \nu/(V_m/N_a)$$

Boundary velocity

(Eq. 3.35)

$$v = \frac{A_2 n_1 \nu_1 V_m^{\,2}}{N_a RT} \exp\left(-\frac{\Delta G^a}{RT}\right)\frac{\Delta G}{V_m}$$

$v \sim \Delta G/V_m$ driving force

→ **F = ΔG/V_m**

$$\text{or } v = M \cdot \Delta G / V_m$$

M: mobility of boundary,
i.e., the velocity under unit driving force

$$\text{where } M = \left\{\frac{A_2 n_1 \nu_1 V_m^{\,2}}{N_a RT}\exp\left(\frac{\Delta S^a}{R}\right)\right\}\exp\left(\frac{-\Delta H^a}{RT}\right)$$

M : mobility = velocity under unit driving force ~ exp (-1/T)

exponentially increase with temp

⇨ **The boundary migration is a thermally activated process.**

(입계 이동은 확산처럼 열활성화 과정)

*3.4.7 Kinetic of grain growth

1) driving force $F = \Delta G/V_m$ → $v = M(\Delta G/V_m)$ **Boundary velocity**

Pulling force

M : exponentially increase with temp.

v : relation to grain coarsening

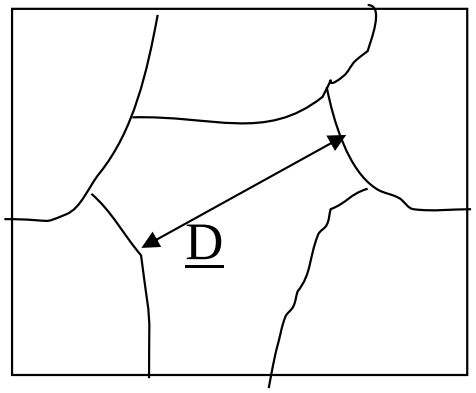

Mean grain size (diameter) : $\underline{D}$

Mean radius of curvature of boundary : r

if $\underline{D} \propto r$,

Mean velocity : $\underline{v} = \alpha M(\Delta G/V_m) = d\underline{D}/dt$ $(\Delta G = 2\gamma V_m/r)$

(Eq. 3.38)

$= \alpha M(2\gamma/\underline{D}) = d\underline{D}/dt$ (α = proportional constant ~ 1)

$\underline{v}$ (rate of grain growth) ~ $1/\underline{D}$, exponentially increase with T

Mean velocity : $\underline{v} = \alpha M (\Delta G/V_m) = d\underline{D}/dt \quad (\Delta G = 2\gamma V_m/r)$

$= \alpha M(2\gamma/\underline{D}) = d\underline{D}/dt \quad (\alpha = \text{proportional constant} \sim 1)$

Integration of previous eq. from D_0 to $\underline{D}$,

$$\rightarrow \int_{D_o}^{\underline{D}} \underline{D}\, d\underline{D} = \int 2\alpha M\gamma dt$$

$$\rightarrow \tfrac{1}{2} (\underline{D}^2 - D_o^2) = 2\alpha M\gamma t$$

$$\rightarrow (\underline{D}^2 - D_o^2) = 4\alpha M\gamma\, t = kt$$

$$\rightarrow \underline{D}^2 = D_o^2 + kt \quad \text{(Eq. 3.39)}$$

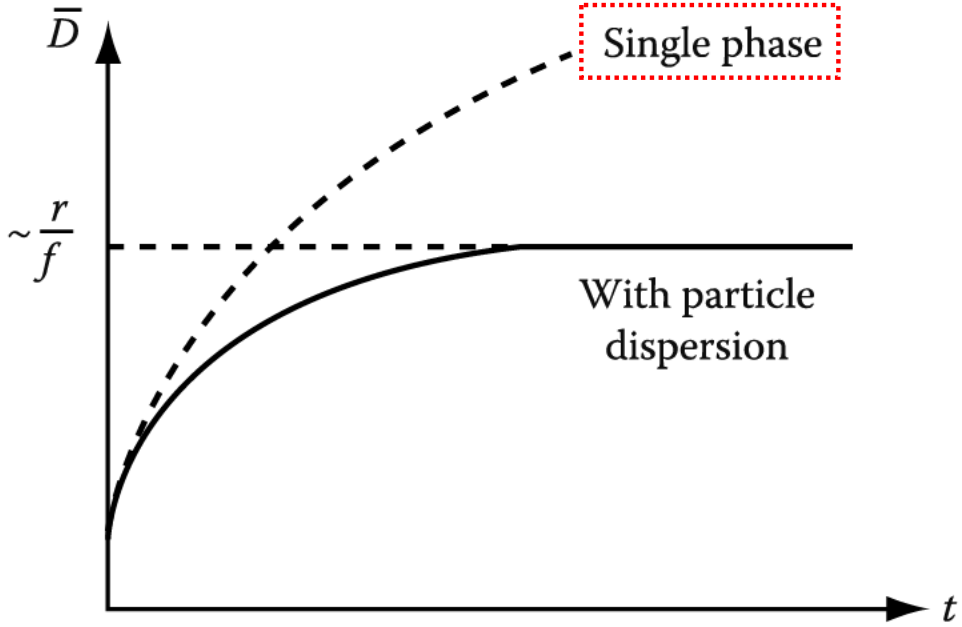

r = average radius of particles

f_v = volume fraction of particles

if $D_o \approx 0 \rightarrow \underline{D} = k't^{1/2}$ (Eq. 3.40)

$\rightarrow \underline{D} = k't^n$ (experimental : n << ½, ½ in very pure metals or only high temp.)

Single phase

∵the velocity of GB migration, v is not linear function of ΔG.
→ M is not a const. but varies with ΔG and thus also with D.
→ Variation of M in alloys could arise from solute drag effects.
(M in alloy is relatively slower than that of pure metal)

Whose mobility would be high between special and random boundaries?

By considering grain boundary structure, (Mobility depending on GB structures)

- High energy G.B. → relatively open G.B. structure → High mobility
- Low energy G.B. → closed (or denser) G.B. structure → Low mobility

But, **Ideal** ⟷ **Real**

2) The other special boundaries are usually more mobile than random high-angle boundary. Why?

If the metal were "perfectly" pure the random boundaries would have the higher mobility.

⇨ **Due to differences in the interactions of alloy elements or impurities with different boundaries**

Same driving force

Ex) 1) coherent twin boundary
~ almost entirely immobile

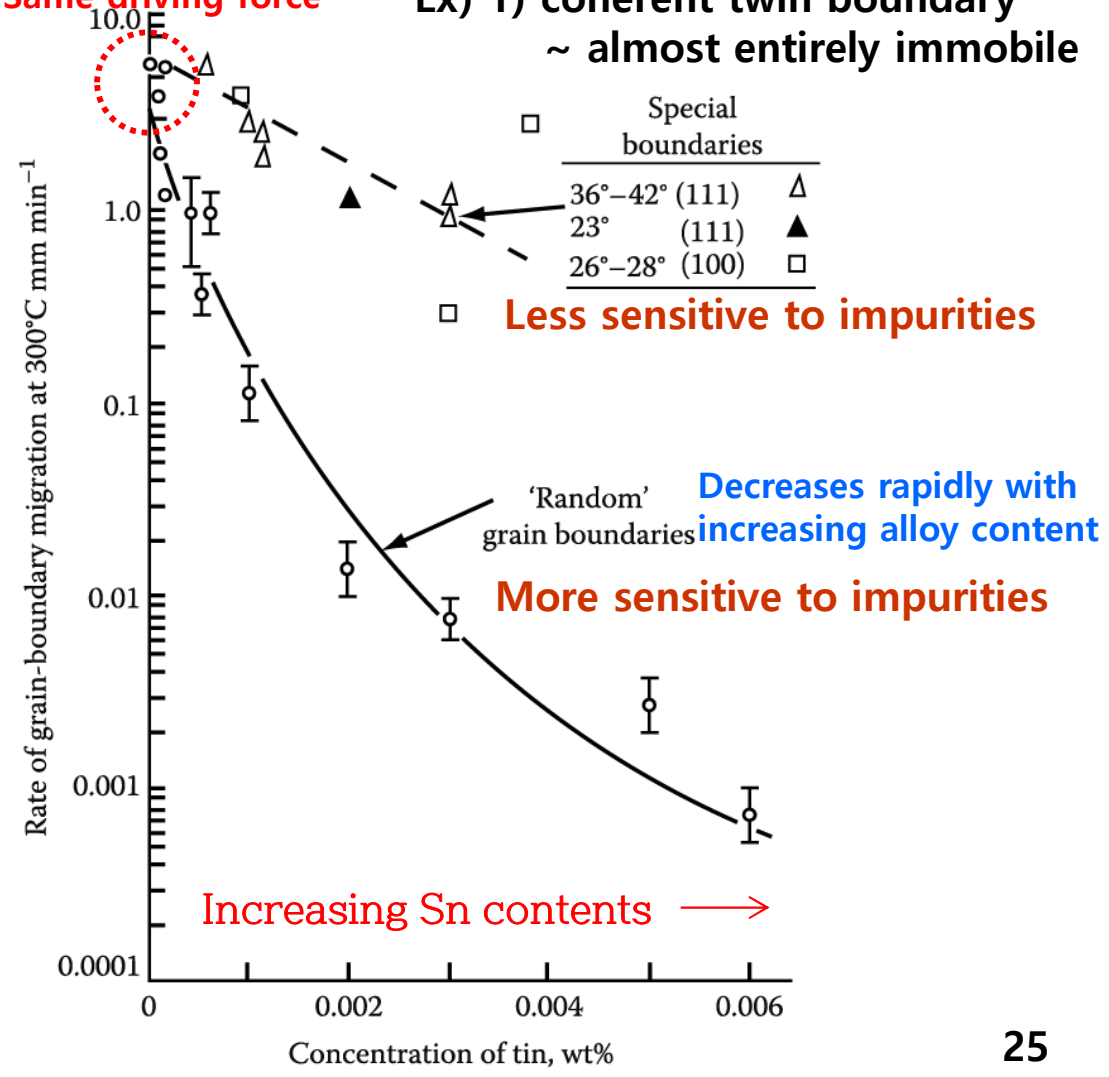

Less sensitive to impurities

Decreases rapidly with increasing alloy content

More sensitive to impurities

Migration rate of special and random boundaries at 300 °C in zone-refined lead alloyed with tin under equal driving forces

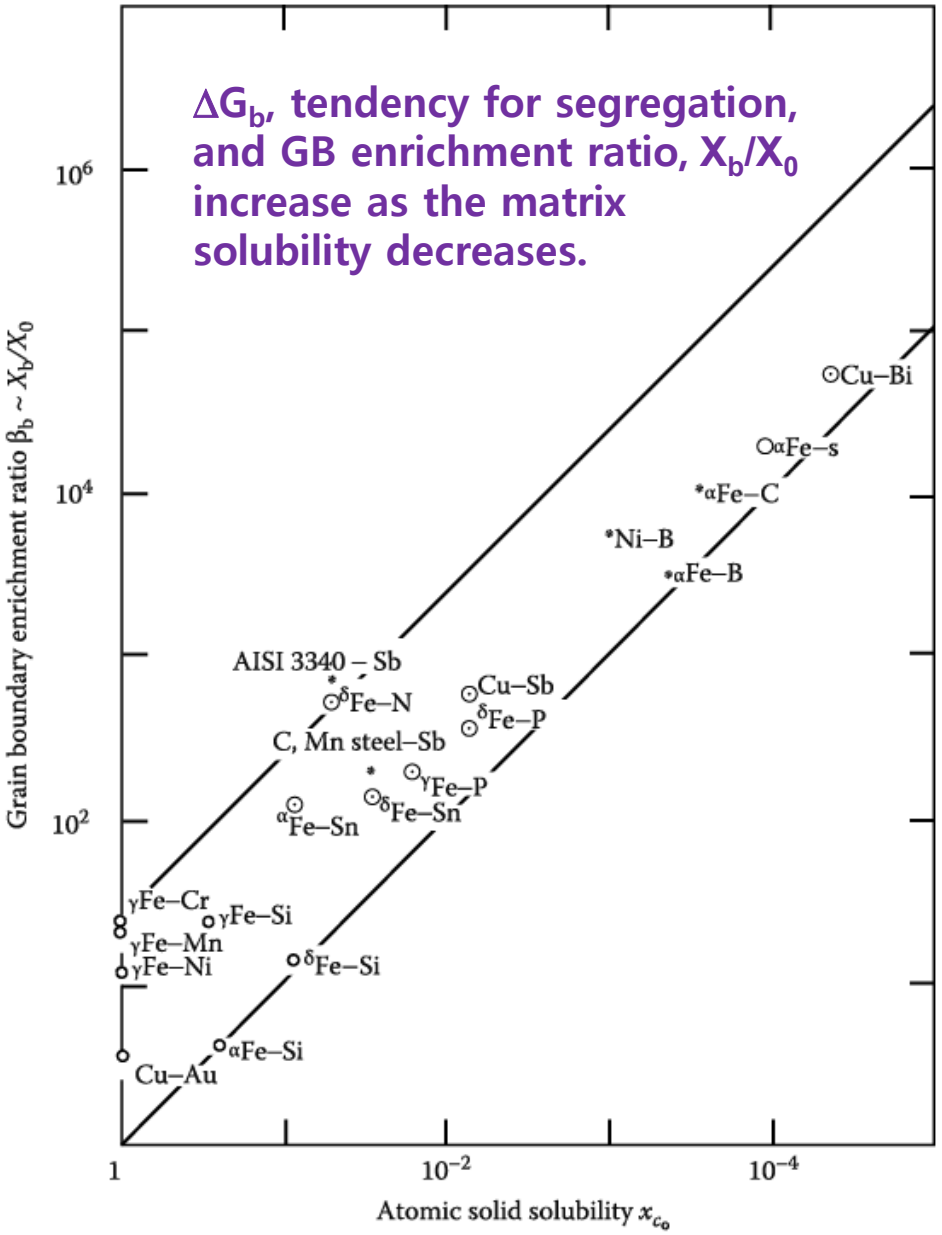

<Increasing GB enrichment with decreasing solid solubility in a range of system>

* Solute drag effect

In general,
G_b (grain boundary E) and mobility of pure metal decreases on alloying.

~Impurities tend to stay at the GB.

Generally, ΔG_b, tendency of segregation, increases as the matrix solubility decreases.

$$X_b = X_0 \exp \frac{\Delta G_b}{RT}$$

X_b/X_0: GB enrichment ratio

- Decreases as temp. increases, i.e., the solute "evaporates" into the matrix

Low T or ΔG_b ⇧ X_b ⇧ Mobility of G.B. ⇩

→ Alloying elements affects mobility of G.B.

X_0 : matrix solute concentration/ X_b : boundary solute concentration

ΔG_b : free energy reduced when one mole of solute is moved to GB from matrix.

→ The high mobility of special boundaries can possibly be attributed to a low solute drag on account of the relatively more close-packed structure of the special boundaries.

3.4.4 Grain boundary energy of dilute binary alloys

- **Grain boundary energy can be expected to change on alloying.**
  There will be a higher concentration of solute at the GBs, and the interaction of the strain files of the solute and boundary will lower the GB energy.

A simple way to modelling GB segregation is to treat the boundary as a separate phase.

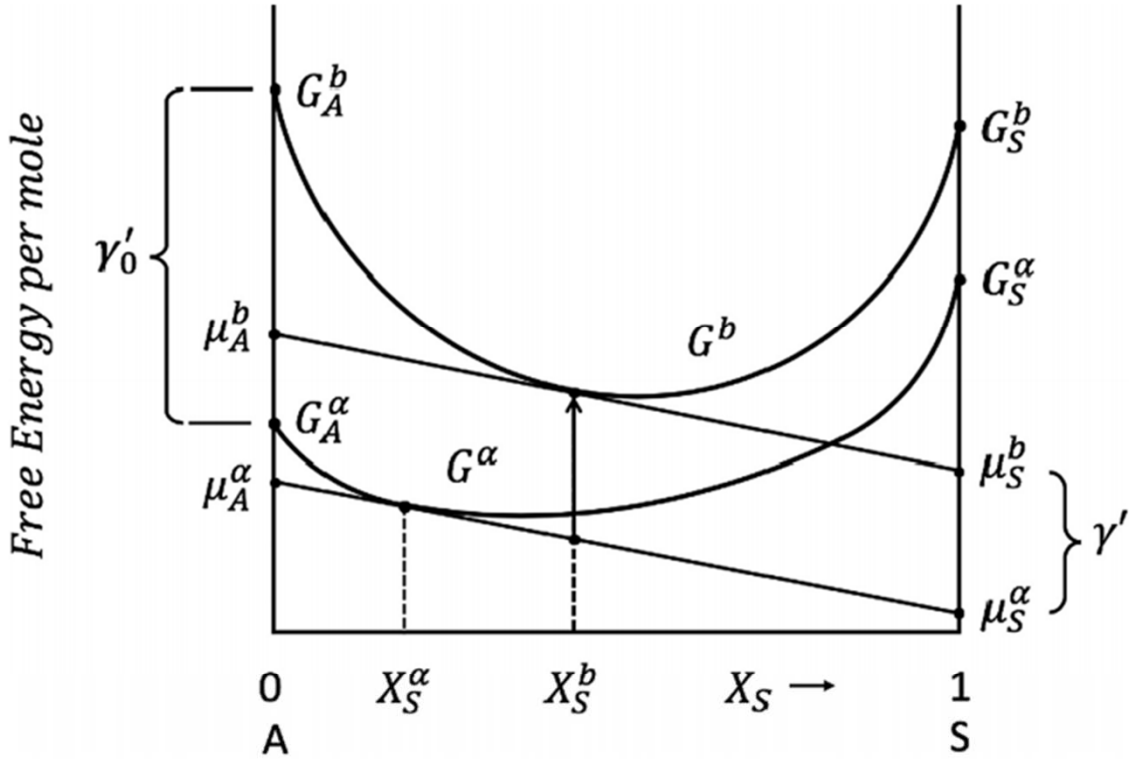

FIGURE 3.22 Free energy diagram for solid α phase and grain boundary phase b for a binary alloy of A containing solute S. X_S^α is the mole fraction of solute in the α grain and X_S^b is the content in the grain boundary. γ_0' is the grain boundary energy of pure A and the length of the vertical arrow (distance between the tangents), γ', the grain boundary energy of the alloy.

A grain phase α and a boundary phase b,
If we transfer dN_A moles of solvent A and dN_S moles of solute S from the grain to the GB,

(3.17) $$dG' = (\mu_A^b - \mu_A^\alpha)dN_A - (\mu_S^b - \mu_S^\alpha)dN_S = 0 \quad (\because \text{Metastable equilibrium btw grain and GB})$$

If total quantity of atoms in the boundary is constant, $dN_A + dN_S = 0$

(3.18) $$\therefore (\mu_A^b - \mu_A^\alpha) = (\mu_S^b - \mu_S^\alpha)$$

If we assume that the grain and boundary phase follow the regular solution model,

(3.19) $$\mu_A^\alpha = G_A^\alpha + \Omega^\alpha (1 - X_A^\alpha)^2 + RT \ln X_A^\alpha \qquad \mu_A^b = G_A^b + \Omega^b (1 - X_A^b)^2 + RT \ln X_A^b$$
$$\mu_S^\alpha = G_S^\alpha + \Omega^\alpha (1 - X_S^\alpha)^2 + RT \ln X_S^\alpha \qquad \mu_S^b = G_S^b + \Omega^b (1 - X_S^b)^2 + RT \ln X_S^b$$

where, Ω^α and Ω^b : the difference in A-A and A-S bond energies in the grain and GB,
and $X_A + X_S = 1$ for each phase.

(3.20) $$\Delta G_b = (G_S^b - G_S^\alpha) - (G_A^b - G_A^\alpha) + (\Omega^b - \Omega^\alpha)$$ ⇨ **(3.21)** $$\frac{X_S^b}{(1 - X_S^b)} = \frac{X_S^\alpha}{(1 - X_S^\alpha)} exp\left\{\frac{-\Delta G_b}{RT}\right\}$$

then substituting Equations (3.19) into Equation (3.18)
and ignoring small terms:

If X_S^α and X_S^b are small, the terms $(1 - X_S^\alpha)$ and $(1 - X_S^b)$ can be ignored:

(3.22) $$X_S^b \approx \frac{X_S^\alpha exp\{-\Delta G_b/RT\}}{1 + X_S^\alpha exp\{-\Delta G_b/RT\}}$$

Here, ΔG_b=Gibbs energy of segregation
~usually negative (In regular solution, strong A-S bonding in the GB, week A-S bonding in the α phase, In real solution, increasing size misfit btw solute and matrix; varies with temp. and atomic structure (misorientation btw the grains and the orientation of the GB plane)

Solute tends to segregate to the boundary to reduce the overall free energy of the system

Derive an expression for how GB segregation affects the GB energy.

: the GB energy is the decrease in free energy that occurs if the atoms in the boundary rearrange themselves into the crystal structure of the α phase ($(\mu_A^b$ and $\mu_S^b) \rightarrow (\mu_A^\alpha$ and $\mu_S^\alpha)$)

If there are n_A^b moles of A atoms and n_S^b moles of S atoms in the boundary, the decrease in free energy is:

$$n_A^b(\mu_A^b - \mu_A^\alpha) + n_S^b(\mu_S^b - \mu_S^\alpha) = (n_A^b + n_S^b)(\mu_A^b - \mu_A^\alpha) = n^b\,(\mu_A^b - \mu_A^\alpha)$$

where, n^b is the total number of moles of boundary $(n_A^b + n_S^b)$

$\therefore$ GB energy per mole : $(\mu_A^b - \mu_A^\alpha) = (\mu_S^b - \mu_S^\alpha) = \gamma'$

Fig. 3.22

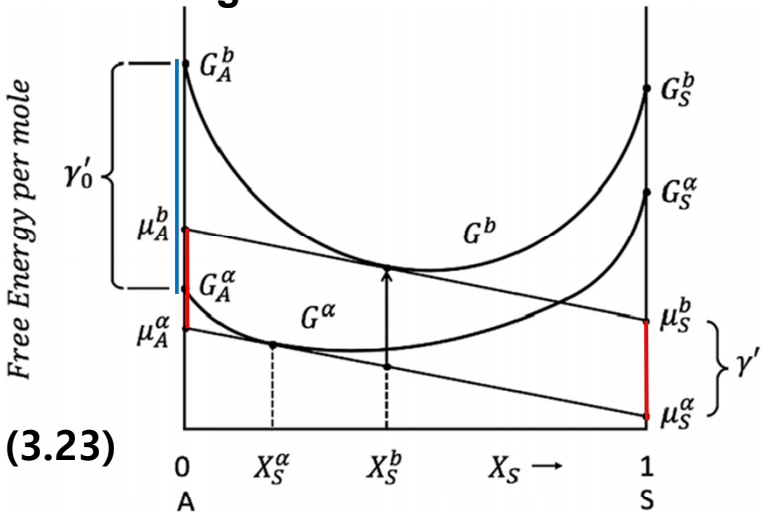

GB energy per unit area $\gamma = (\mu_A^b - \mu_A^\alpha)\delta/V_m^b$ J/m^2 **(3.23)**

where, δ is the thickness of the boundary phase and V_m^b is the molar volume of the boundary, assumed to be independent of the boundary composition. V_m^b/δ is the area of GB containing 1 mole.

In a similar way,

GB energy per mole for pure A is γ_0', i.e., $G_A^b - G_A^\alpha$ and per unit area $\gamma_0 = (G_A^b - G_A^\alpha)\delta/V_m^b$ J/m^2 **(3.24)**

GB energy for binary alloys $\gamma = \gamma_0 - \frac{\delta RT}{V_m^b} \ln\{1 + X_S^\alpha \exp(-\Delta G_b/RT)\}$ **(3.25)**

Since ln (1+x) → x as x→ 0, for very dilute solutions, i.e., metals containing impurities

The rate of change of GB energy with increasing X_S^α is given by

$$\frac{\partial \gamma}{\partial X_S^\alpha} = -\frac{\delta RT}{V_m^b} \exp(-\Delta G_b/RT)\} \quad \textbf{(3.26)}$$

GB energy for binary alloys $\gamma = \gamma_0 - \frac{\delta RT}{V_m^b} \ln \{1 + X_S^\alpha \exp(-\Delta G_b/RT)\}$ **(3.25)**

Since ln (1+x) → x as x→ 0, for very dilute solutions, i.e., metals containing impurities The rate of change of GB energy with increasing X_S^α is given by

$$\frac{\partial \gamma}{\partial X_S^\alpha} = -\frac{\delta RT}{V_m^b} \exp(-\Delta G_b/RT)\} \quad \textbf{(3.26)}$$

- **The stronger the tendency for solute or impurities to segregate to the grain boundary, the greater is the reduction in the GB energy.** Note that, in the case of impurity contents, is essential the same as the total impurity content in the alloy.

For example, Putting δ=0.75 nm, V_m^b=7 cm³, R =8.314 J/mol·K and T =773 K (500 ℃) gives X_S^α = 1,650 J/m² for ΔG_b = -50 kJ/mol, which is a strong free energy of segregation.

In such a case, an addition of just 0.0001 mole fraction (0.01 atomic %) would reduce the GB energy by 165 mJ/m², which is an appreciable effect considering that random high-angle GB energies are typically of the order of 1,000 mJ/m².

Putting the same value of ΔG_b into Equation (3.22) predicts that the enrichment ratio X_S^b / X_S^α is 2,000 giving the mole fraction of solute in the boundary as 0.2.

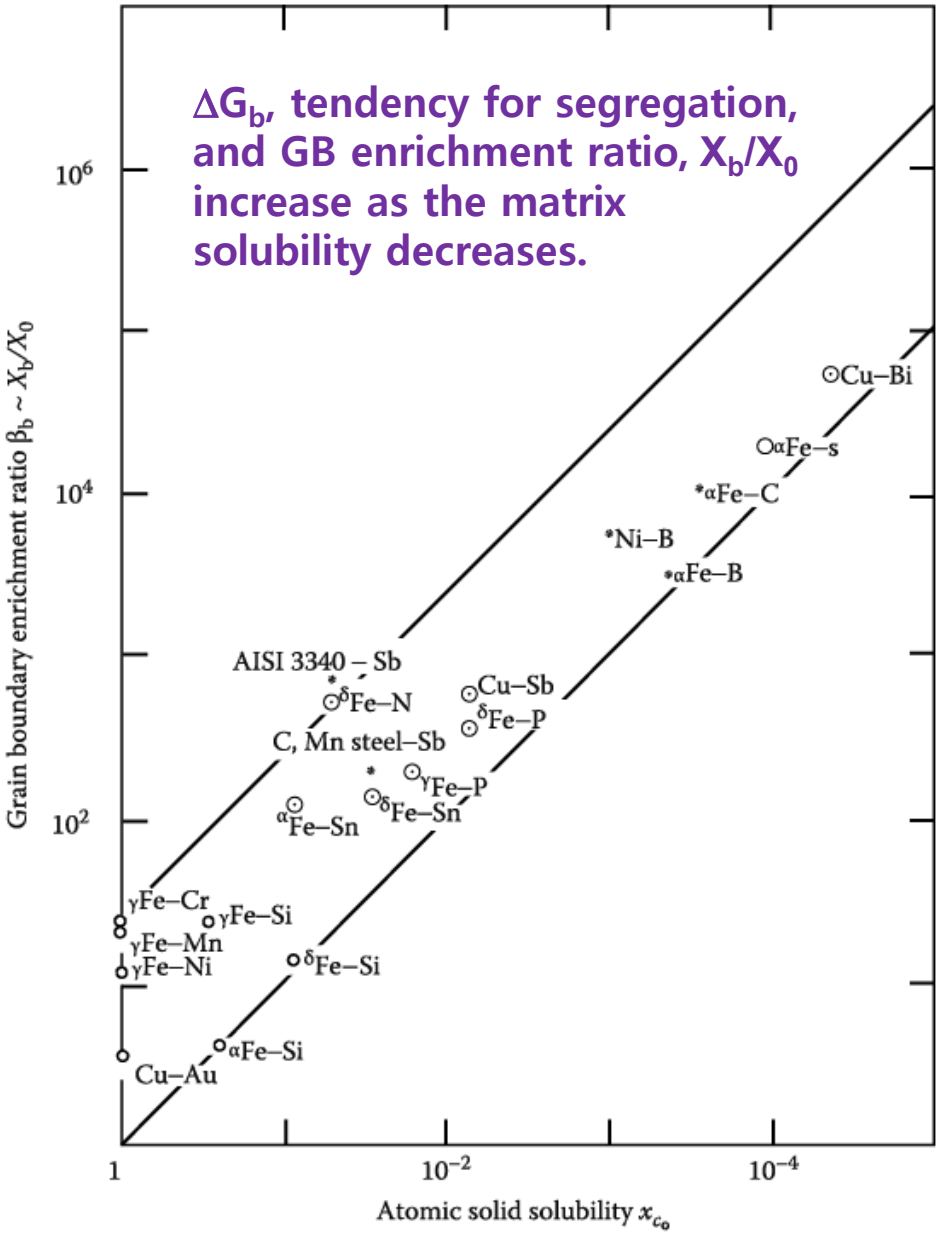

<Increasing GB enrichment with decreasing solid solubility in a range of system>

* Solute drag effect

In general,
G_b (grain boundary E) and mobility of pure metal decreases on alloying.

~Impurities tend to stay at the GB.

Generally, ΔG_b, tendency of segregation, increases as the matrix solubility decreases.

$$X_b = X_0 \exp \frac{\Delta G_b}{RT}$$

X_b/X_0: GB enrichment ratio

- Decreases as temp. increases, i.e., the solute "evaporates" into the matrix

Low T or ΔG_b ⇧ X_b ⇧ Mobility of G.B. ⇩

→ Alloying elements affects mobility of G.B.

X_0 : matrix solute concentration/ X_b : boundary solute concentration

ΔG_b : free energy reduced when one mole of solute is moved to GB from matrix.

→ The high mobility of special boundaries can possibly be attributed to a low solute drag on account of the relatively more close-packed structure of the special boundaries.

Normal Grain Growth

- Grain boundary moves to reduce area and total energy
- Large grain grow, small grains shrink
- Average grain size increases
- Little change of size distribution

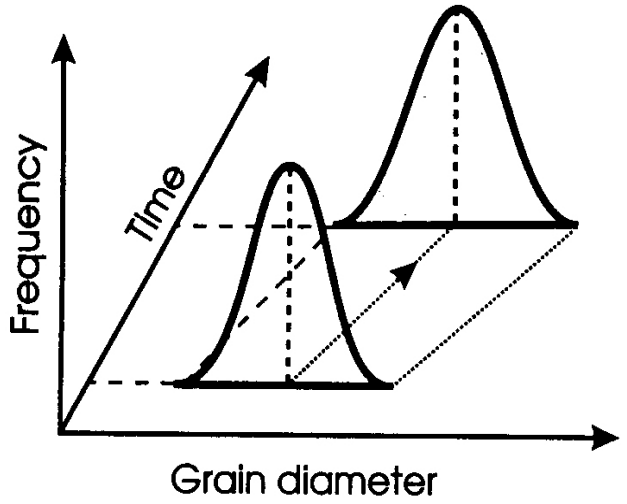

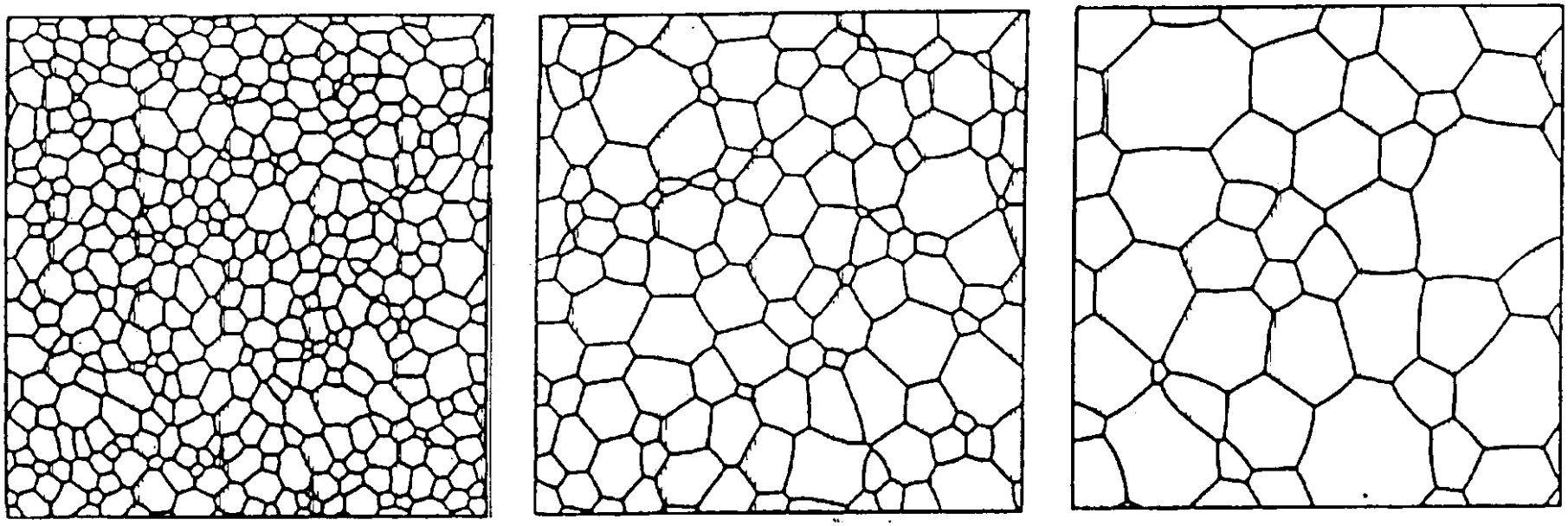

Ref. Hillert ACTA Mater. 13 227 (1965)

Abnormal Grain Growth

(high mobility of special GBs → development of recrystallization textures)

❑ **Discontinuous grain growth of a few selected grains**

- Local breaking of pinning by precipitates
- Anisotropy of grain boundary mobility
- Anisotropy of surface & grain boundary energy
- Selective segregation of impurity atoms
- Inhomogeneity of strain energy

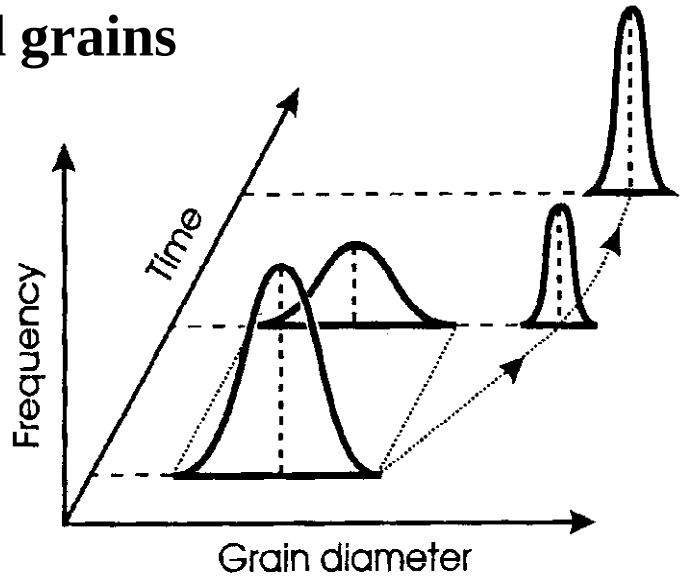

❑ **Bimodal Size distribution**

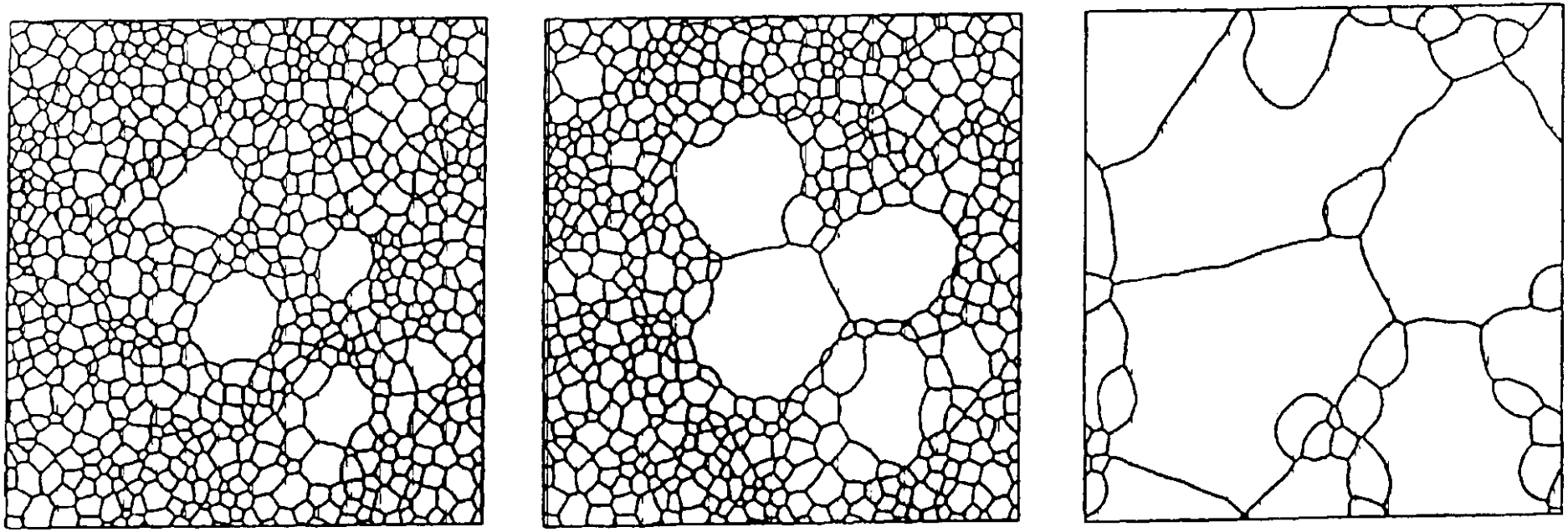

Abnormal Grain Growth

ex) Si steel → improvement of "soft magnetic property"

= discontinuous grain growth or secondary recrystallization

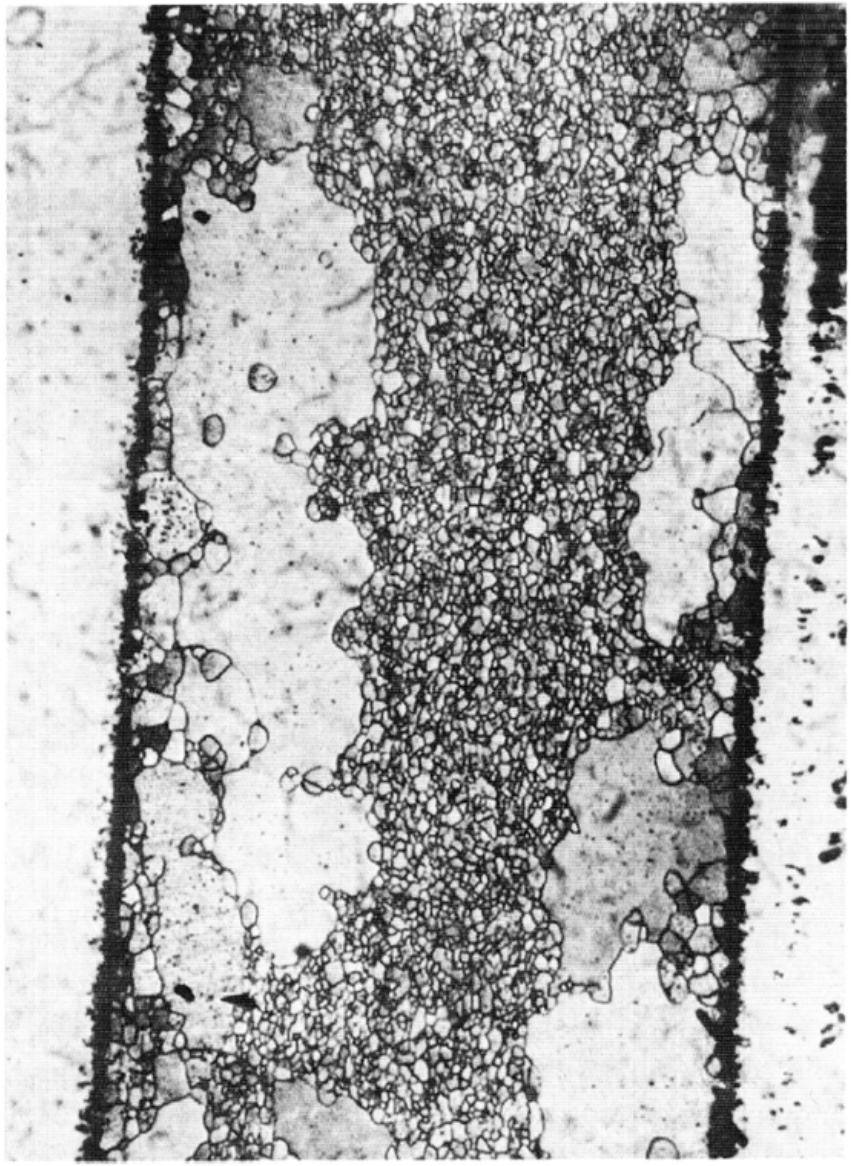

Figure 5.87 Optical micrograph showing abnormal grain growth in a fine grain steel containing 0.4 wt% carbon. The matrix grains are prevented from growing by a fine dispersion of carbide particles that are not revealed. Magnification ×135. (After Gawne and Higgins 1971. Courtesy of the Metals Society.)

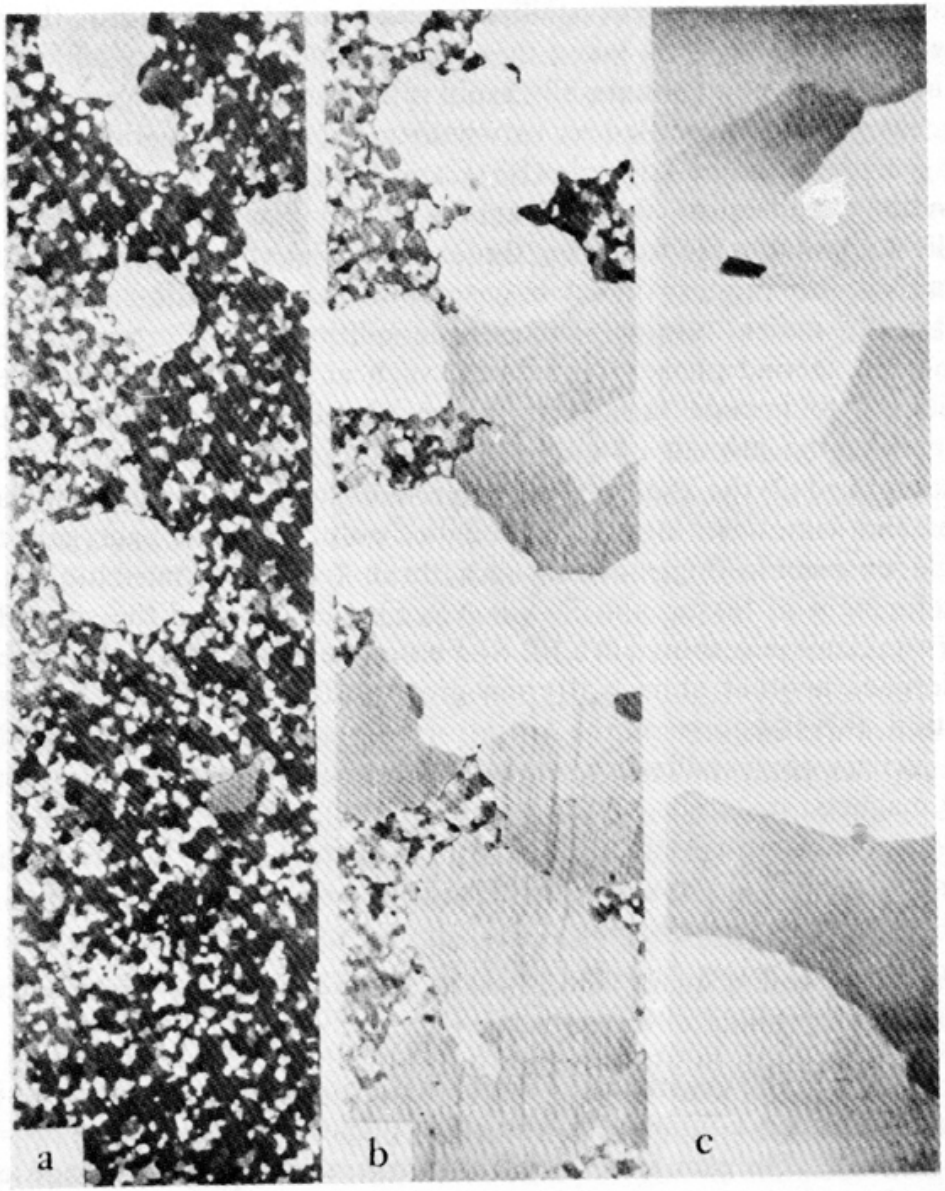

Fig. 5.48. Evidence for the preferential formation of (110)[001]-oriented grains by secondary recrystallization in 5% Si–Fe (Graham [1969]).

Q: Grain boundary (α/ α interfaces)

= Boundaries in Single-Phase Solids

(a) Low-Angle and High-Angle Boundaries

(b) Special High-Angle Grain Boundaries

(c) Equilibrium in Polycrystalline Materials

④ Effect of second-phase particle on GB migration

: Zener Pinning

$$\bar{D}_{max} = \frac{4r}{3f_v}$$

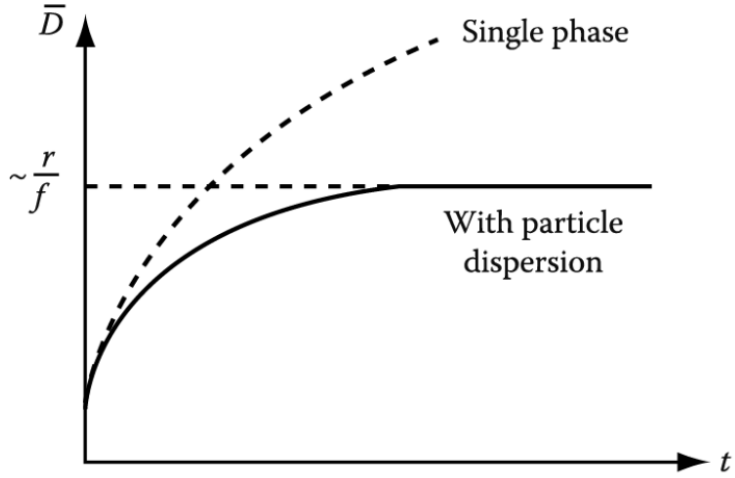

Schematic diagram illustrating the possible interactions of second phase particles and migrating grain boundaries.

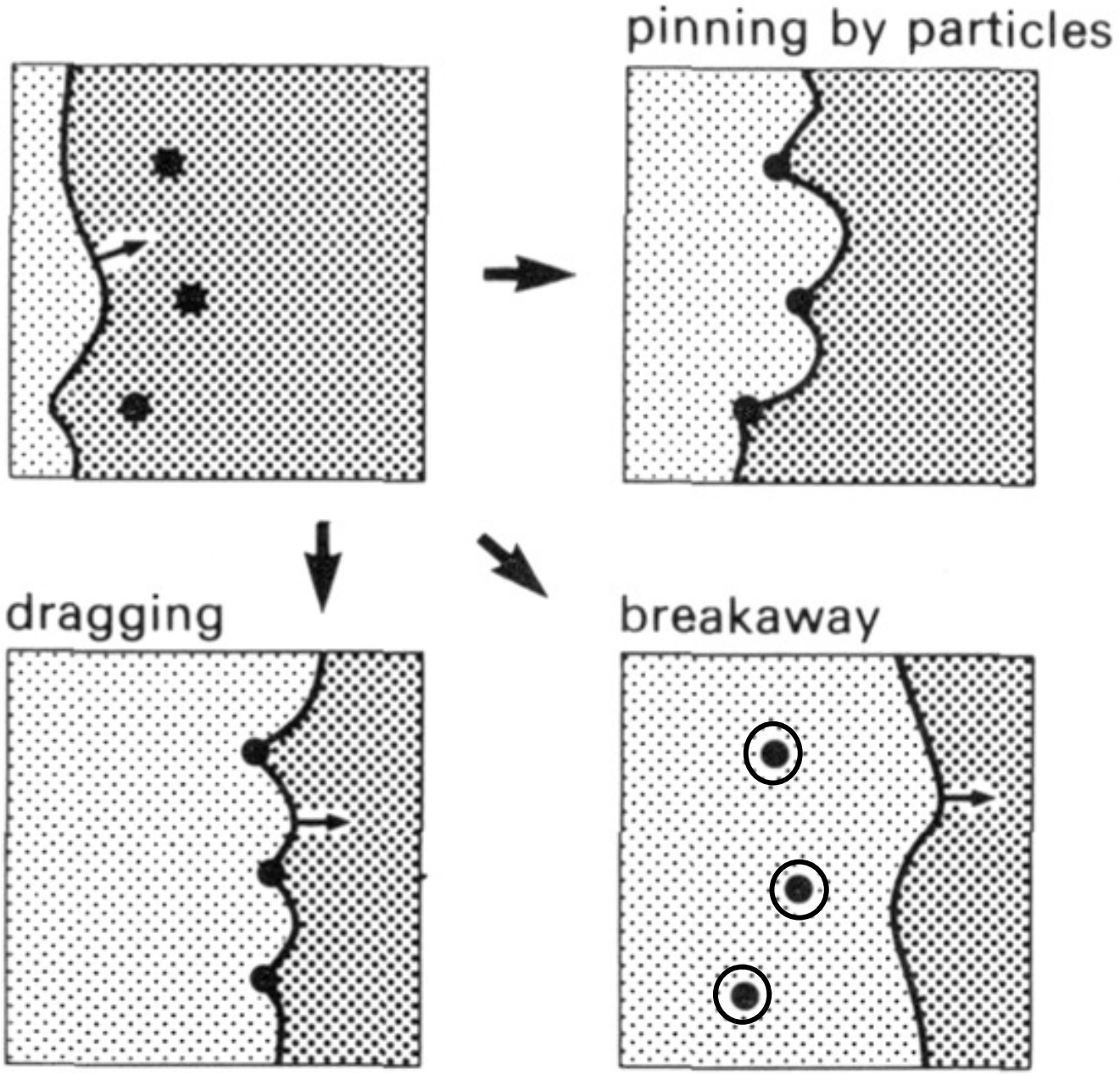

Pinning by particle

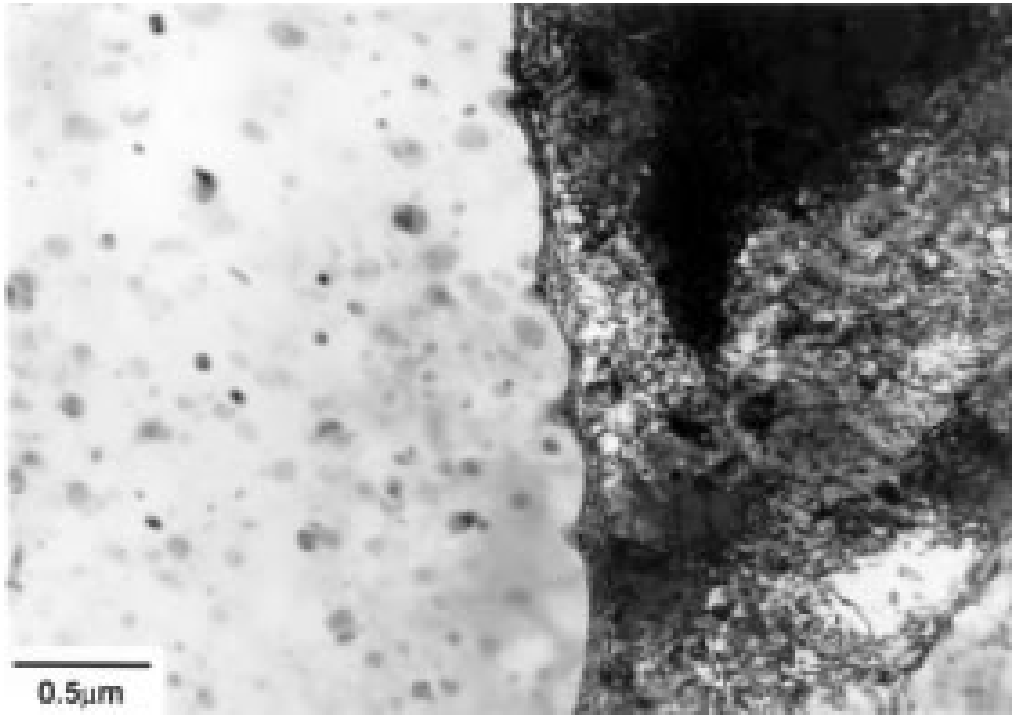

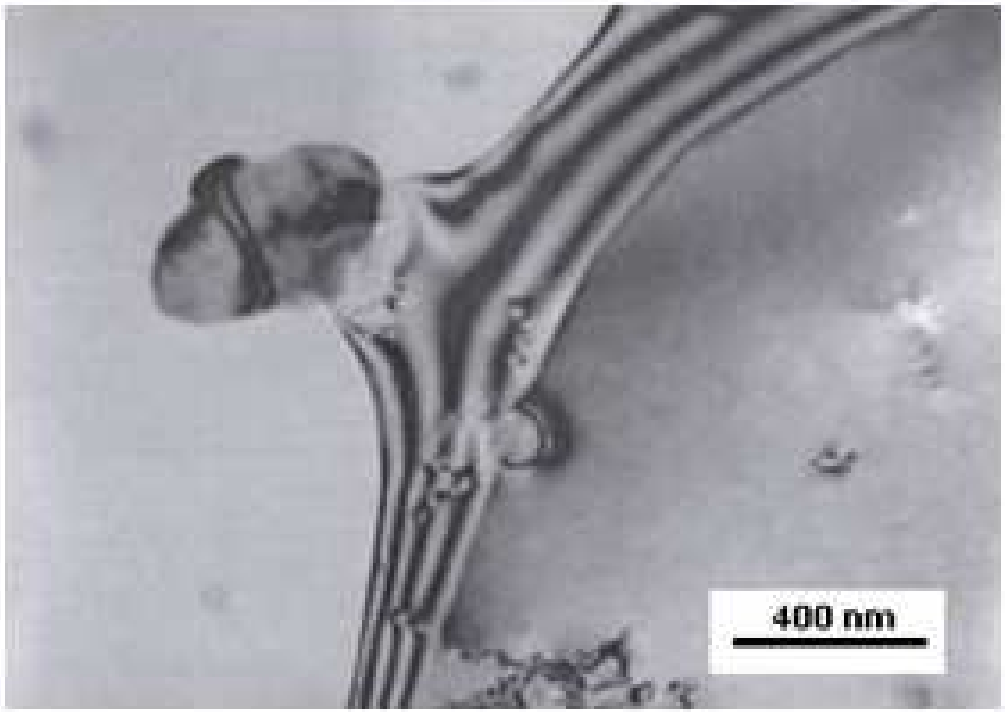

Effect of Second-Phase Particles on GB migration

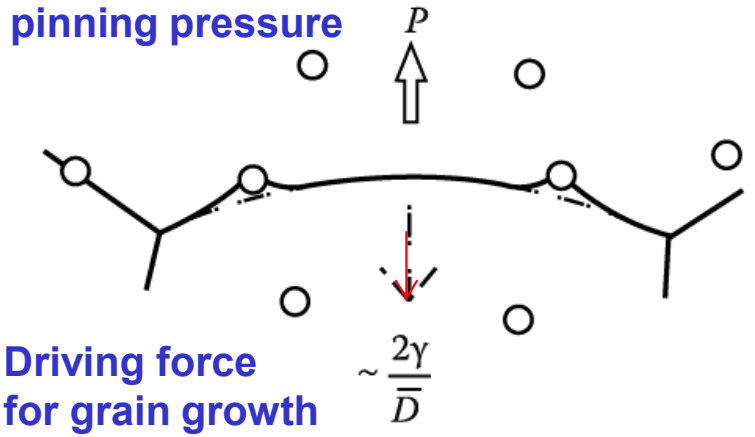

Interaction with particles

Zener Pinning

Derive the expression for the pinning effect of grain boundary migration by precipitates.

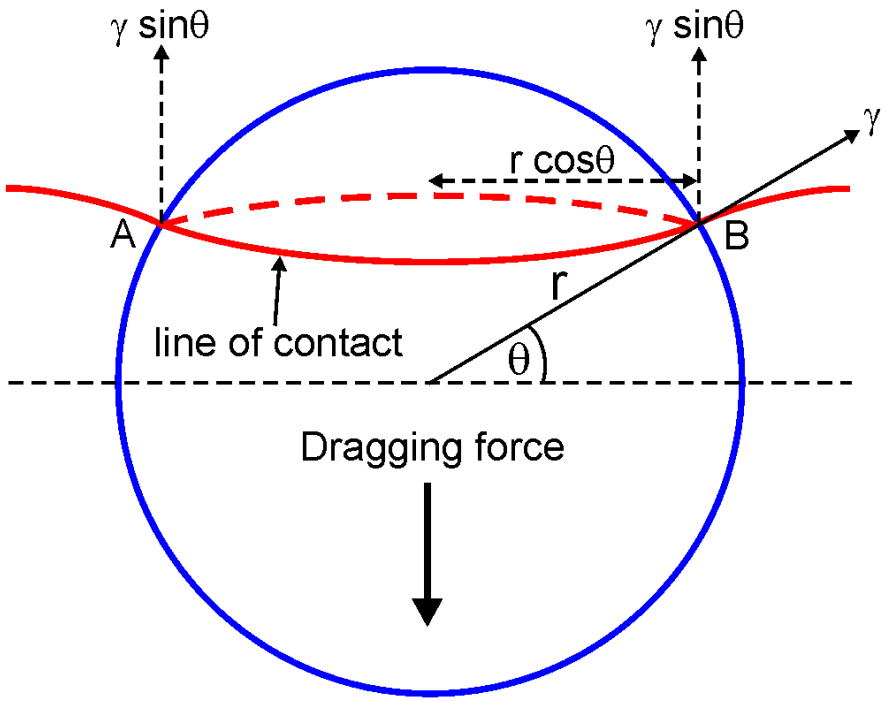

since $\gamma \sin\{\theta\} =$ force per unit length

$$F = \gamma \sin\{\theta\} \times 2\pi r \cos\{\theta\} = \text{AB}$$

circumference

so that at $\theta = 45^\circ$

$$F_{max} = \gamma \pi r$$

Maximum force exerted by a single particle

Interaction with particles **Zener Pinning**

f_v = volume fraction of randomly distributed particles of radius r

N_{total} = number of particles per unit volume $\quad N = \dfrac{f_v}{\frac{4}{3}\pi r^3}$

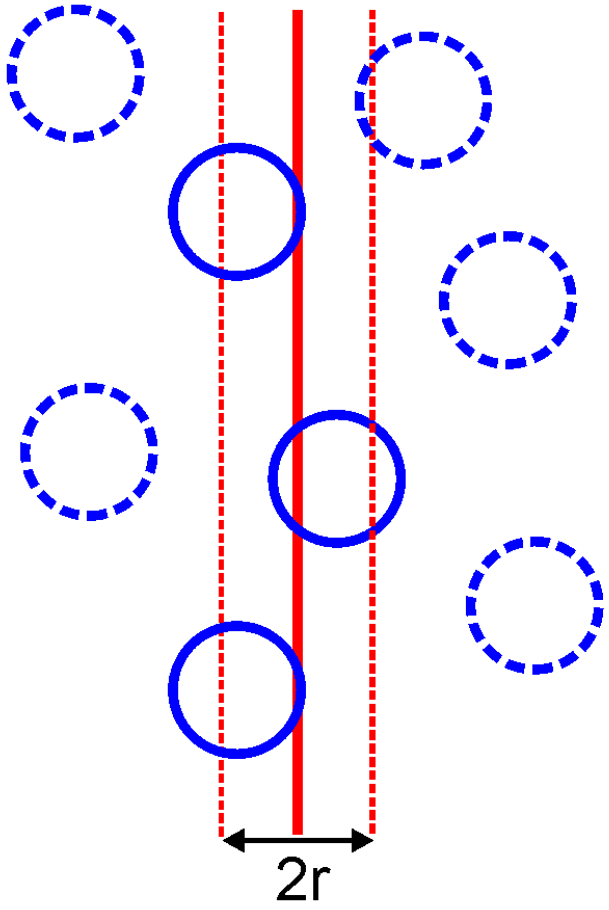

Only particles within one radius (solid circles) can intersect a planar boundary

If the boundary is essentially planar,

$$N_{interact} = 2rN_{total} = 3f_v/2\pi r^2$$

Mean # of particles intersecting unit area of a random plane

Given the assumption that

all particles apply the maximum pinning force,

the total pinning pressure

$$P = \frac{3f_v}{2\pi r^2} \cdot \pi r \gamma = \frac{3f_v \gamma}{2r}$$ (Eq. 3.41)

This force will oppose the driving force for grain growth, $2\gamma/\bar{D}$ **.**

Interaction with particles

Zener Pinning

$$P = \frac{3f_v}{2\pi r^2} \cdot \pi r \gamma = \frac{3f_v \gamma}{2r}$$

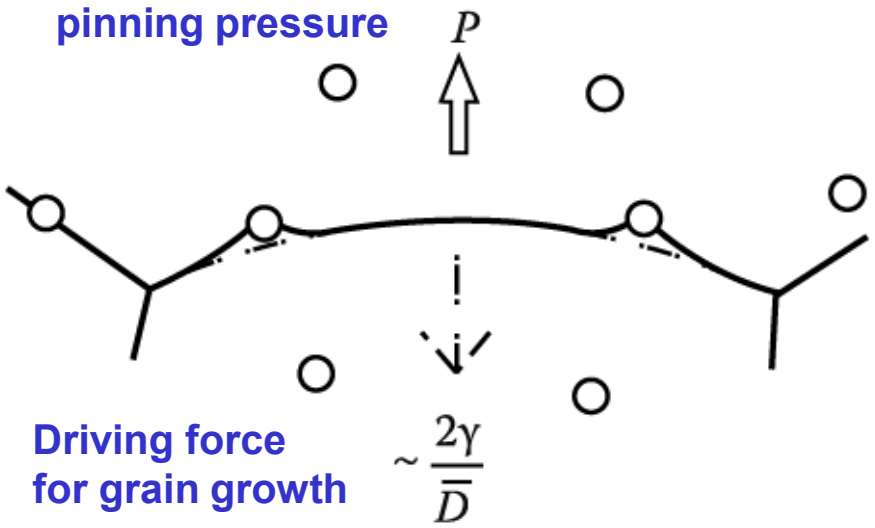

→ F = 2γ/r = ΔG/V_m (by curvature)

This force will oppose the driving force for grain growth, $2\gamma/\bar{D}$.

(Eq. 3.42)

$$\frac{2\gamma}{\bar{D}} = \frac{3f_v \gamma}{2r} \rightarrow \bar{D}_{max} = \frac{4r}{3f_v}$$

Driving force will be insufficient to overcome the drag of the particles and grain growth stagnates.

For fine grain size
→ a large volume fraction of very small particles

* Effect of second-phase particles on grain growth

$$\bar{D}_{max} = \frac{4r}{3f_v}$$

: Stabilization of a fine grain size during heating at high temp. → large volume fraction (f ↑) of very small particles (r ↓).

$$\bar{D}_{max} = \frac{4r}{3f_v} \downarrow$$

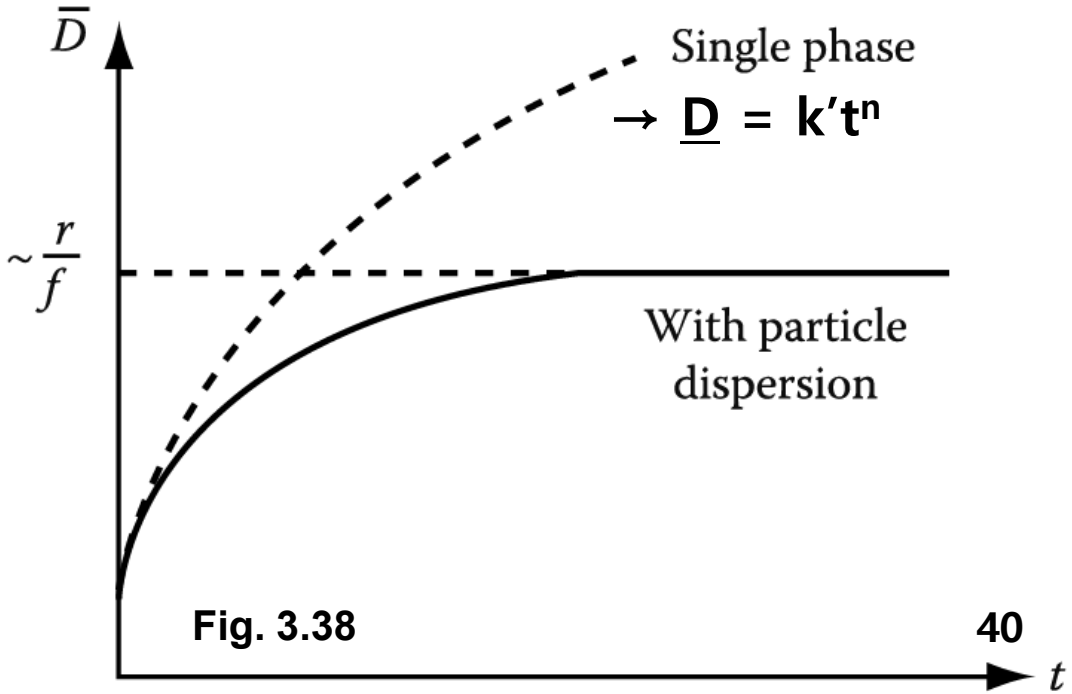

Fig. 3.38

- **Thermally Activated Migration of Grain Boundaries:**

  Metastable equilibrium of grain boundary (Balances of 1) boundary E + 2) surface tension)

  → real curvature (ΔP → ΔG: Gibbs Thomson Eq.) → $F = 2\gamma/r = \Delta G/V_m$ (by curvature)

  (Pulling force per unit area of boundary)

  → Grain coarsening at high T annealing

- **Kinetics of Grain Growth**

  - Grain boundary migration (v) by thermally activated atomic jump

Boundary velocity $$v = \frac{A_2 n_1 v_1 V_m^{\,2}}{N_a RT} \exp\left(-\frac{\Delta G^a}{RT}\right) \frac{\Delta G}{V_m}$$

$v \sim \Delta G/V_m$ driving force → $F = \Delta G/V_m$

M : mobility = velocity under unit driving force ~ exp (-1/T)

rate of grain growth $dD/dt \sim 1/D$, exponentially increase with T

→ $D = k't^n$ (Experimental: n << 1/2, ½ at pure metals or high Temp.)

- Mobility of GB~ affected by both type of boundaries and GB segregation or 2nd phase precipitation

Ex) Effect of second-phase particle - Zener Pinning

$$\bar{D}_{max} = \frac{4r}{3f_v}$$

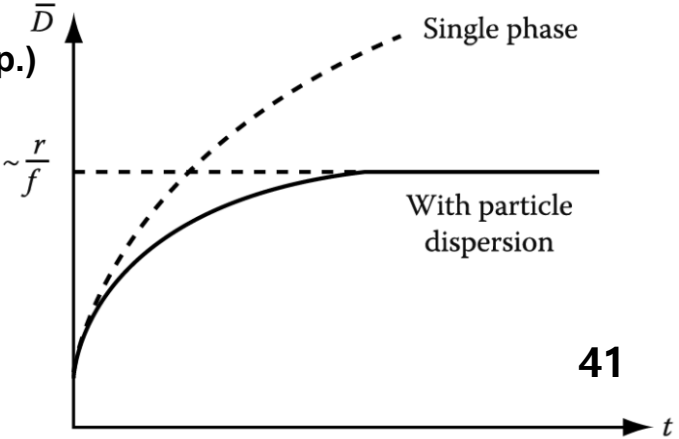

Summary for today's class

- **Grain Growth**

- Normal grain growth ⟺ **Abnormal grain growth**

(high mobility of special GBs
→ development of recrystallization textures)

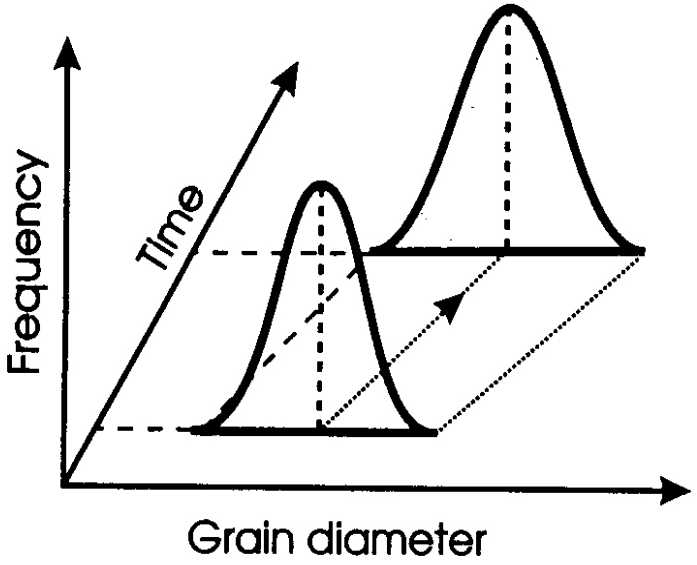

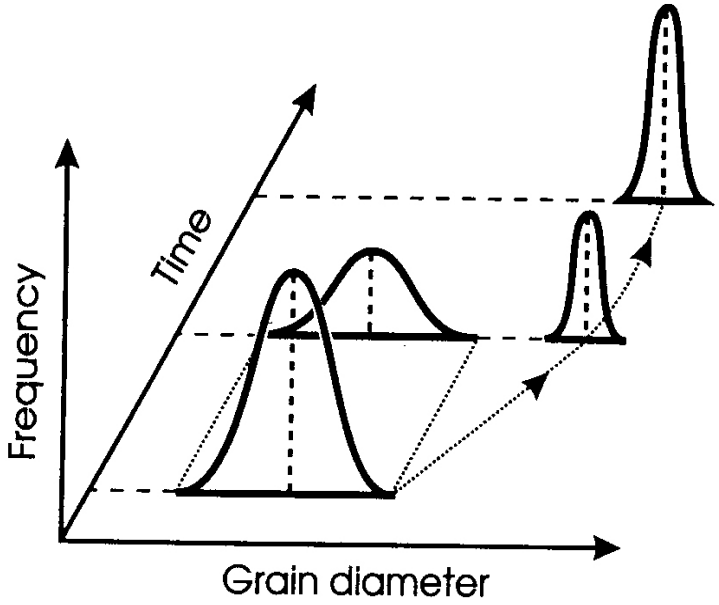

< Bimodal Size distribution >

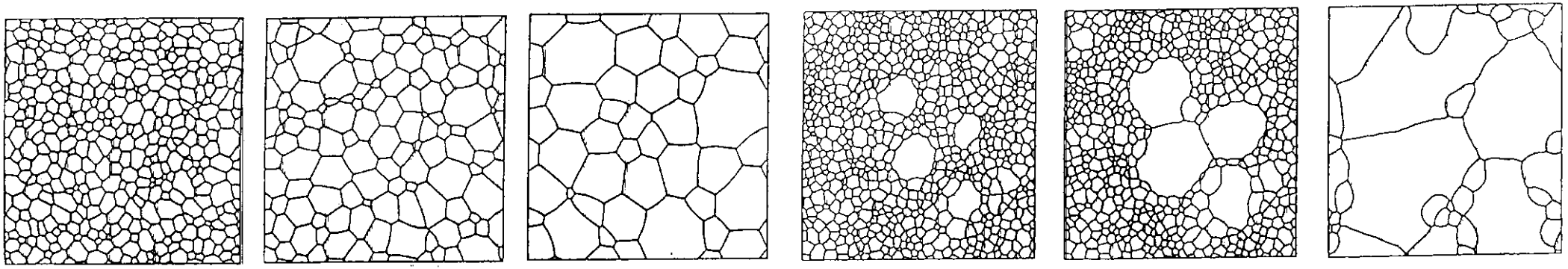

2023 Fall

"Phase Transformation *in* Materials"

10.18.2023

Eun Soo Park

Office: 33-313
Telephone: 880-7221
Email: espark@snu.ac.kr
Office hours: by an appointment

Chapter 3 Crystal Interfaces and Microstructure

1) Interfacial Free Energy

2) Solid/Vapor Interfaces

3) Solid/Liquid Interfaces

4) Boundaries in Single-Phase Solids

(c) Equilibrium in Polycrystalline Materials

① GB intersection: Balance of 1) boundary E & 2) surface tension

GBs in a polycrystal can adjust themselves during annealing to produce "a metastable equilibrium at the GB intersections" and "inverse relationship between relative GB E and relative GB area".

- **Thermally Activated Migration of Grain Boundaries:**

  Metastable equilibrium of grain boundary (Balances of 1) boundary E + 2) surface tension)

  → real curvature (ΔP → ΔG: Gibbs Thomson Eq.) → $F = 2\gamma/r = \Delta G/V_m$ (by curvature)

  (Pulling force per unit area of boundary)

  → Grain coarsening at high T annealing

- **Kinetics of Grain Growth**

  - Grain boundary migration (v) by thermally activated atomic jump

Boundary velocity $$v = \frac{A_2 n_1 v_1 V_m^{\,2}}{N_a RT} \exp\left(-\frac{\Delta G^a}{RT}\right) \frac{\Delta G}{V_m}$$

$v \sim \Delta G/V_m$ driving force → $F = \Delta G/V_m$

M : mobility = velocity under unit driving force ~ exp (-1/T)

rate of grain growth $d\underline{D}/dt \sim 1/\underline{D}$, exponentially increase with T

→ $\underline{D} = k't^n$ (Experimental: n << 1/2, ½ at pure metals or high Temp.)

- Mobility of GB~ affected by both type of boundaries and GB segregation or 2nd phase precipitation

Ex) Effect of second-phase particle - Zener Pinning

$$\bar{D}_{max} = \frac{4r}{3f_v}$$

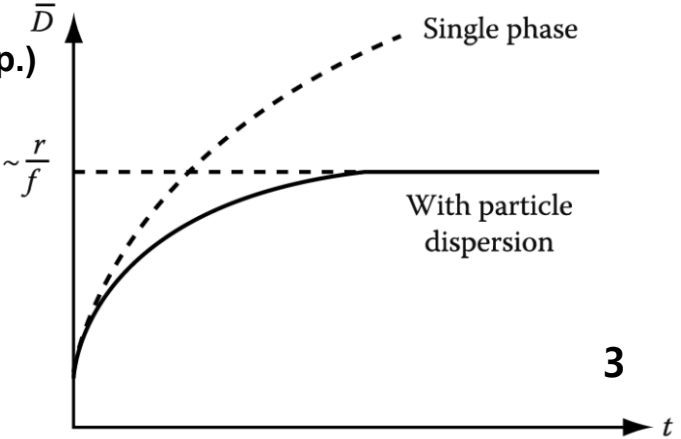

Contents for previous class

- **Grain Growth**

- Normal grain growth ⟺ **Abnormal grain growth**

(high mobility of special GBs
→ development of recrystallization textures)

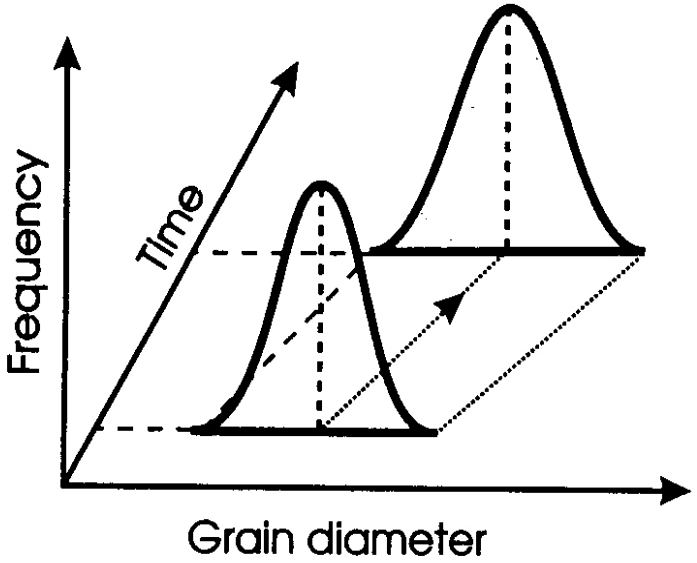

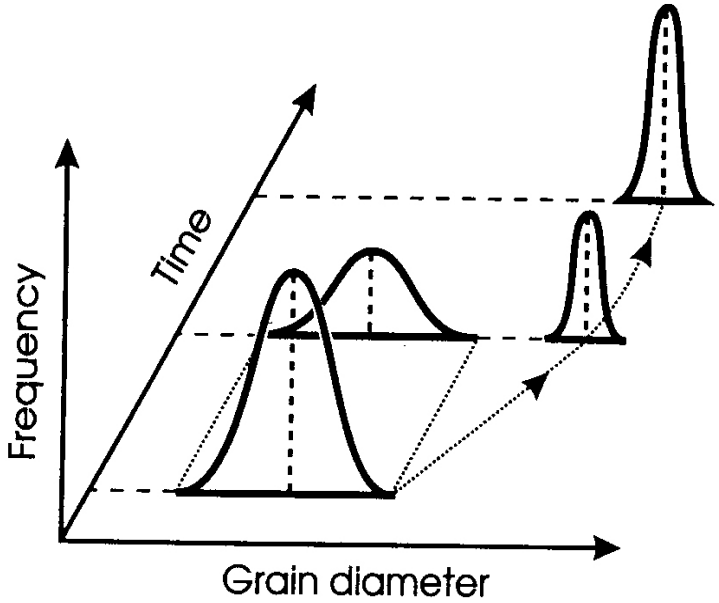

< Bimodal Size distribution >

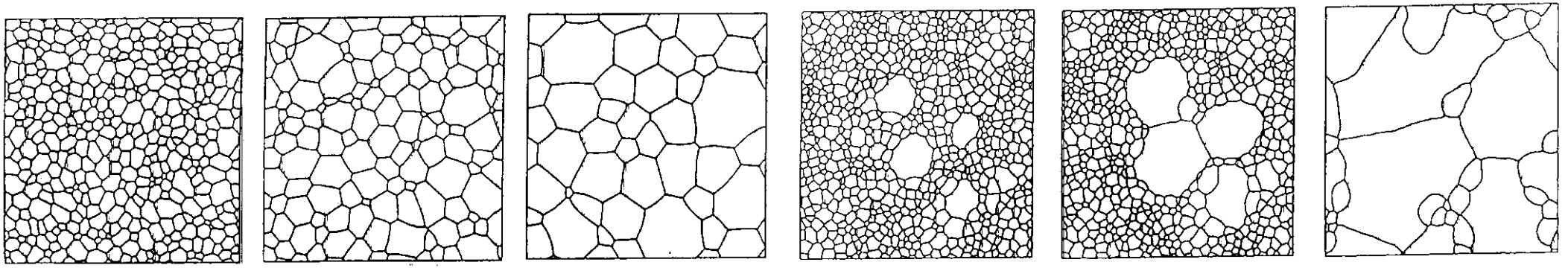

Contents for today's class

Chapter 3 Crystal Interfaces and Microstructure

1) Interfacial Free Energy (vs E_{sv})

2) Solid/Vapor Interfaces

4) Boundaries in Single-Phase Solids

5) Interphase Interfaces in Solid (α/β)

3) Solid/Liquid Interfaces

6) Interface migration

Contents for today's class

- **Interphase Interfaces in Solid (α/β)**

  - Types of interphase interfaces in solid (α/β)

  - Second-Phase Shape

    $$\sum A_i \gamma_i + \Delta G_S = minimum$$

    - Interface Energy Effects
      - Coherent / Semi-coherent / incoherent
    - Misfit Strain Effects

  - Coherency Loss

  - Glissil Interfaces ⟺ Solid/Liquid Interfaces

- Interface migration

  - Interface controlled growth ⟺ Diffusion controlled growth

Q: What kind of interphase interfaces in solid (α/β) exist?

= coherent/ semi-coherent / incoherent/ complex semi-coherent

→ different interfacial free energy, γ

3.5 Interphase Interfaces in Solids

Interphase boundary
- different two phases : different crystal structure or different composition

{ **coherent,**
semicoherent
incoherent

3.5.1 Fully Coherent interfaces

Disregarding chemical species, if the interfacial plane has the same atomic configuration in both phases,

Perfect atomic matching at interface

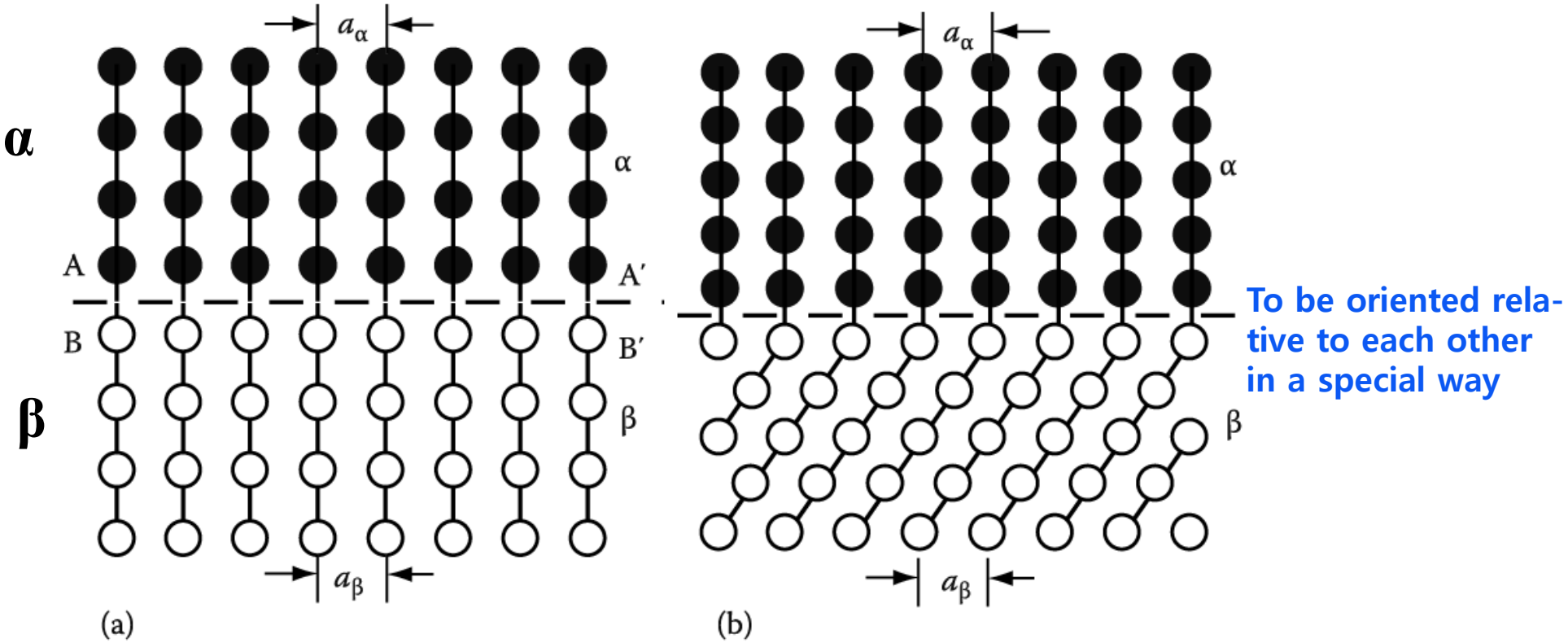

To be oriented relative to each other in a special way

Fig. 3.39 Two-dimensional cross-sections through strain-free coherent interfaces. (a) Each crystal has a different chemical composition but the same crystal structure. (b) The two phases have different lattices. They may or may not have different chemical compositions.

8

3.5.1 Fully Coherent interfaces

Which plane and direction will be coherent between FCC and HCP?

: **Interphase interface will make lowest energy and thereby the lowest nucleation barrier**

ex) hcp silicon-rich κ phase in fcc copper-rich α matrix of Cu-Si alloy

→ the same atomic configuration & interatomic distance

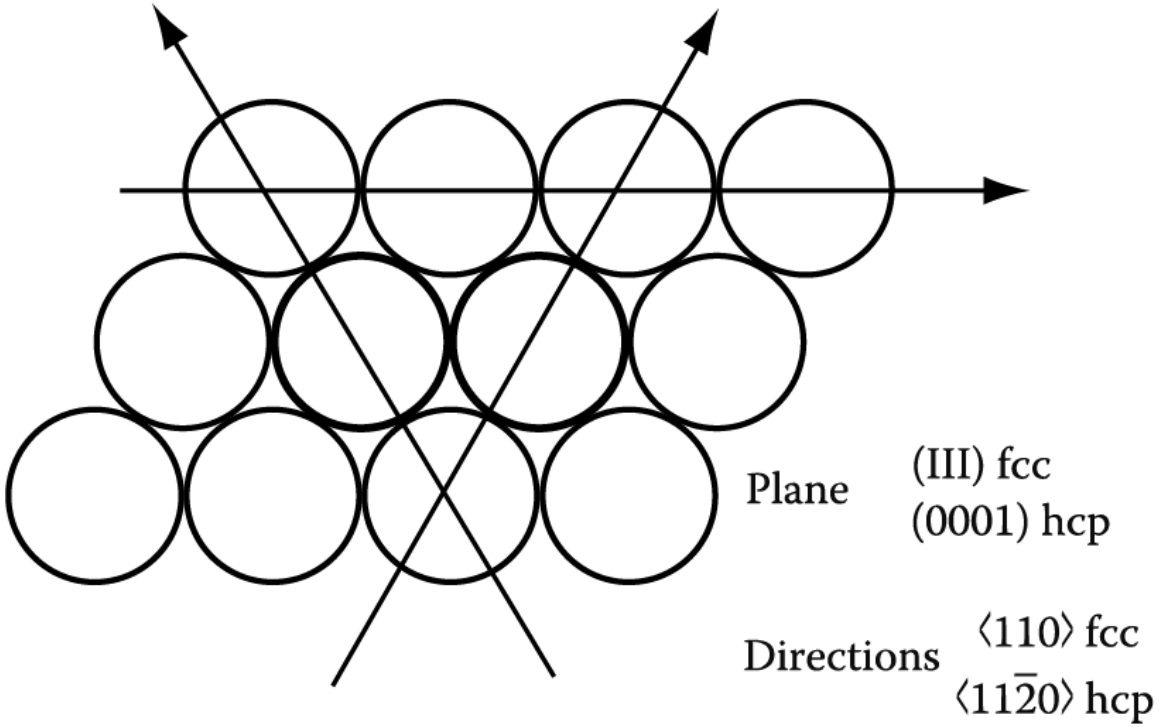

Fig. 3.40 The close-packed plane and directions in fcc and hcp structures.

→ Orientation relation

Cu $(111)_\alpha // (0001)_\kappa$ Si

$[\bar{1}10]_\alpha // [11\bar{2}0]_\kappa$

$\gamma_{\alpha\text{-}\kappa}$ of Cu-Si ~ 1 mJm^{-2}

In general,

γ (coherent) ~ 200 mJm^{-2}

$\gamma_{coherent} = \gamma_{structure} + \gamma_{chemical}$

$= \gamma_{chemical}$

γ (coherent) = γ_{ch} (Eq. 3.43)

hcp/ fcc interface: only one plane that can form a coherent interface

When the atomic spacing in the interface is not identical between the adjacent phase, what would happen?

Possible to maintain coherency by straining one or both crystal lattices.

→ lattice distortion

→ Coherency strain

→ strain energy

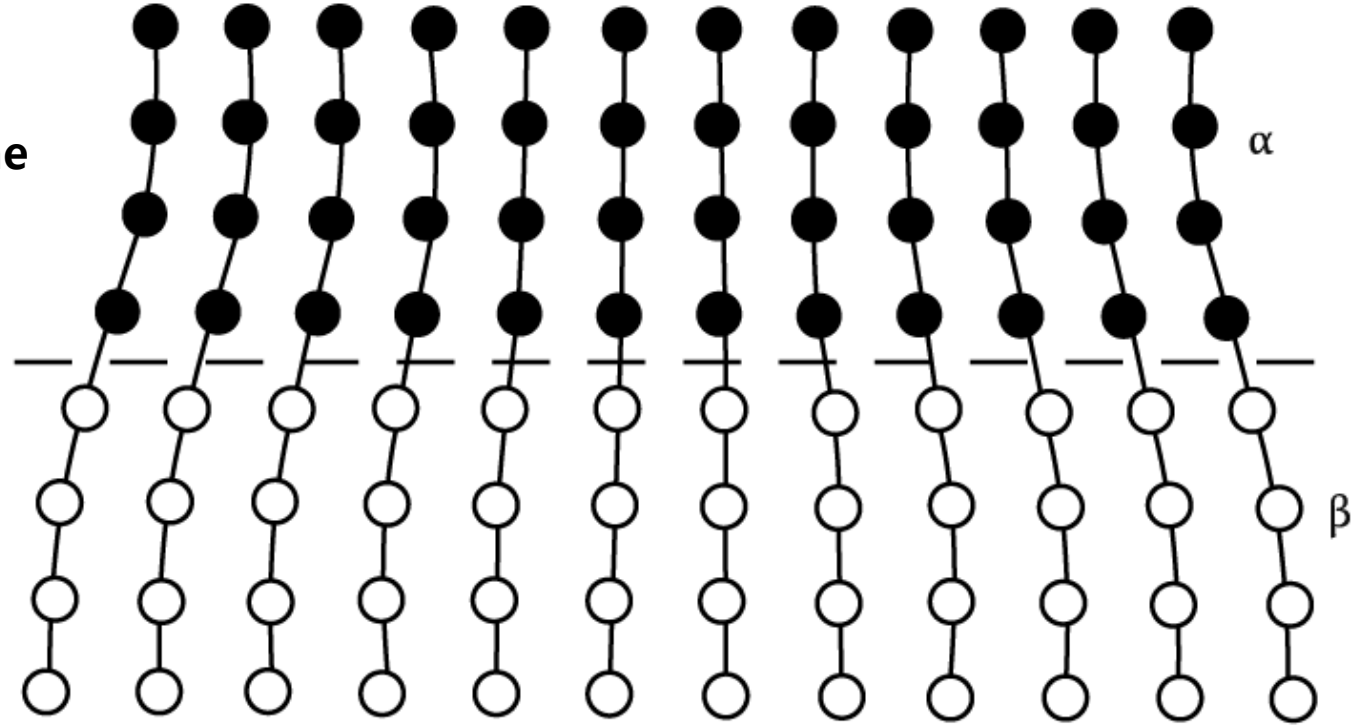

Fig. 3.41 A coherent interface with slight mismatch leads to coherency strains in the adjoining lattices.

The strains associated with a coherent interface raise the total energy of the system.

How can this coherent strain can be reduced?

If coherency strain energy is sufficiently large, → "misfit dislocations"

→ semi-coherent interface

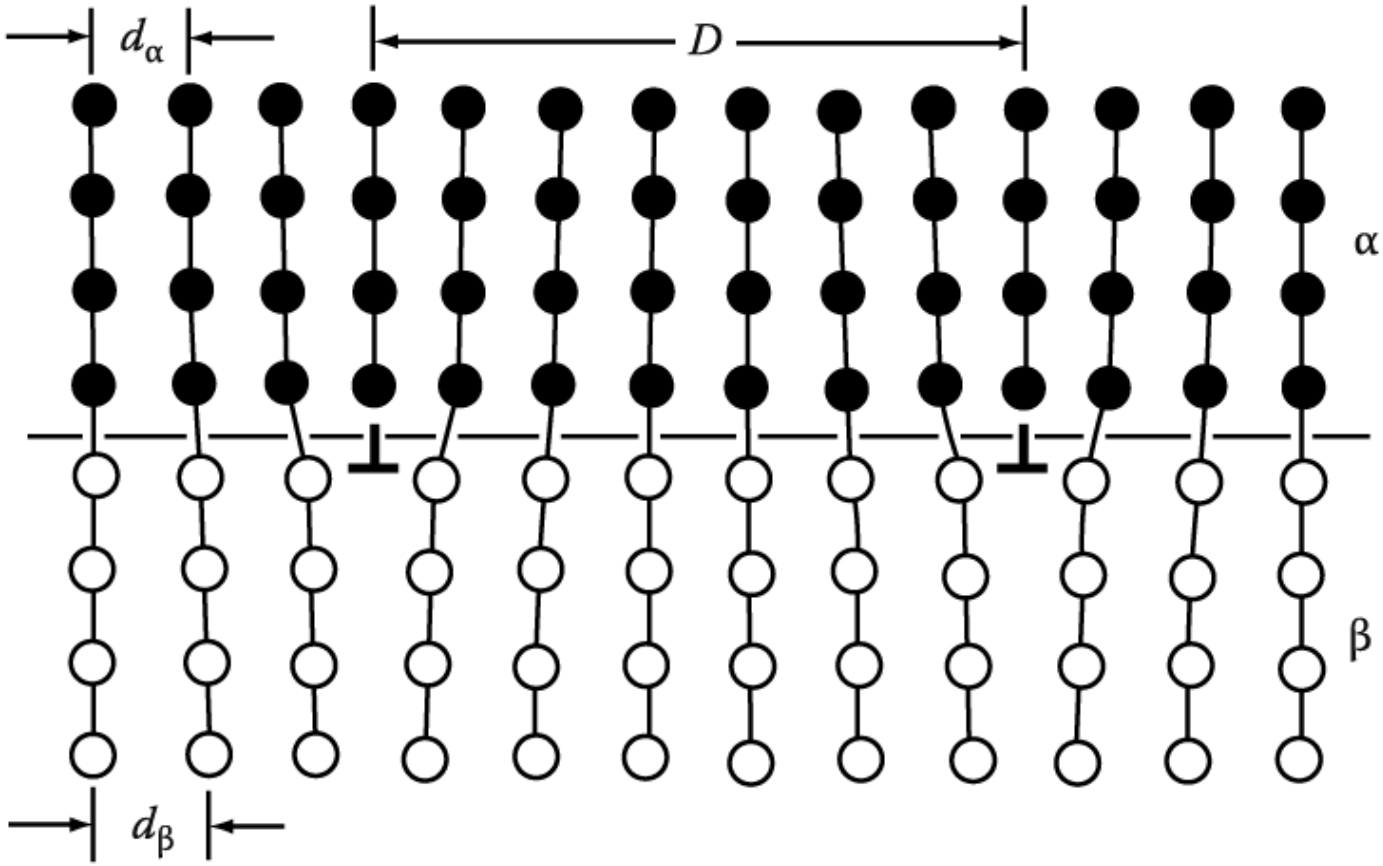

Misfit between the two lattices

$$D = nd_\alpha = (n+1)d_\beta$$

$$\delta = \frac{d_\beta - d_\alpha}{d_\alpha}$$

δ~ small,

$$D = \frac{b}{\delta}$$

δ: misfit (disregistry)

b: Burgers vector of disl.

$[b=(d_\alpha + d_\beta)/2]$

Fig. 3.42 A cross-section parallel to a (100) plane through a partly coherent interface between two simple cubic lattices in a parallel orientation relationship. **The misfit parallel to the interface is accommodated by a series of edge dislocations.** Between the dislocations, there are coherent patches.

3.5.2 Partially Coherent Interfaces

$$\gamma(semicoherent) = \gamma_{ch} + \gamma_{st}$$

γ_{st} → due to **structural distortions** caused by the misfit dislocations

$$\gamma_{st} \propto \delta \text{ for small } \delta$$

In general,
γ (semicoherent) ~ 200~500 mJm^{-2}

$d_\alpha < d_\beta$

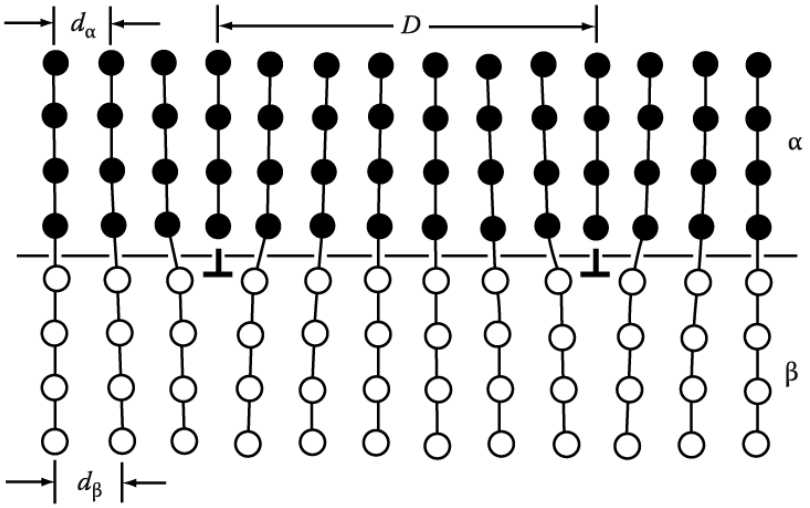

$\delta = (d_\beta - d_\alpha)/ d_\alpha$: misfit

→ D vs. δ vs. n

$(n+1)\, d_\alpha = n\, d_\beta = D$

$\delta = (d_\beta/ d_\alpha) - 1, (d_\beta/ d_\alpha) = 1 + 1/n = 1 + \delta$

→ $\delta = 1/n$

$D = d_\beta / \delta \approx b / \delta$ $[b=(d_\alpha + d_\beta)/2]$ (Eq. 3.49)

δ~ small, Burgers vector of dislocation

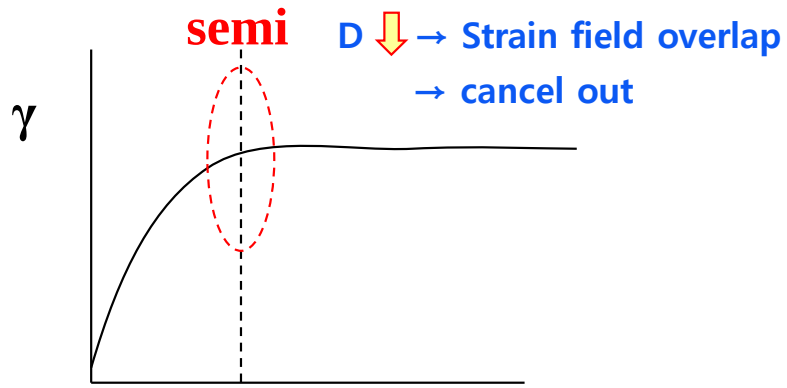

1 dislocation per 4 lattices
n=4

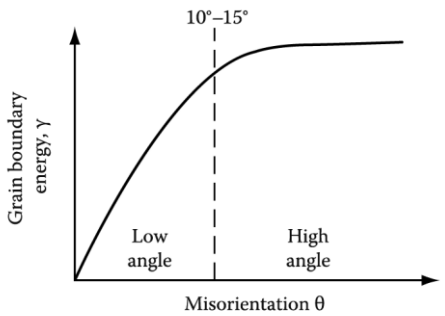

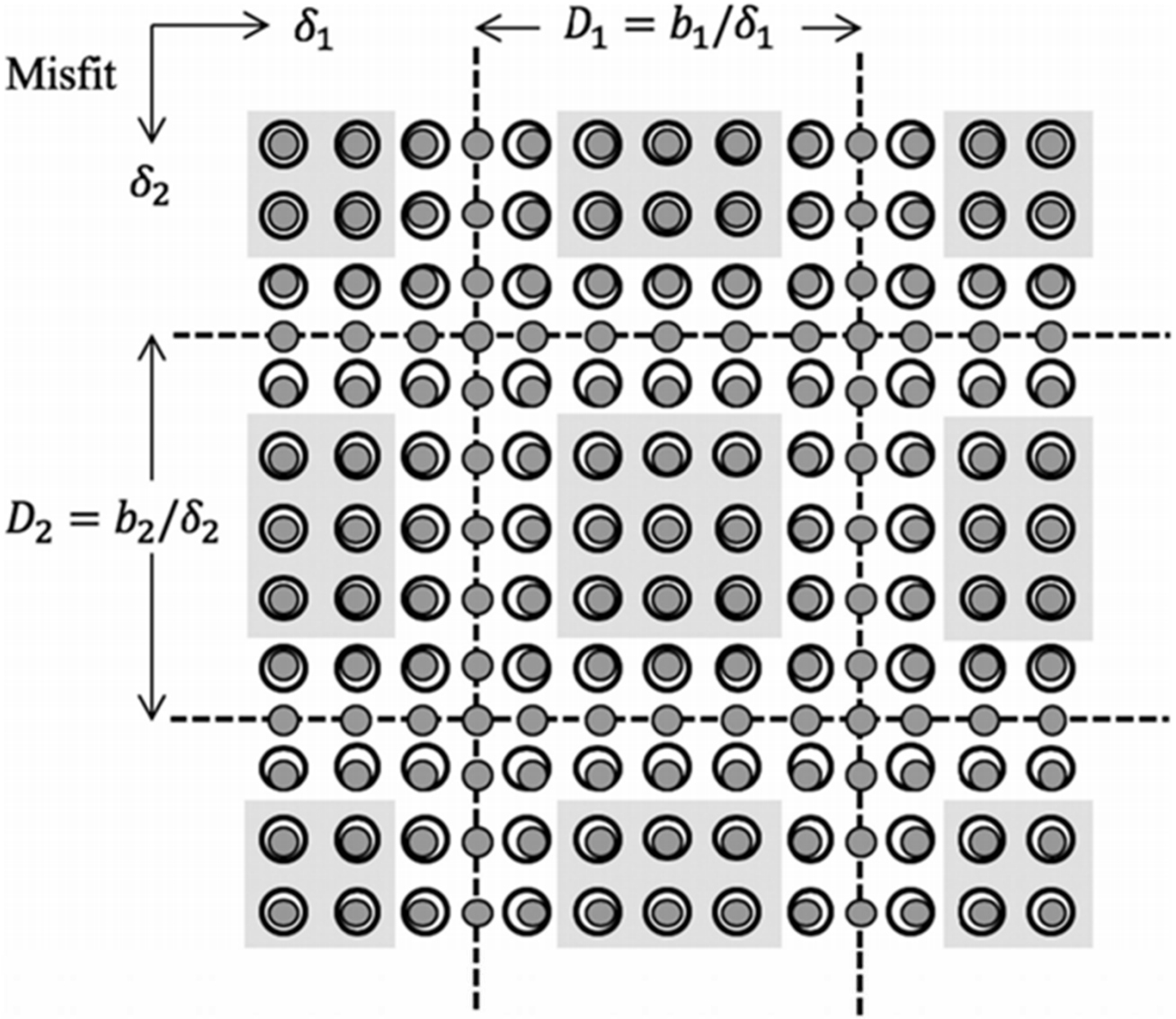

FIGURE 3.43 Schematic diagram of the interface atomic positions in Figure 3.42. Filled circles are the atoms adjacent to the interface plane in the α phase and the open circles in the β phase. In the case of equal misfit in the [100] and [010] directions, the misfit can be accommodated by a square array of edge dislocations (dashed lines) with $D_1 = D_2$. Note how the dislocations separate patches of coherent interface (shaded).

3.5.3

Incoherent Interfaces ~ high angle grain boundary

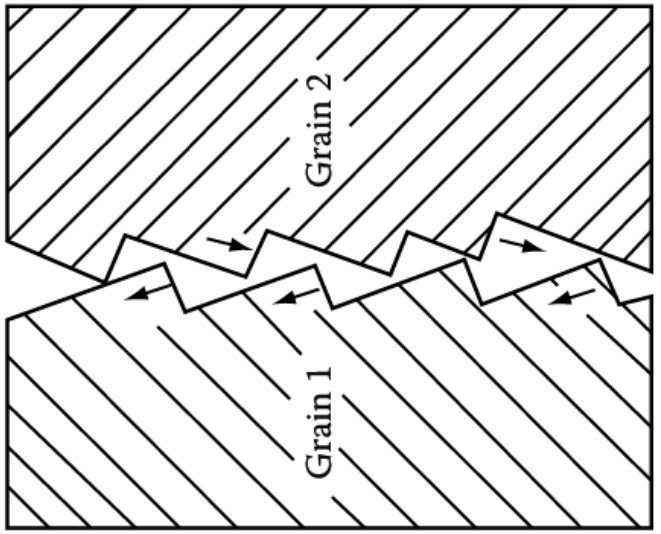

1) δ > 0.25 No possibility of good matching across the interface

2) different crystal structure (in general)

In general,
γ (incoherent) ~ 500~1000 mJm^{-2}

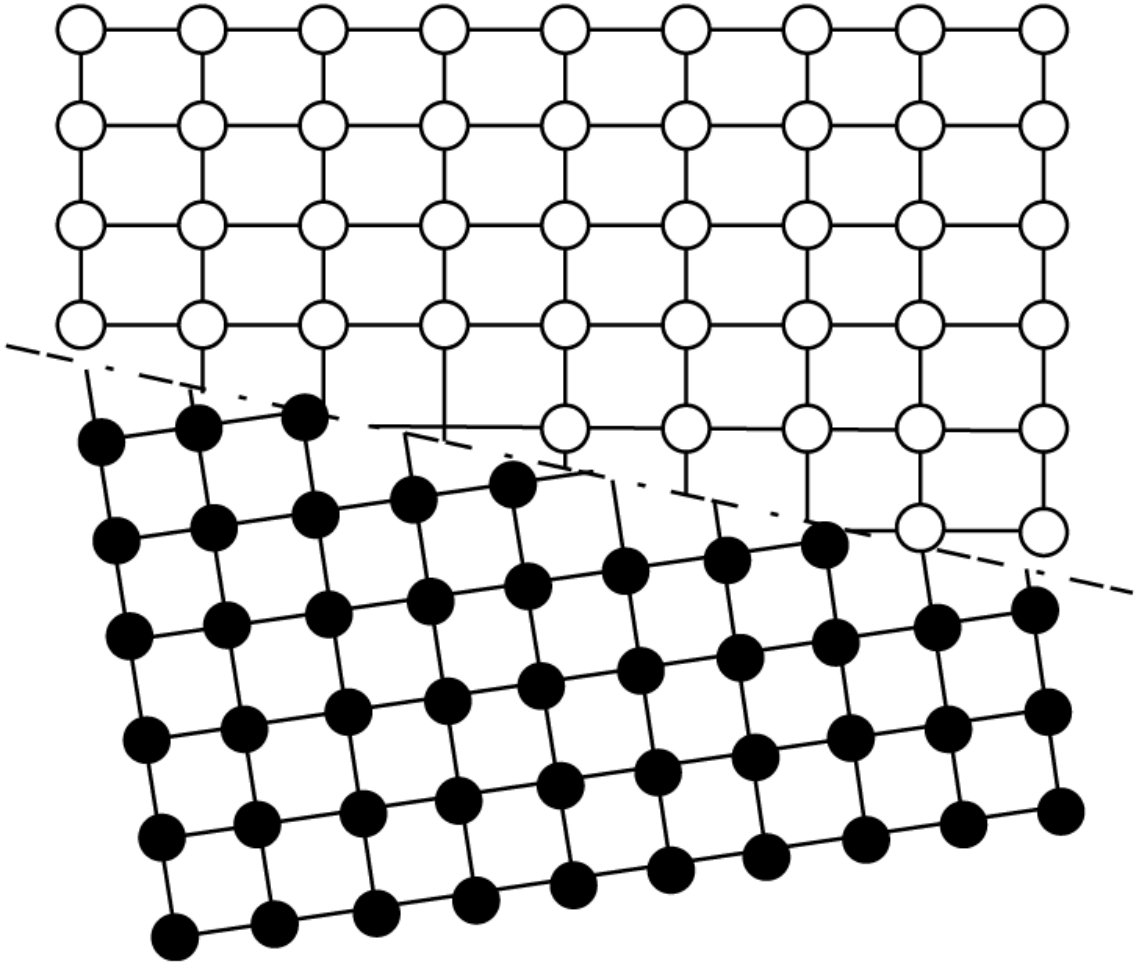

incoherent

Fig. An incoherent interface.

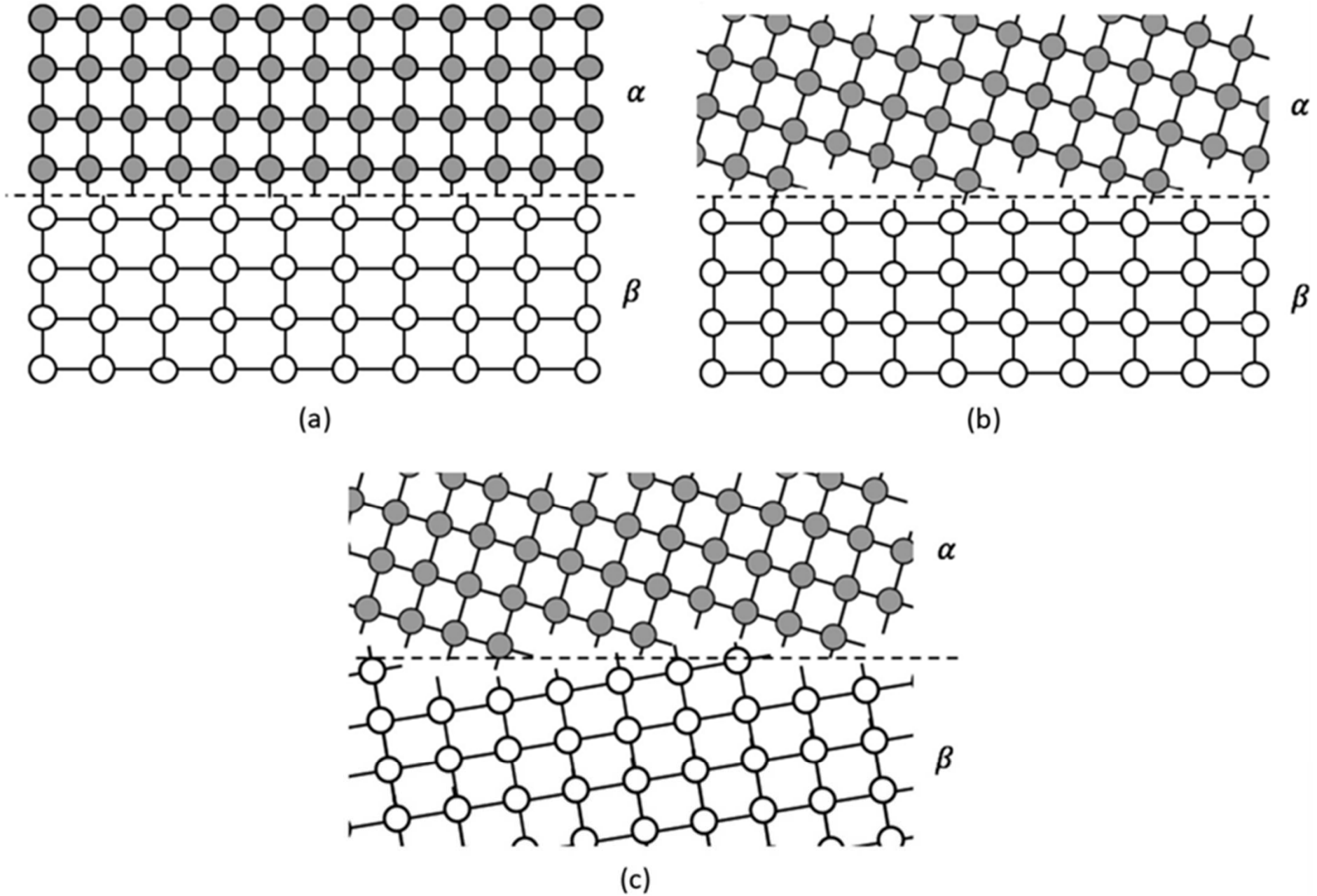

FIGURE 3.44 Incoherent interfaces. (a) Orientation relationship but $\delta > 0.25$. (b) No simple orientation relationship but interface plane is a low-index plane in one phase. (c) No simple orientation relationship and no low-index planes in the interface.

3.5.4 Complex Partial Coherent Interfaces

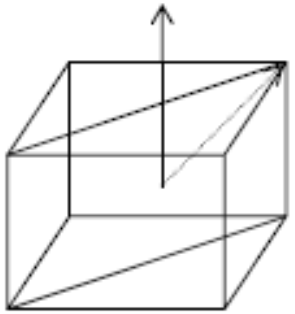

a_α=2.87

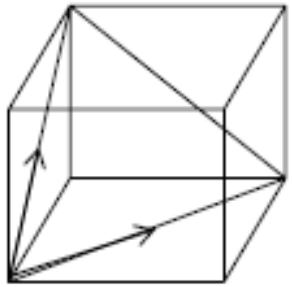

a_γ=3.57

If bcc α is precipitated from fcc γ, which interface is expected?

Which orientation would make the lowest interface energy?

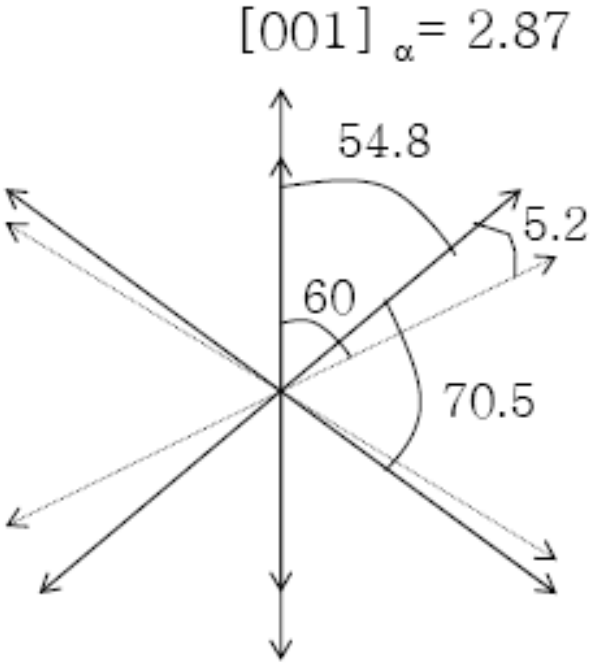

For fcc and bcc crystals ~ closest-pack planes in each phase almost parallel to each other

Nishiyama-Wasserman (N-W) Relationship

$$(110)_{bcc} // (111)_{fcc}, \quad [001]_{bcc} // [\bar{1}01]_{fcc}$$

Kurdjumov-Sachs (K-S) Relationships

$$(110)_{bcc} // (111)_{fcc}, \quad [1\bar{1}1]_{bcc} // [0\bar{1}1]_{fcc}$$

(The only difference between these two is a rotation in the closest-packed planes of 5.26°.)

Pitsch relationship

in which slightly less close-packed planes and directions are parallel:

$$(111)_{bcc} \| (110)_{fcc}, [\bar{1}10]_{bcc} \| [001]_{fcc}$$

Complex Partial Coherent Interfaces

Semicoherent interface observed at boundaries formed by low-index planes.

(atom pattern and spacing are almost equal.)

N-W relationship

Good fit is restricted to small diamond-shaped areas that only contain ~8% of the orientation relationship.

A similar situation can be shown to exist for the K-S orientation relationship.

⇨ **But, impossible to form a large interfaces**

→ Incoherent interface

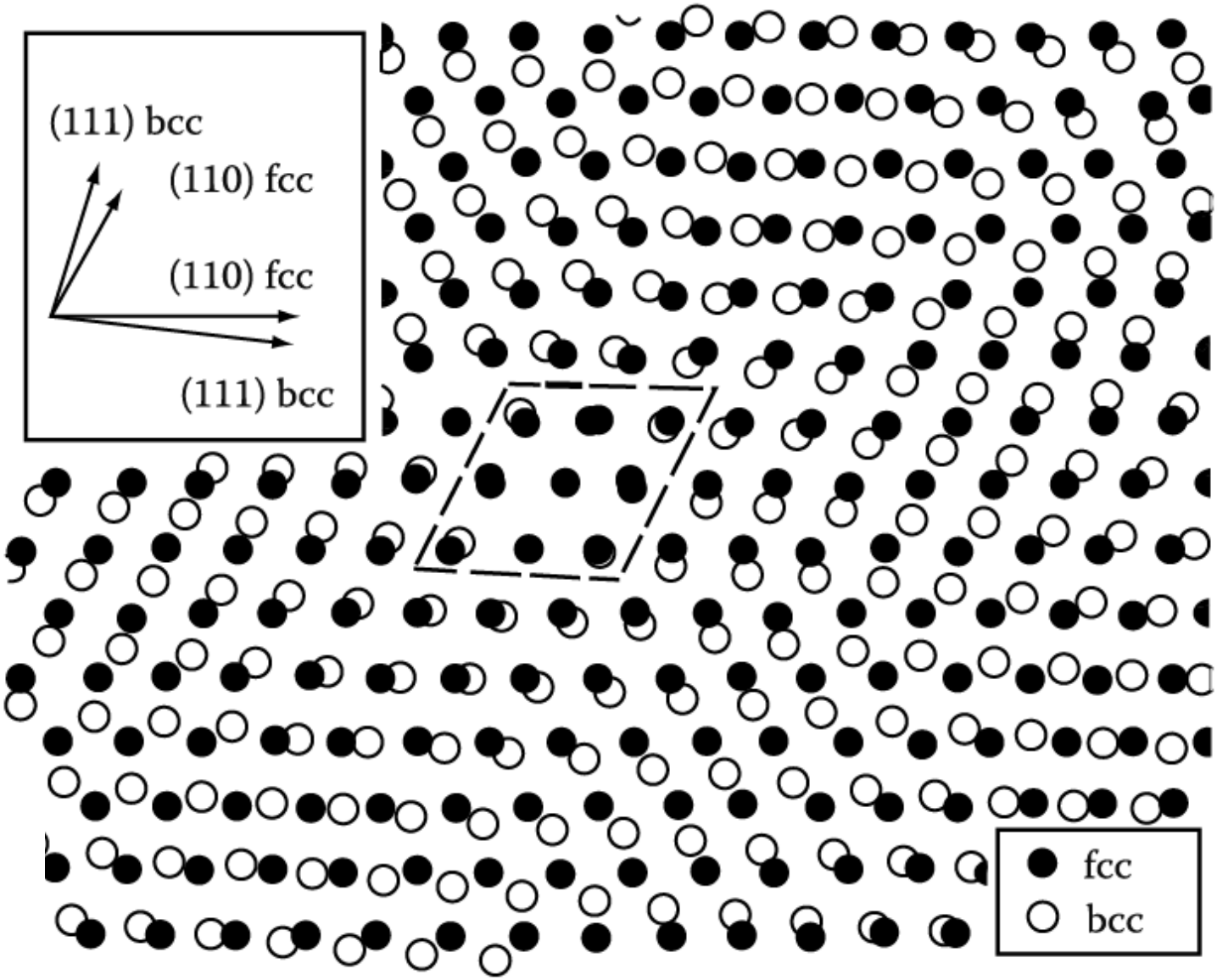

Fig. Atomic matching across a (111)fcc/(110)bcc interface bearing the NW orientation relationship for lattice parameters closely corresponding to the case of fcc and bcc iron.

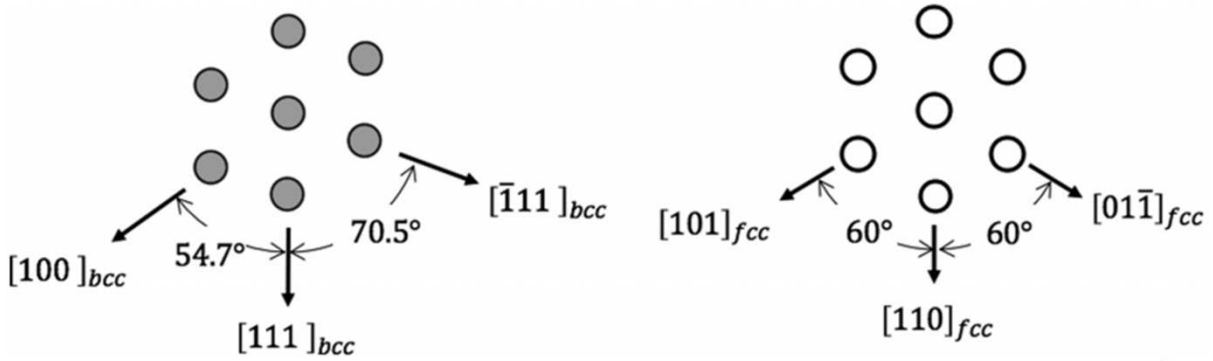

FIGURE 3.45 The pattern of lattice points centered on closest neighbor atoms in a $(01\bar{1})$ bcc plane (left) and a $(\bar{1}11)$ fcc plane (right).

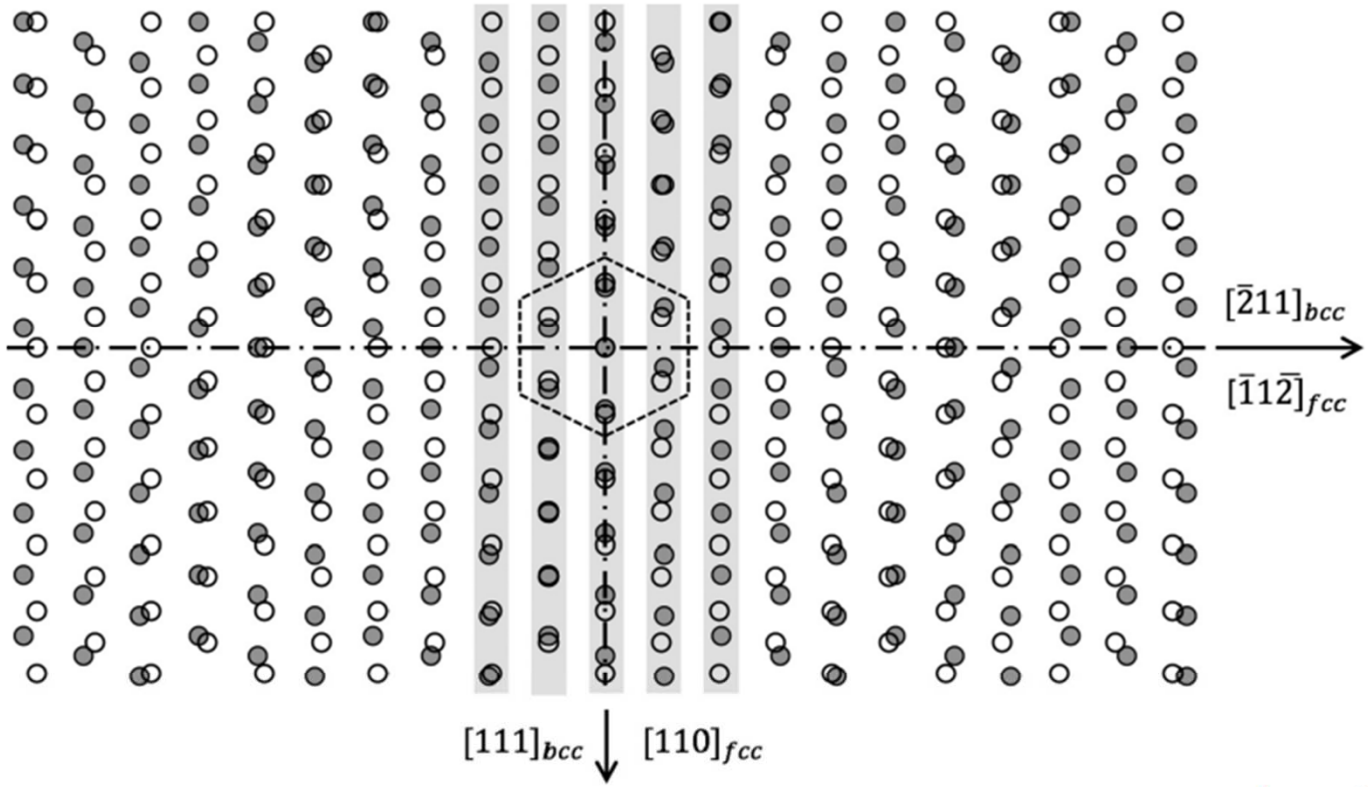

FIGURE 3.46 The pattern of lattice points (atom centers) on the close-packed $(01\bar{1})$ bcc and $(\bar{1}11)$ fcc planes in the K-S orientation relationship when the lattice parameter ratio $a_{\text{fcc}} / a_{\text{bcc}} = 1.30$ corresponding to a hard-sphere atom diameter ratio $d_{\text{fcc}} / d_{\text{bcc}} = 1.06$. Filled circles bcc, open circles fcc.

Complex Partial Coherent Interfaces

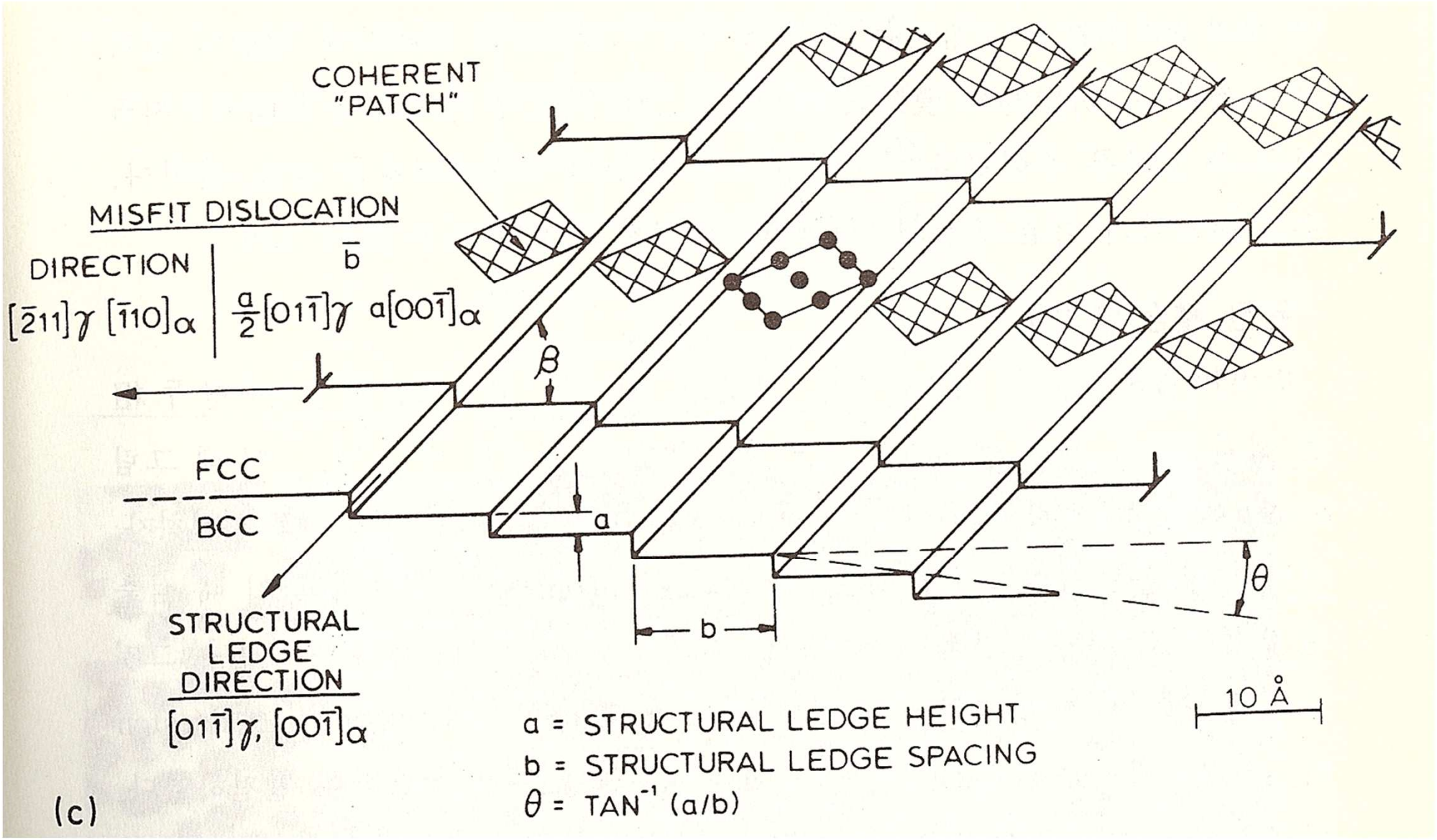

The degree of coherency can, however, be greatly increased if a macroscopically irrational interface is formed. The detailed structure of such interfaces is, however, uncertain due to their complex nature.

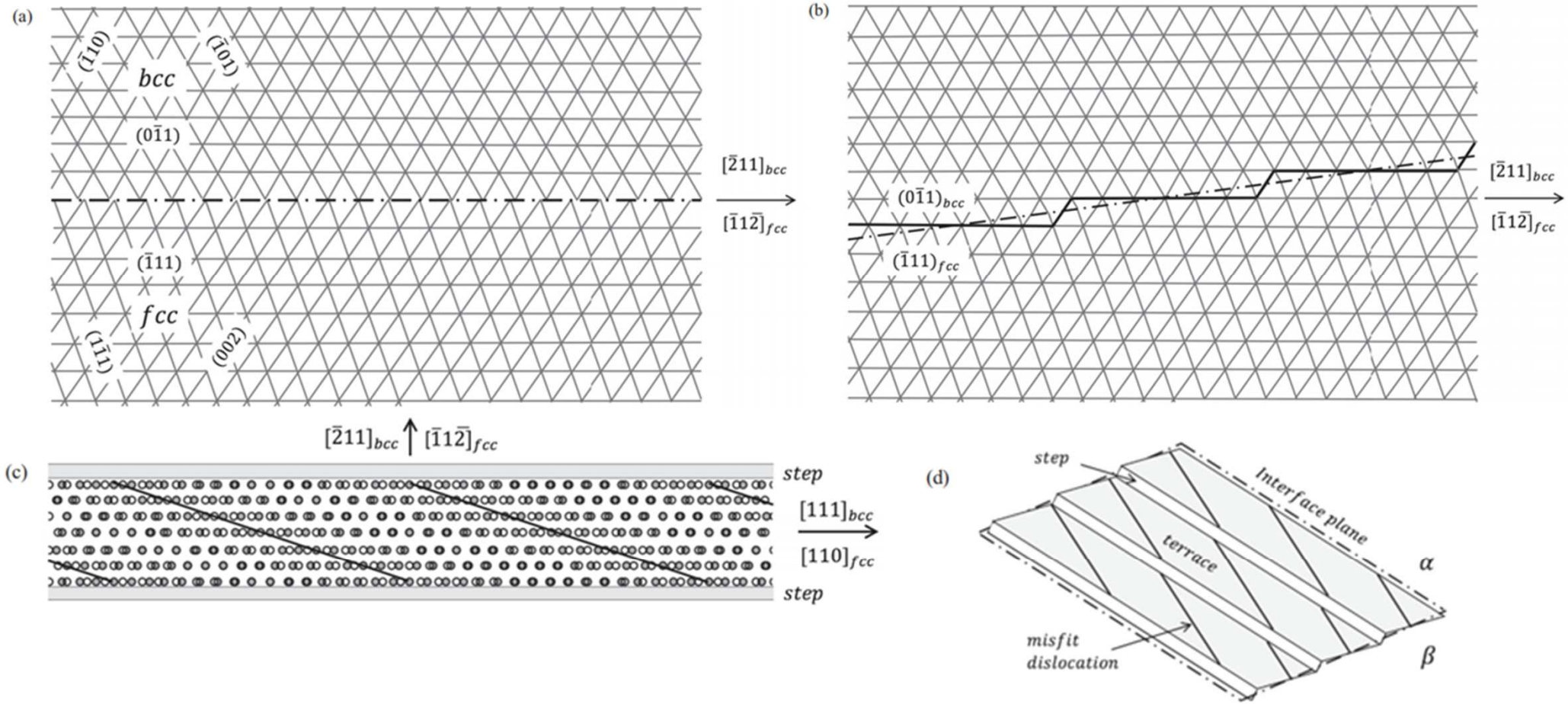

FIGURE 3.47 Vertical section through the lattices in Figure 3.46 showing the traces of some of the lattice planes in the $[111]_{bcc}$ and $[110]_{fcc}$ zones. Note that only some of the intersections contain lattice points. In (a) the dash-dotted line representing the interface plane follows the close-packed planes $(0\bar{1}1)_{bcc}$ / $(\bar{1}11)_{fcc}$. In (b) the dash-dotted line is the mathematical interface plane across which the bcc and fcc planes in the $[111]_{bcc}$ and $[110]_{fcc}$ zones are continuous. It has the high indices $(1\bar{7}6)_{bcc}$ / $(\bar{3}34)_{fcc}$. The atomic structure of the interface follows the close-packed planes that project into the boundary. For simplicity, the positions of the atoms are not shown. (c) A low-magnification plan view of the lattice points in one terrace plane rotated 90° with respect to the other figures to save space. The distances between the close-packed rows have been made equal to emphasize the pattern of good and bad matching between the lattices on the terrace. The heavy diagonal lines mark the positions of misfit dislocations that can accommodate the misfit along the close-packed rows. (d) Schematic perspective view of the terraces and steps.

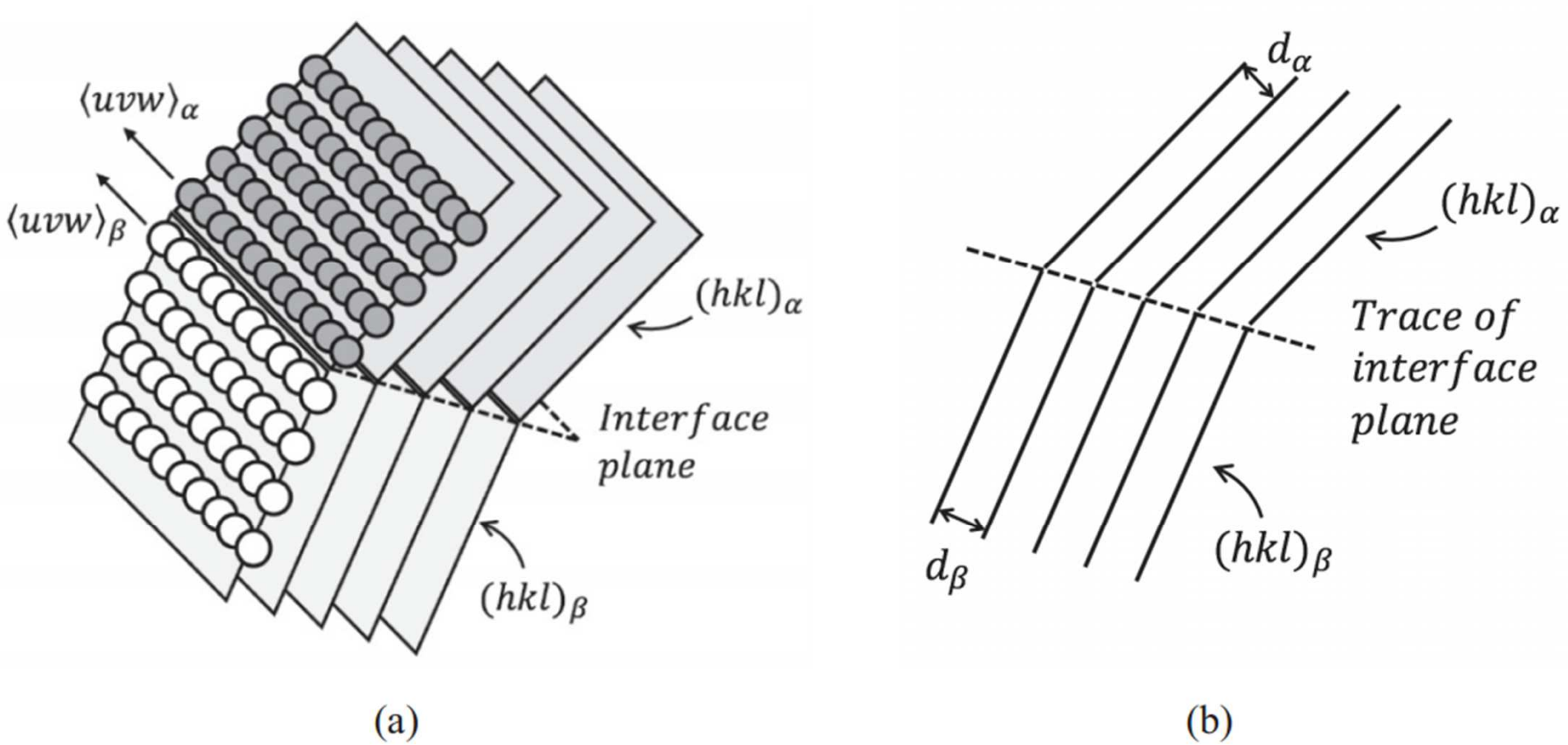

FIGURE 3.48 Minimizing the energy of partly coherent interfaces between different Bravais lattices. (a) The mathematical interface plane is a plane that allows relatively close-packed (low-index) planes (hkl) in the two lattices to meet edge to edge such that the edges contain relatively close-packed directions $\langle uvw \rangle$. (b) Cross-section through (a) normal to the close-packed directions to show that the edge-to-edge planes can be inclined to each other and have different spacings, provided the mathematical interface plane is suitably chosen.

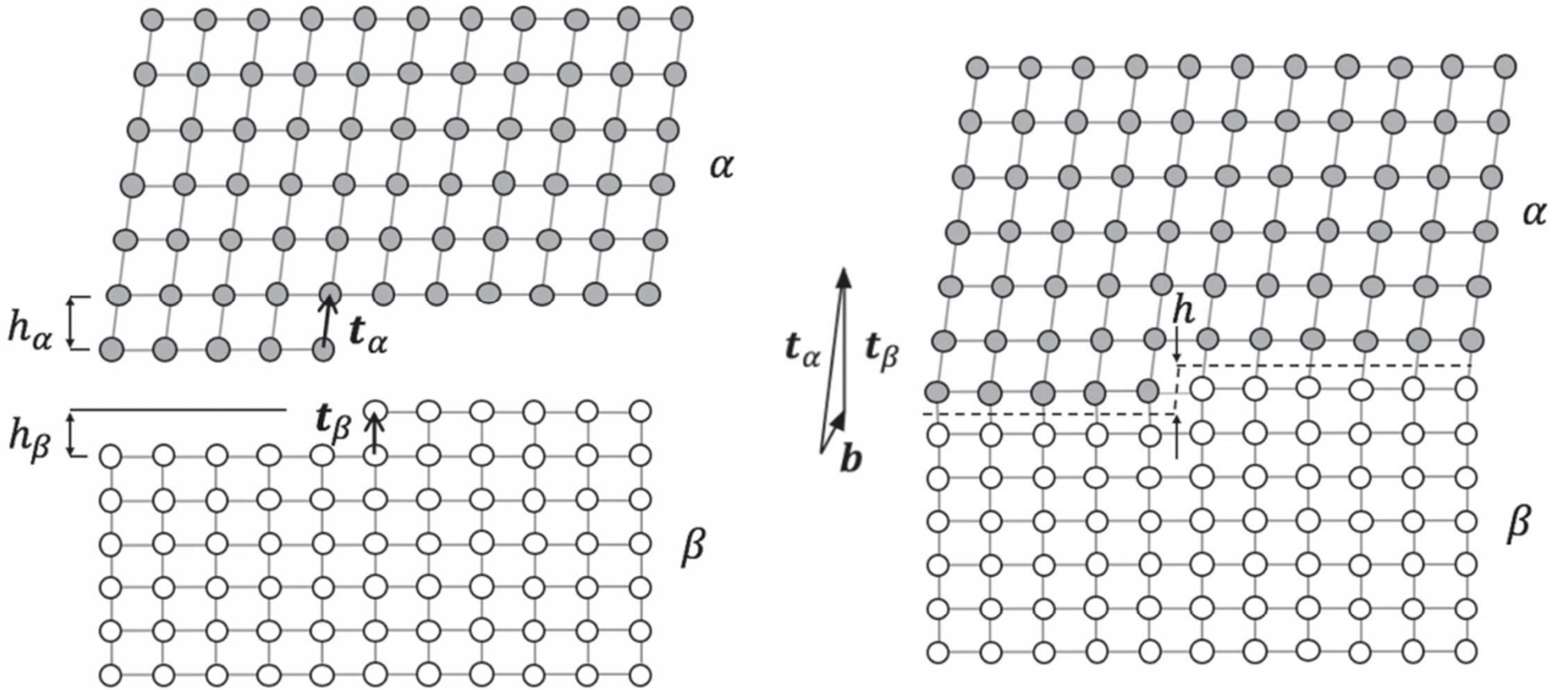

(a) (b)

FIGURE 3.49 Dislocation content of an interfacial step, also known as a disconnection. (a) Stepped surfaces in two separate lattices. (b) Lattices joined across an interface. The Burgers vector of the disconnection $\boldsymbol{b} = \boldsymbol{t}_\alpha - \boldsymbol{t}_\beta$ is drawn magnified for clarity.

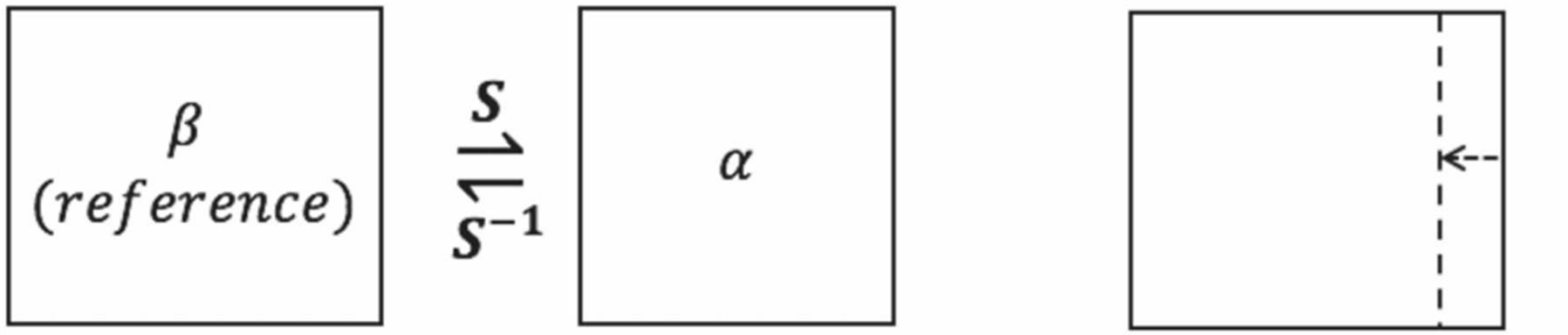

(a)

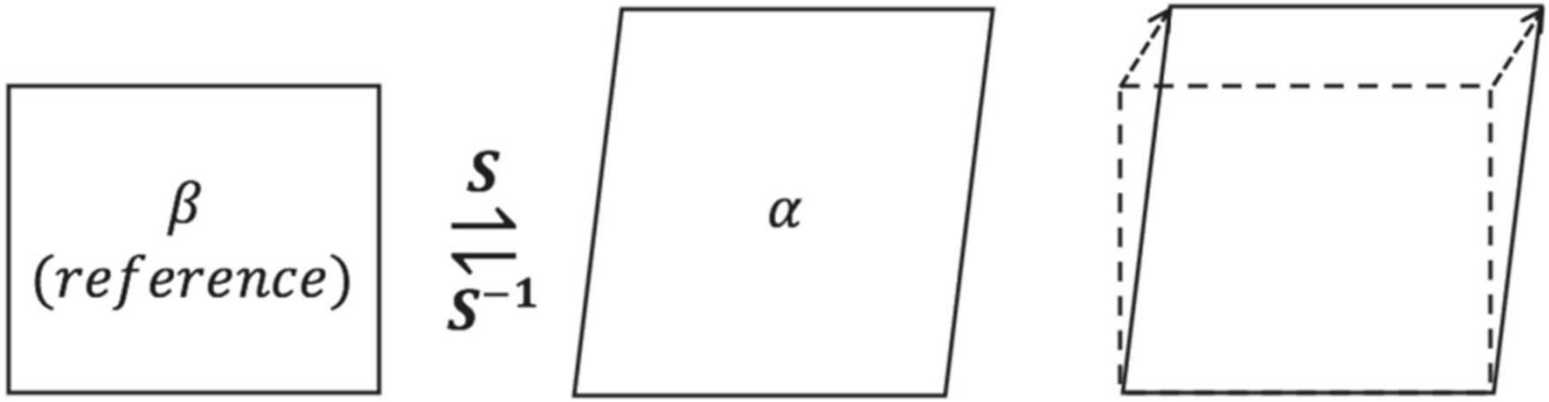

(b)

FIGURE 3.50 Strains that convert the two-dimensional α and β lattices in Figures 3.42 and 3.49 into each other. (a) The strain $\boldsymbol{S}$ is a simple contraction parallel to the interface (–1/6). (b) The strain is an expansion of 0.26 perpendicular to the base close-packed plane followed by a shear of 0.12 parallel to the base. In each case, $\boldsymbol{S}^{-1}$ is just the opposite strain.

3.4 Interphase Interfaces in Solids

Interphase boundary - different two phases : different crystal structure
different composition

coherent, **Perfect atomic matching at interface**

γ (coherent) = γ_{ch} γ (coherent) ~ 200 mJM^{-2}

partially coherent $\gamma(semicoherent) = \gamma_{ch} + \gamma_{st}$

γ_{st} → due to structural distortions
caused by the misfit dislocations

γ(semicoherent) ~ 200~500 mJM^{-2}

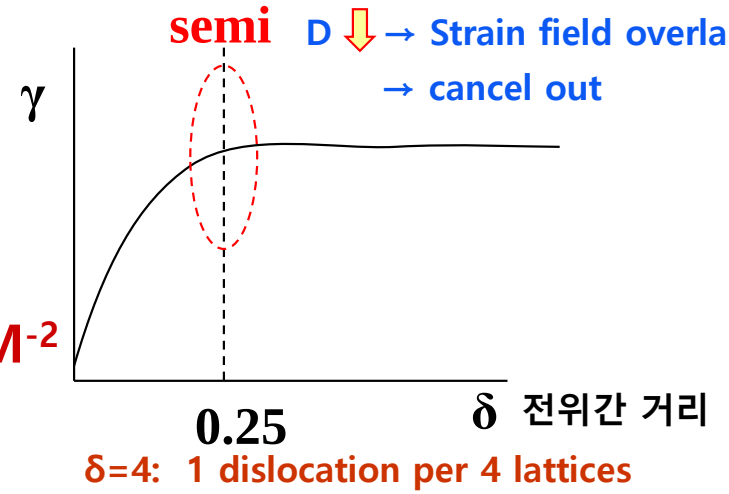

incoherent

1) δ > 0.25 No possibility of good matching across the interface

2) different crystal structure (in general)

γ (incoherent) ~ 500~1000 mJM^{-2}

Complex Partial Coherent Interfaces

Nishiyama-Wasserman (N-W) Relationship **Kurdjumov-Sachs (K-S) Relationships**

(The only difference between these two is a rotation in the closest-packed planes of 5.26°.)

The degree of coherency can, however, be greatly increased if a macroscopically irrational interface is formed.

3.5.7

Q: How is the second-phase shape determined?

If misfit is small,
Equilibrium shape of a coherent precipitate or zone **can only be predicted from the "γ-plot"**

$$\sum A_i \gamma_i$$

⇒ Misfit

$$\sum A_i \gamma_i + \Delta G_S = minimum$$

"γ-plot" + "Elastic strain energy"

Lowest total interfacial free energy
by optimizing the shape of the precipitate and its orientation relationship

Fully coherent precipitates

γ_{ch} ⇒ γ_{ch} + *Lattice misfit* ⇒ γ_{ch} + $Volume\ Misfit\ \ \Delta = \frac{\Delta V}{V}$

different composition — Coherency strain energy — Chemical and structural interfacial E

Incoherent inclusions

(a) Precipitate shapes : $\sum A_i \gamma_i$ ⇩

(b) Calculation of misfit strain energy

3.4.2 Second-Phase Shape: Interfacial Energy Effects

How is the second-phase shape determined? $\sum A_i \gamma_i = minimum$

Lowest total interfacial free energy
by optimizing the shape of the precipitate and its orientation relationship

A. Fully Coherent Precipitates (G.P. Zone)

- If α, β have the same structure & a similar lattice parameter
- Happens during early stage of many precipitation hardening
- Good match ⇨ can have any shape ⇨ spherical

A zone with no misfit

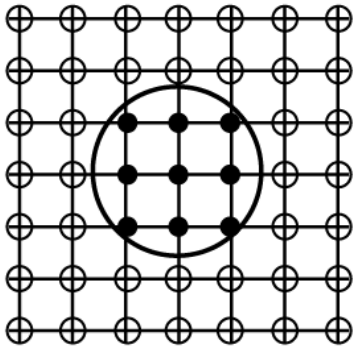

Fig. 3.61 (a) GP(Guinier- Preston) Zone in Al – Ag Alloys

$$\varepsilon_a = \frac{r_A - r_B}{r_A} = 0.7\%$$

→ negligible contribution to the total free energy

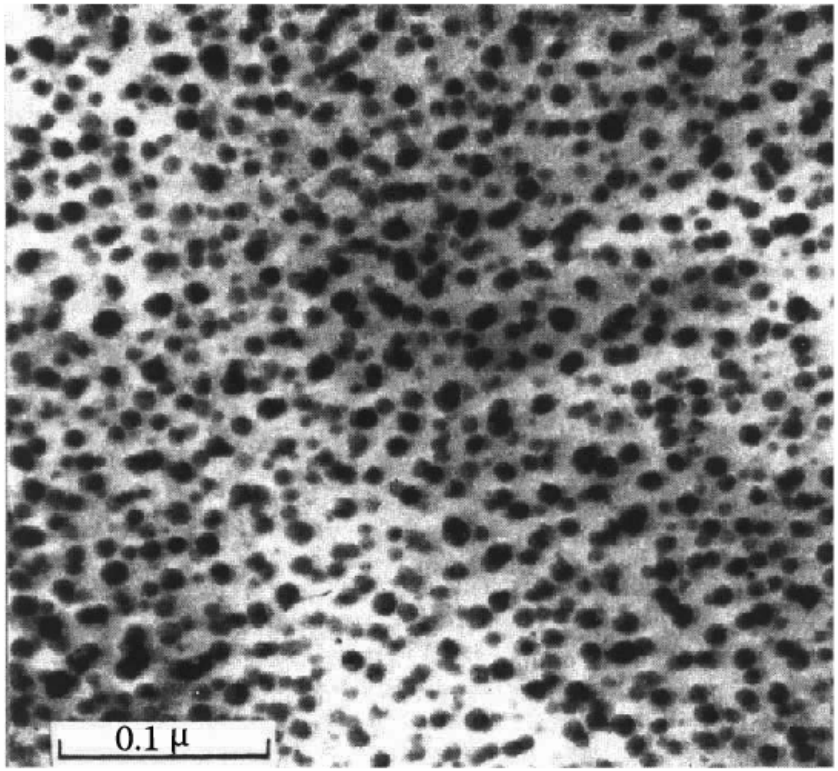

(b) Ag-rich GP zones (Dia. ~10 nm) in Al-4at% Ag alloy

B. Partially Coherent Precipitates

- α, β have different structure and one plane which provide close match

- Coherent or Semi-coherent in one Plane;
  Disc Shape (also plate, lath, needle-like shapes are possible)

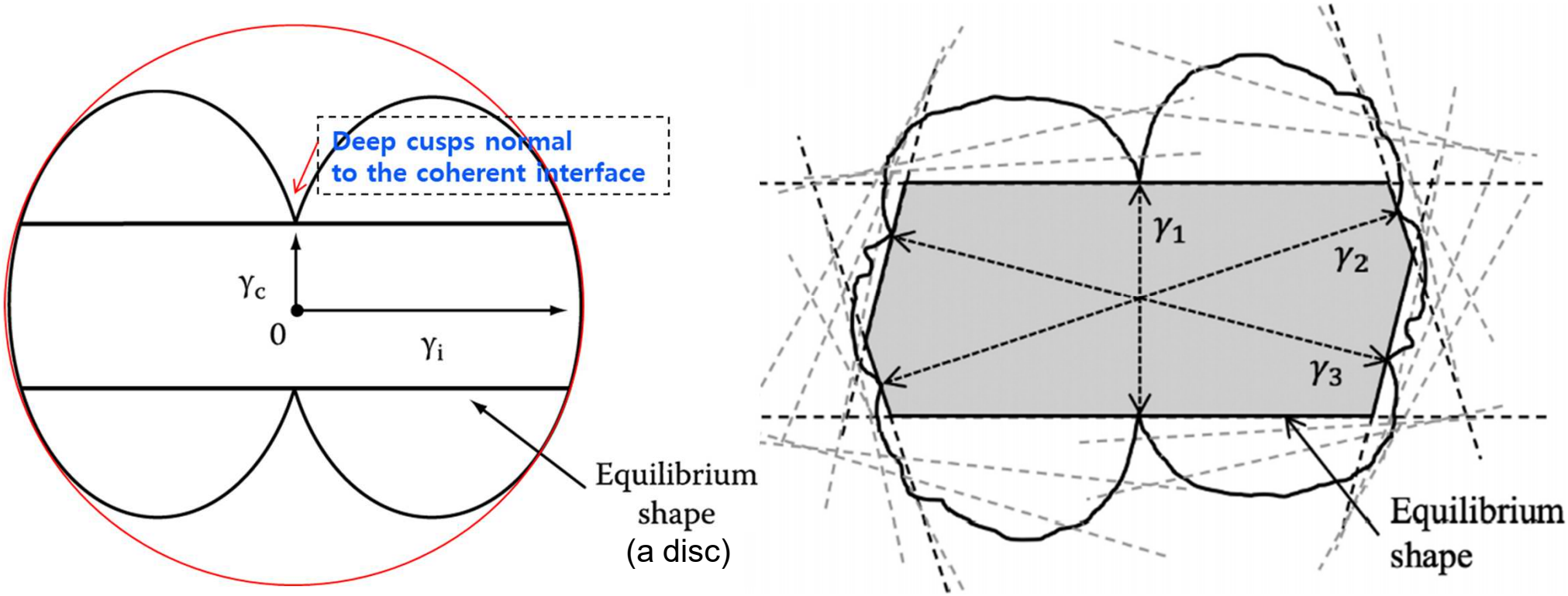

Fig. 3.62 A schematic section through a γ-plot for a precipitate and matrix having different crystal lattices. Some lines of the Wulff construction are shown. Those forming the predicted interface facets are drawn with bold dashed lines. The horizontal habit plane corresponds to the interface plane with the lowest energy.

Precipitate shapes observed in practice
~ not equilibrium shape through a γ-plot
why? 1) misfit strain E effects ~ ignored.
2) different growth rates depending on directions

hcp γ′ Precipitates in Al – 4%Ag Alloys → plate

Semicoherent broad face parallel to the $\{111\}_\alpha$ matrix planes

(usual hcp/fcc orientation relationship)

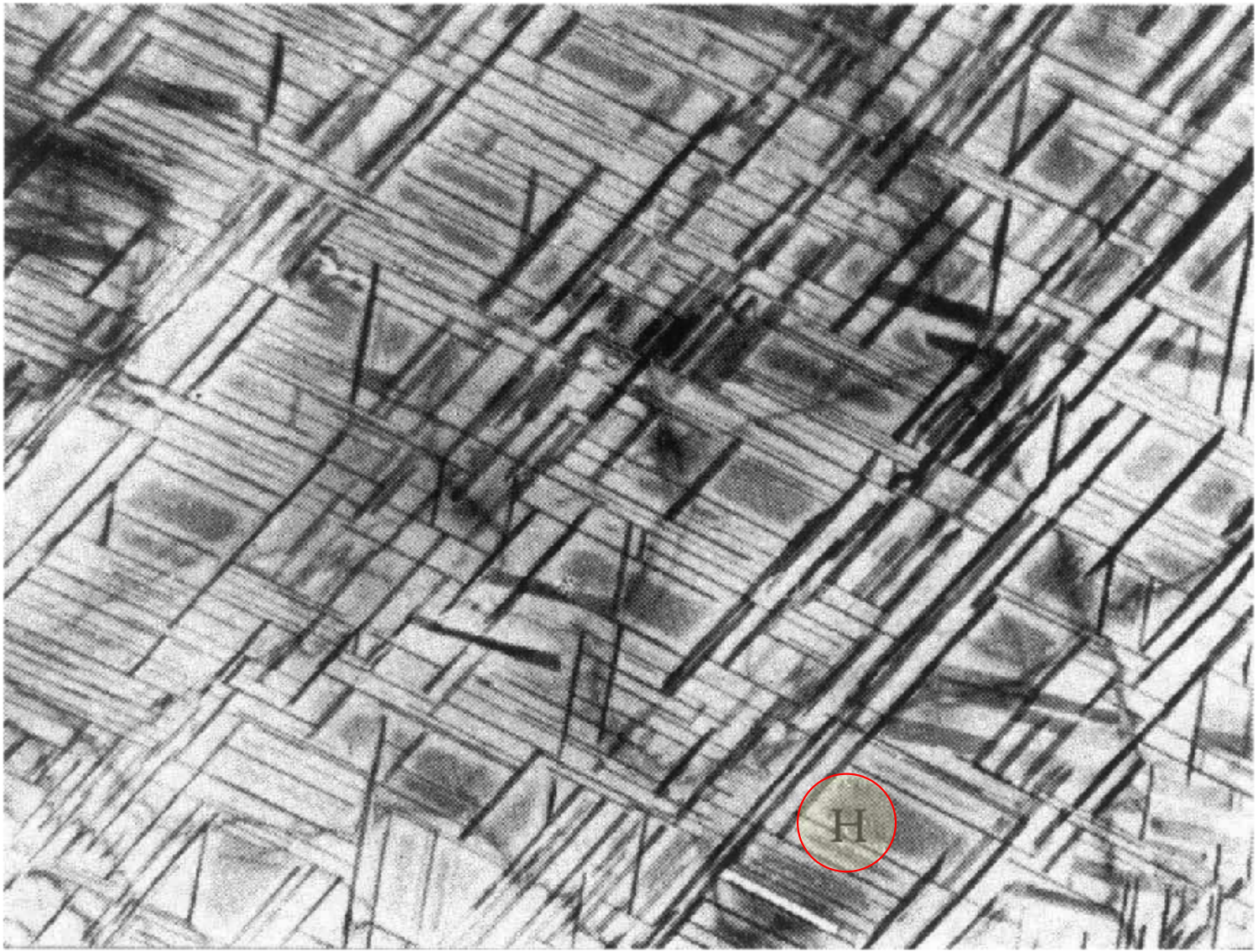

Fig. 3. 42 Electron micrograph showing the Widmanstatten morphology of γ' precipitates in an Al-4 atomic % Ag alloy. GP zones can be seen between the γ' e.g. at H (x 7000).

C. Incoherent precipitates

- when α, β have completely different structure ⇨ Incoherent interfaces
  or When the two lattices are in a random orientation
- Interface energy is high for all plane ⇨ spherical shape
  with smoothly curved interface
- Polyhedral shapes: certain crystallographic planes of the inclusion lie at cusps in the γ-plot

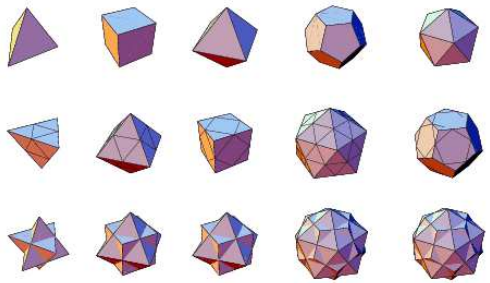

θ phase in $Al-Cu$ alloys (Al_2Cu)

Q: Example of Second-Phase Shape

precipitates from solid solution in Al-Cu alloys

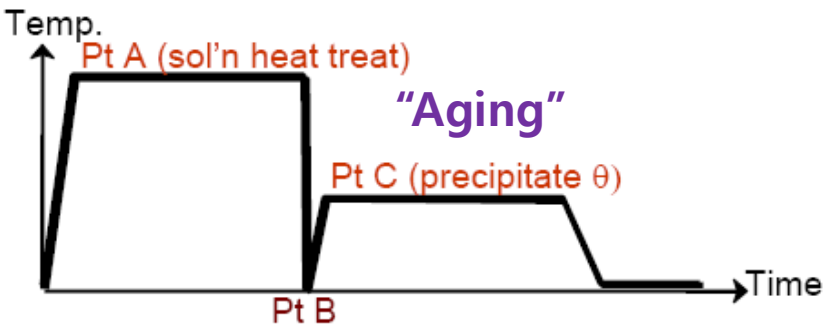

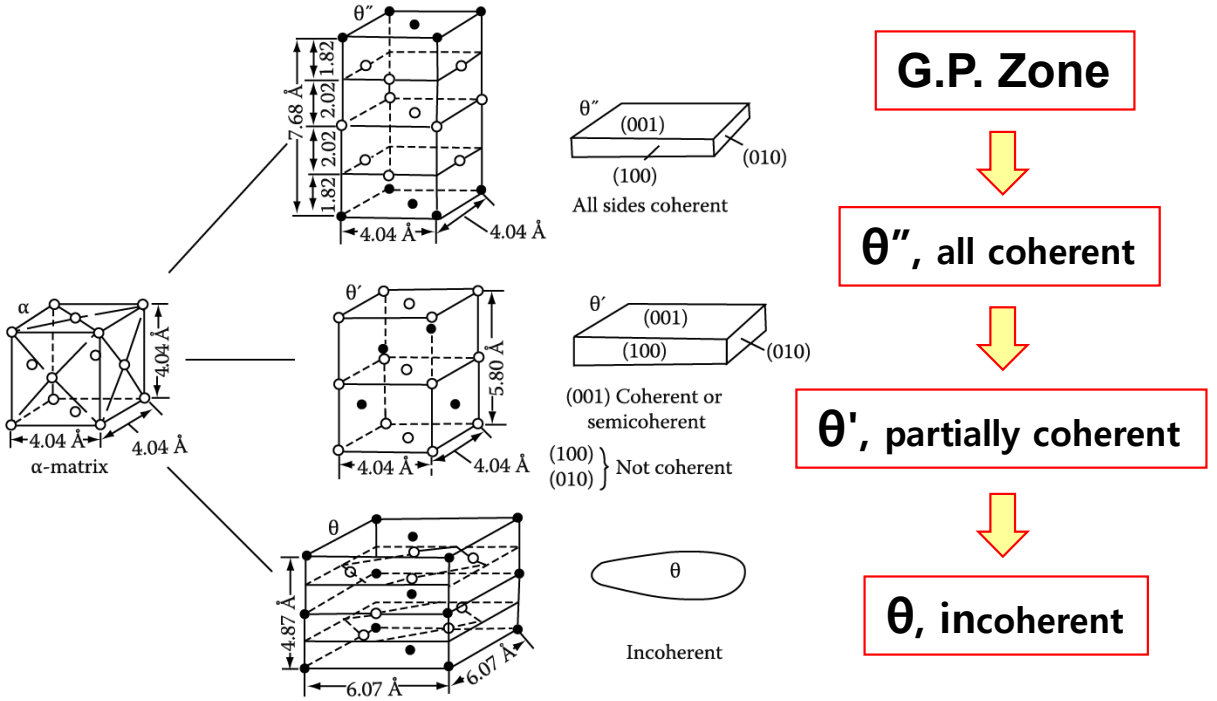

Precipitation Hardening

- Ex: Al-Cu system
- Procedure:

- *Pt A: solution heat treat (get a solid solution)*
- *Pt B: quench to room temp.*
- *Pt C: reheat to nucleate small θ crystals within α crystals.*

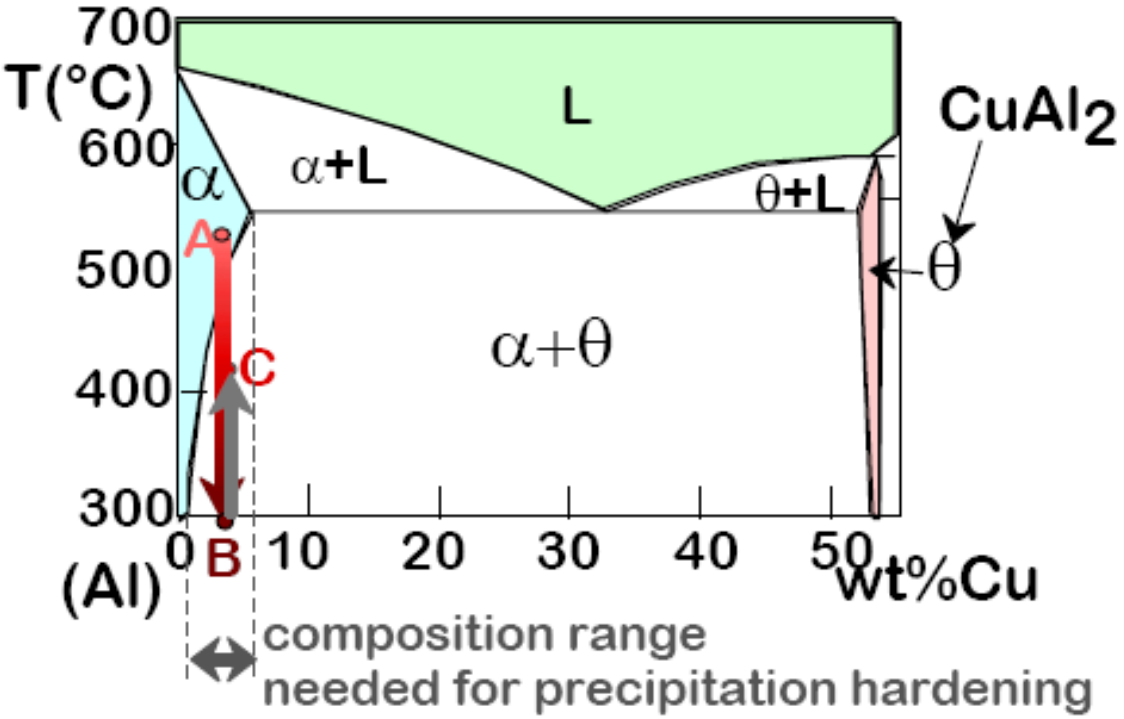

$\alpha + \theta \rightarrow$ Heat (~550°C) $\rightarrow$ Quench (0°C) $\rightarrow$ α (ssss) $\rightarrow$ Heat/age (~150°C) $\alpha + \theta_{ppt}$

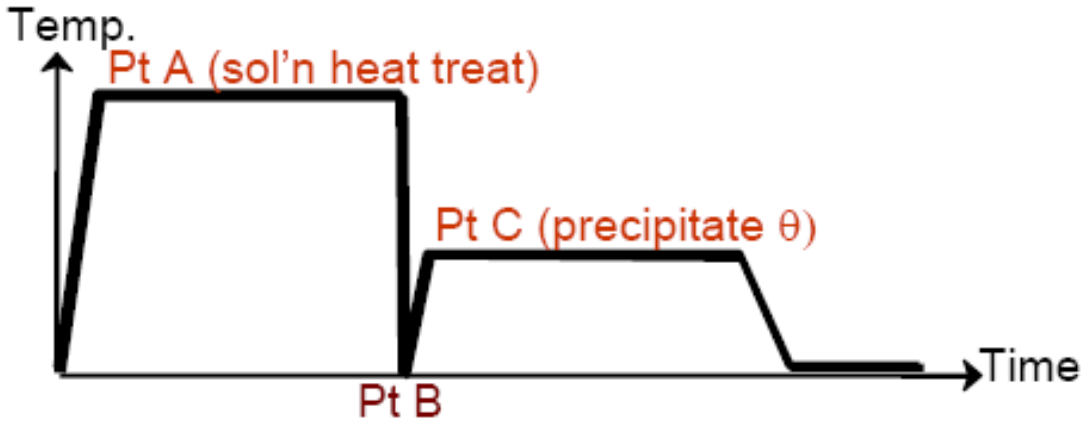

Al-Cu ppt structures

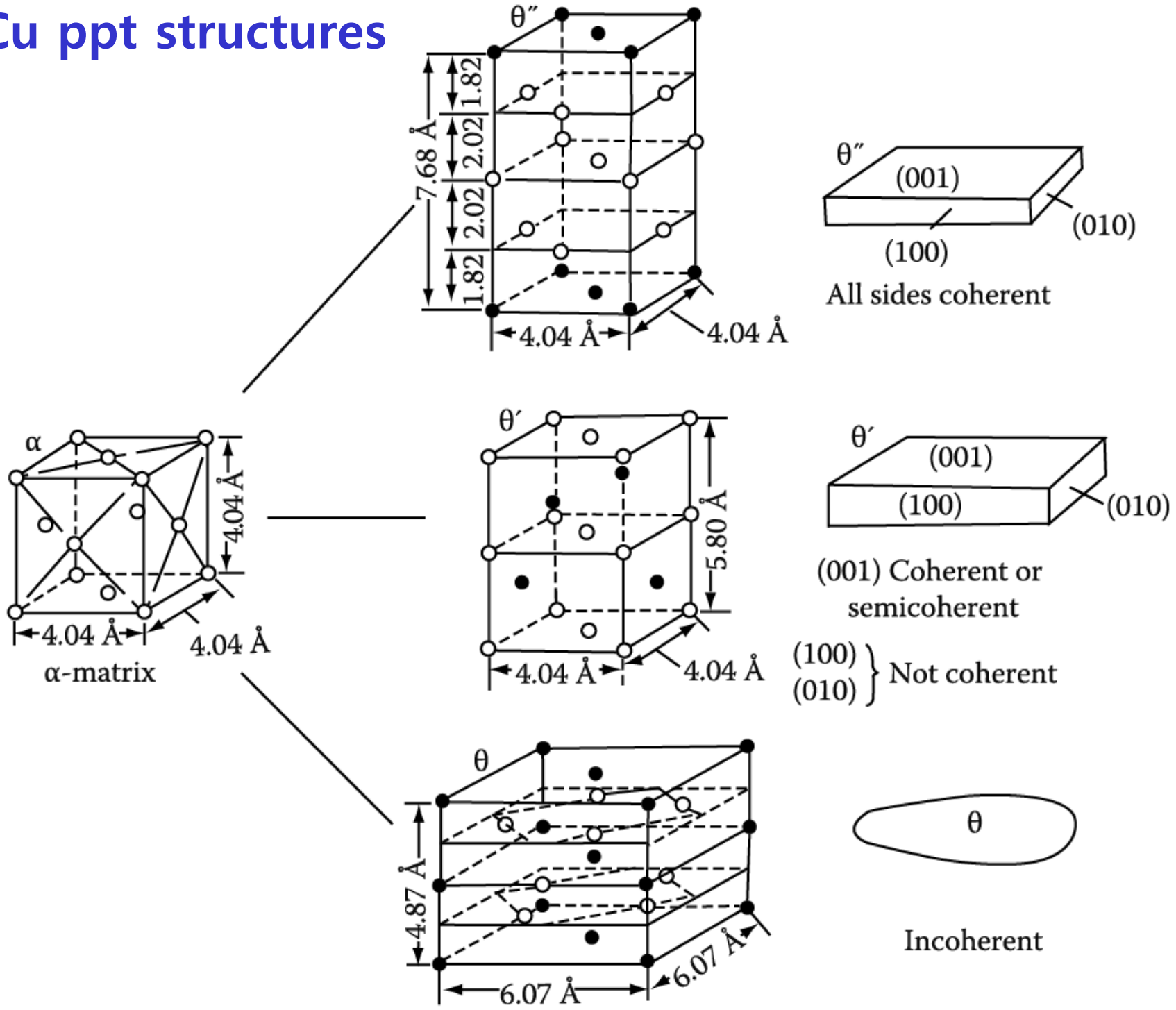

Al-Cu ppt structures

GP zone structure

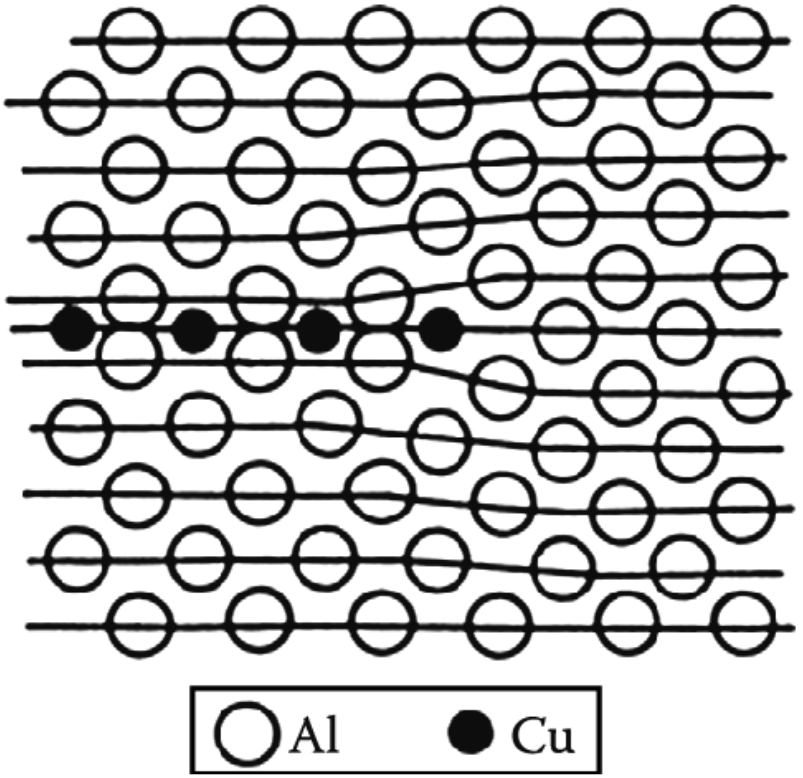

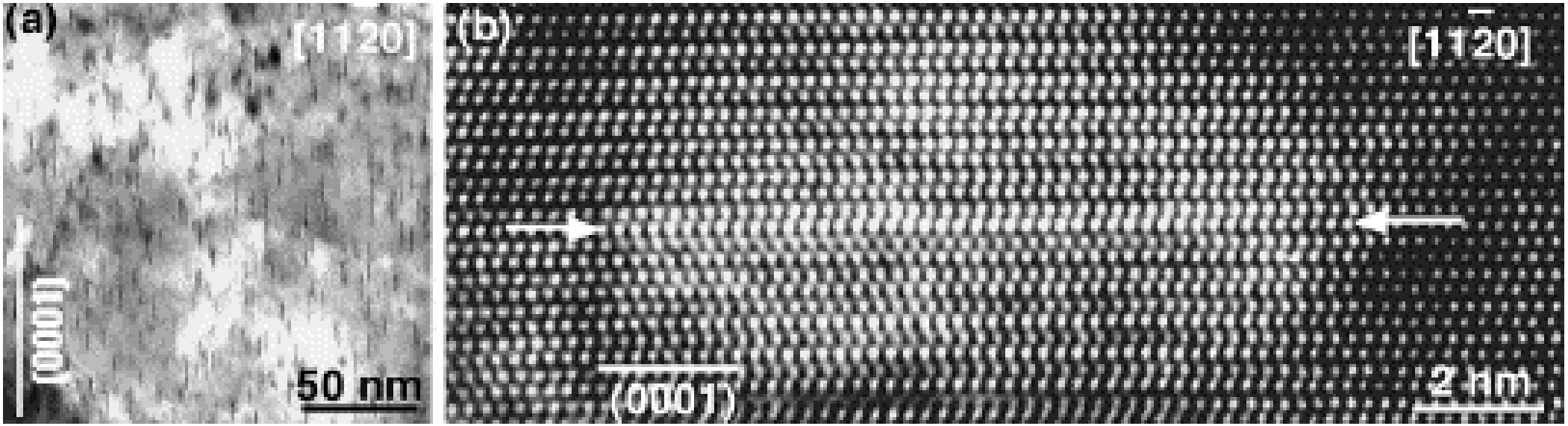

(a) Bright-field TEM image showing G.P. zones, and (b) HRTEM image of a G.P. zone formed on a single $(0\ 0\ 0\ 1)_{\alpha}$ plane. Electron beam is parallel to in both (a) and (b).

θ' Phase Al – Cu Alloys

Semicoherent broad face parallel to the $\{100\}_\alpha$ matrix planes (habit plane)

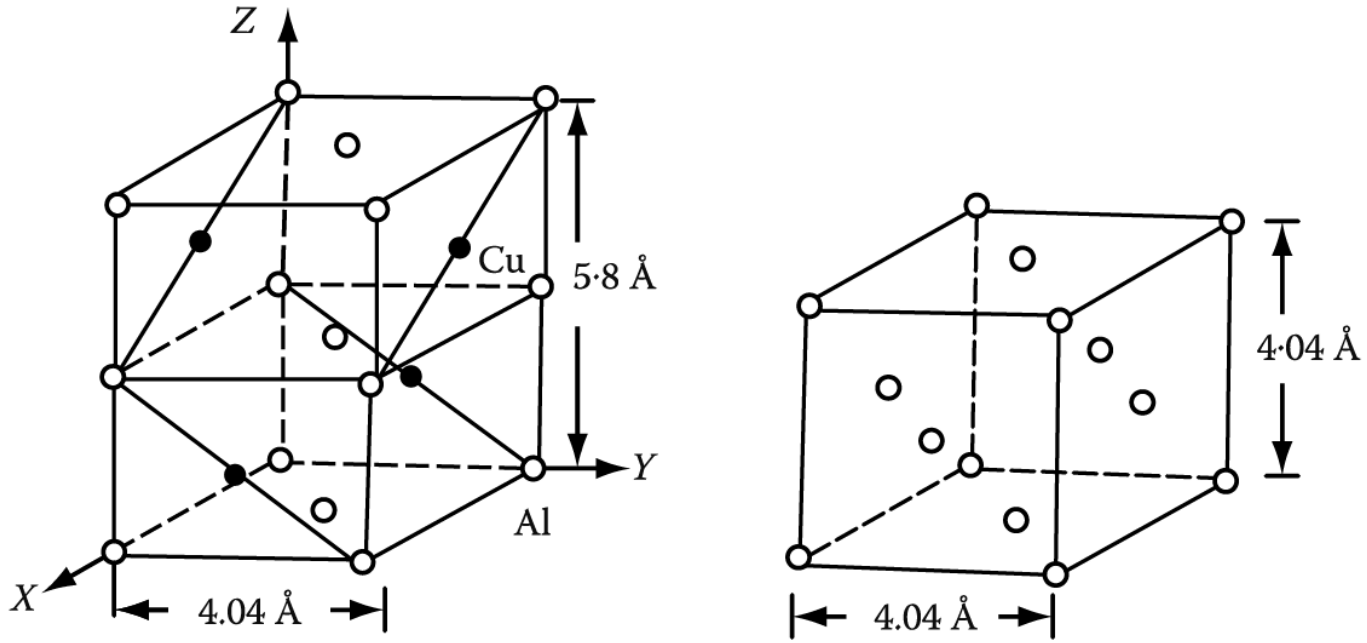

(a) The unit cell of the Θ′ precipitate in Al-Cu alloys

(b) The unit cell of the matrix

Orientation relationship between α and θ'

$$(001)_{\theta'} \;//\; (001)_{\alpha} \qquad [100]_{\theta'} \;//\; [100]_{\alpha}$$

→ Cubic symmetry of the Al-rich matrix (α) ~
many possible orientations for the precipitate plates within any given grain

S phase in Al-Cu-Mg alloys ; Lath shape

β' phase in Al-Mg-Si alloys ; Needle shape

} **Widmanstätten morphology**

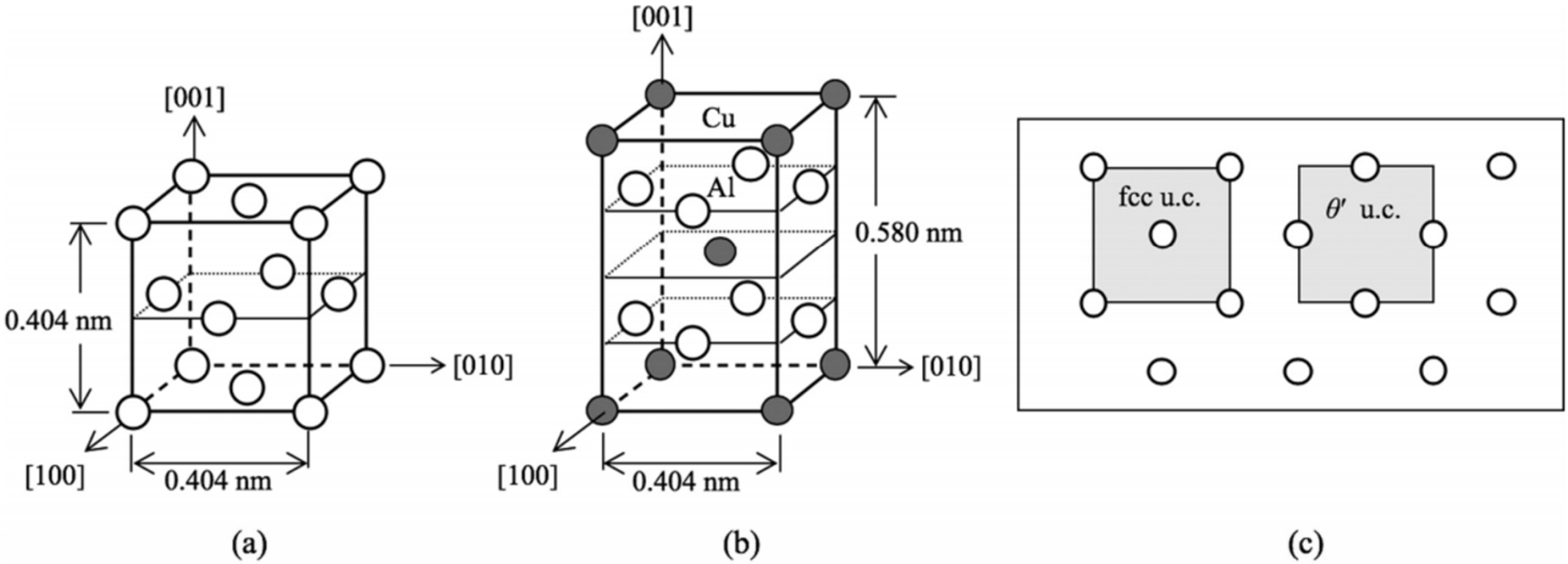

FIGURE 3.63 Unit cells of θ' Al_2Cu precipitates and the matrix in Al–Cu alloys. (a) The unit cell of the fcc Al matrix. Note that some of the atoms will be Cu. (b) The unit cell of the bct θ' precipitate showing the positions of the smaller Cu atoms (dark) and larger Al atoms (light). Note that the arrangement of the Al atoms parallel to the (001) planes in both lattices is identical as shown in (c).

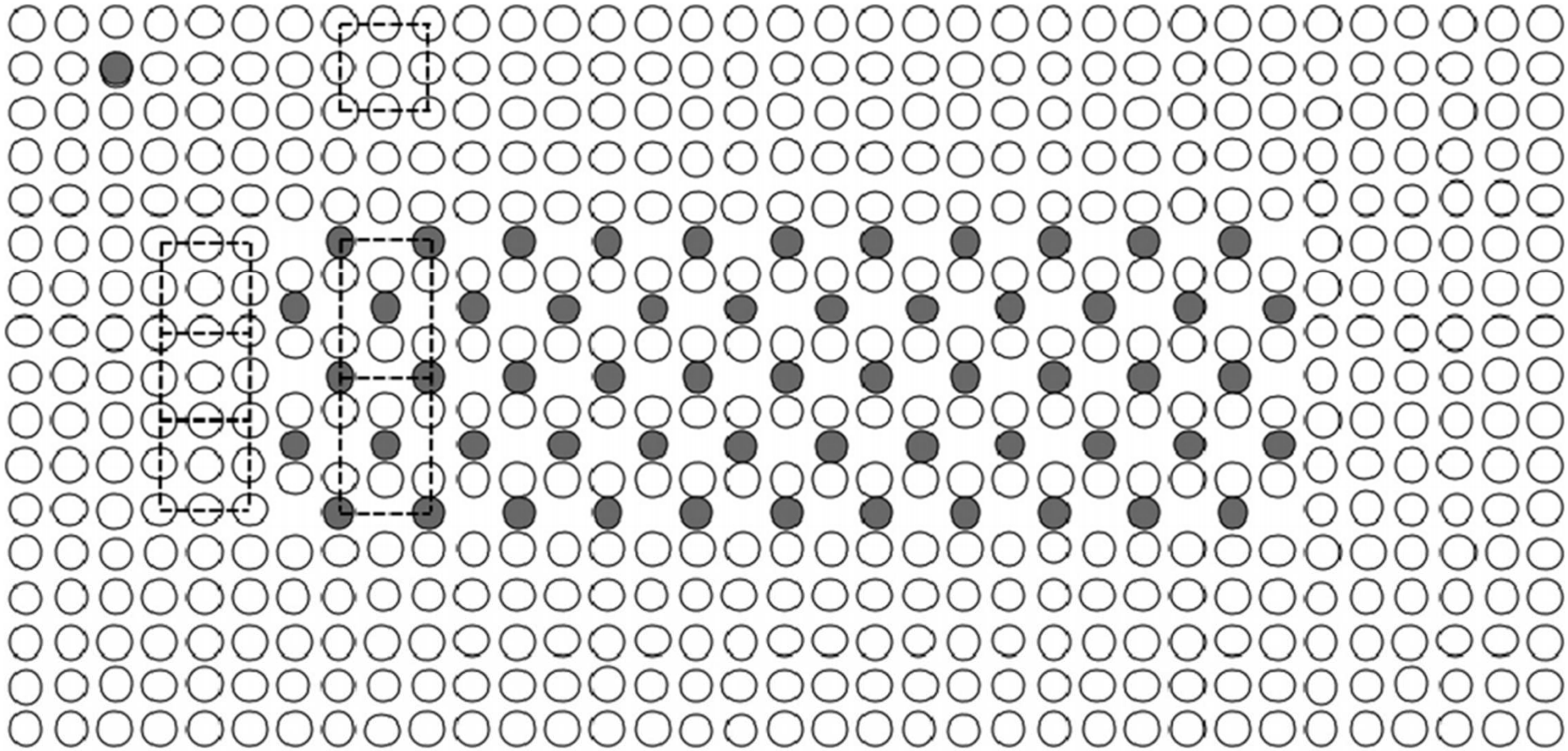

FIGURE 3.64 A schematic cross-section through a θ' Al_2Cu plate-like precipitate in an Al matrix in an Al–Cu alloy showing the positions (but not sizes) of the Al atoms (open circles) and Cu atoms (filled circles). The [100] direction of both the fcc matrix and θ' precipitate is out of the plane of the diagram. Note that several layers of atoms are superimposed. The precipitate is just two unit cells thick. Projections of the unit cells of the two lattices are outlined with dashed lines. There is perfect matching of the Al atoms across the coherent broad face of the plate $(001)_{\theta'}$, while there is poor matching of the atoms and atomic planes across the partly coherent plate edges $(010)_{\theta'}$. Coherency strains are present in both precipitate and matrix in the [001] direction.

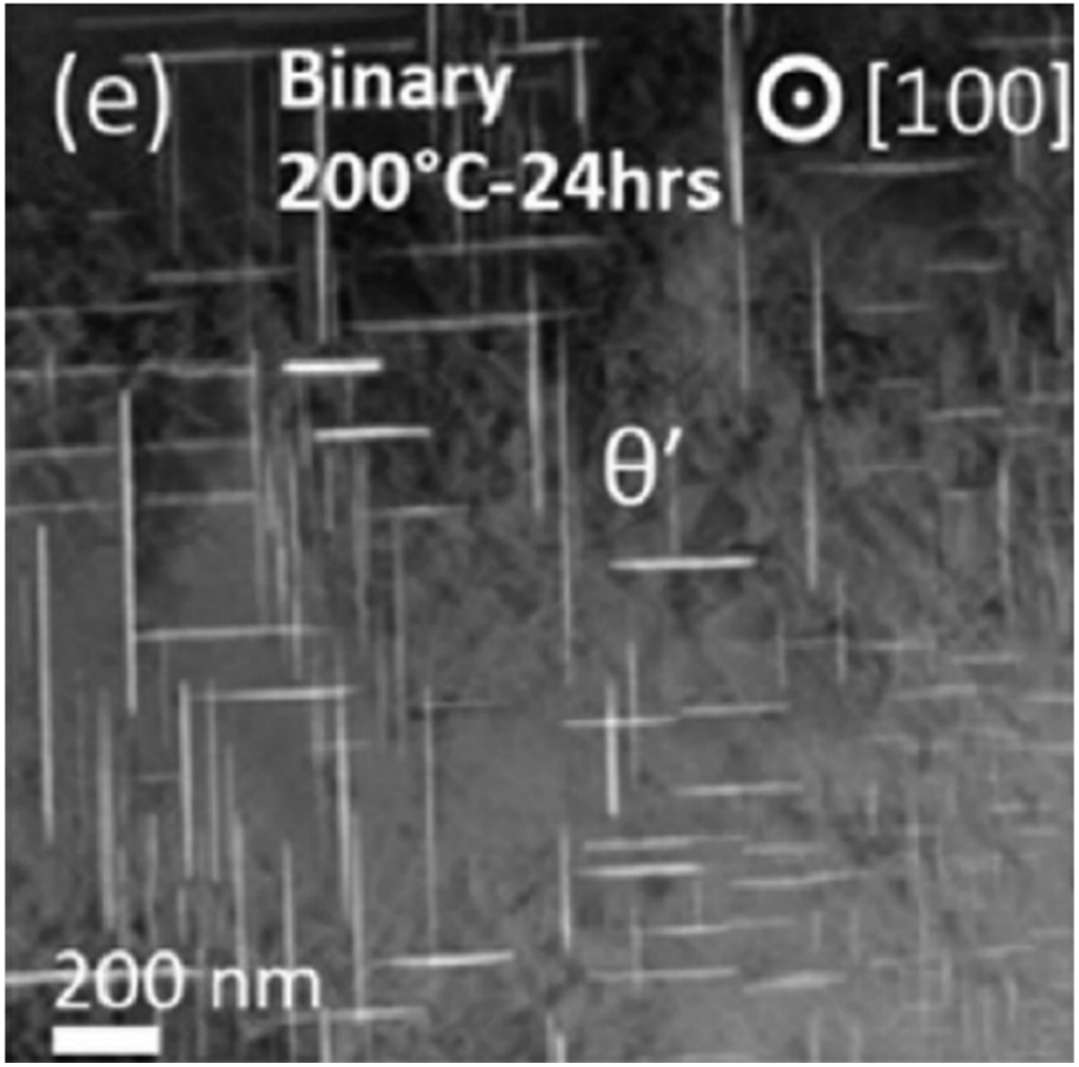

FIGURE 3.65 Thin foil specimen of an Al–1.7 at.% Cu alloy solution treated, quenched and aged at 200°C for 24h showing θ' precipitates in a Widmanstätten morphology on $(010)_{Al}$ and $(001)_{Al}$ planes. Annular dark field scanning transmission electron microscope image. (Reprinted from *Acta Materialia*, Vol. 125, Y. Chen, Z. Zhang, Z. Chen, A. Tsalanidis, M. Weyland, S. Findlay, L.J. Allen, J. Li, N.V. Medhekar, L. Bourgeois, The enhanced theta-prime (θ') precipitation in an Al-Cu alloy with trace Au additions, 340–350 (2017), with permission from Elsevier.)

θ phase in $Al-Cu$ alloys (Al_2Cu)

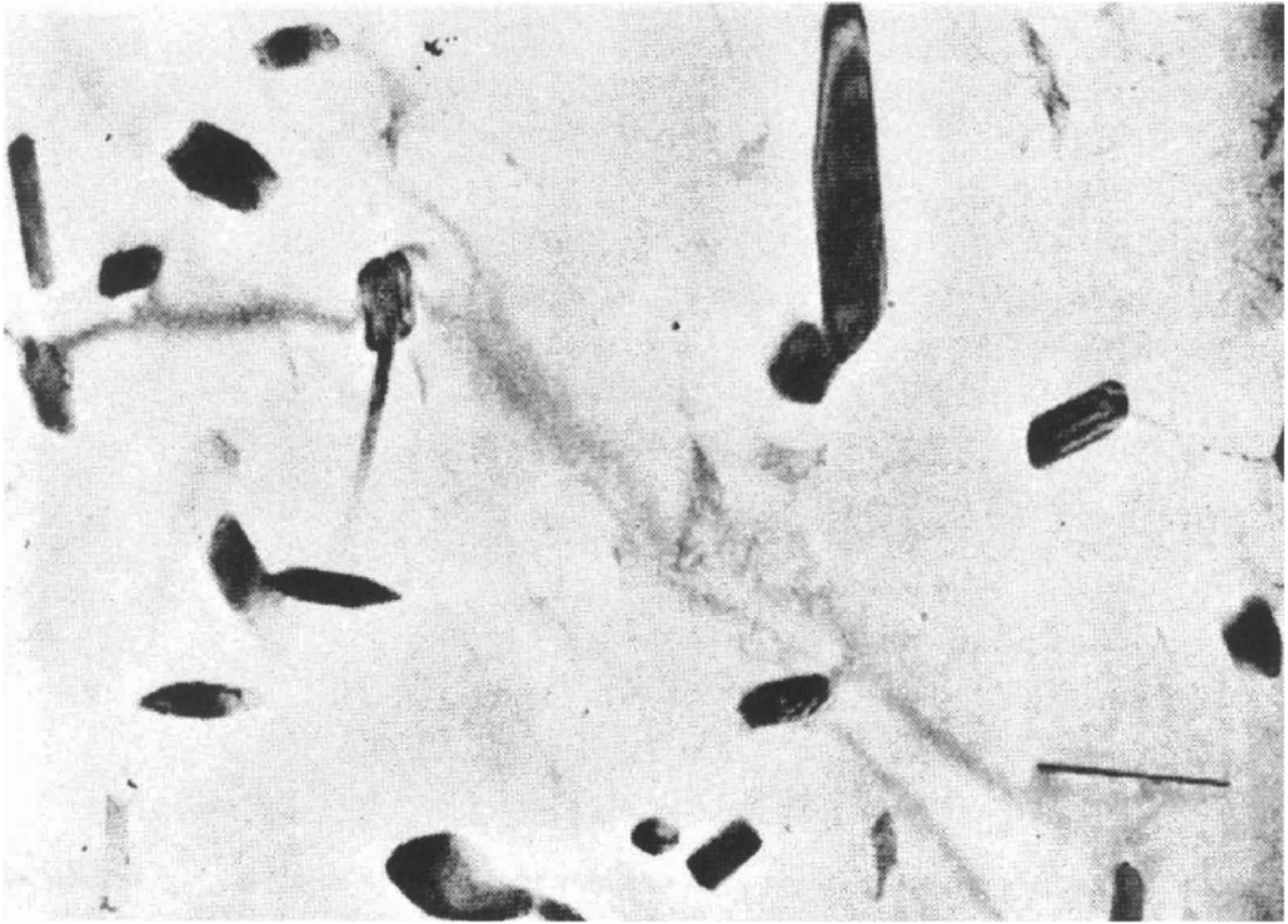

- **Polyhedral shapes:** certain crystallographic planes of the inclusion lie at cusps in the γ-plot

5.5.4. Age Hardening

Transition phase precipitation → great improvement in the mechanical properties
Coherent precipitates → highly strained matrix → dislocations~forced during deformation

Hardness vs. Time by Aging

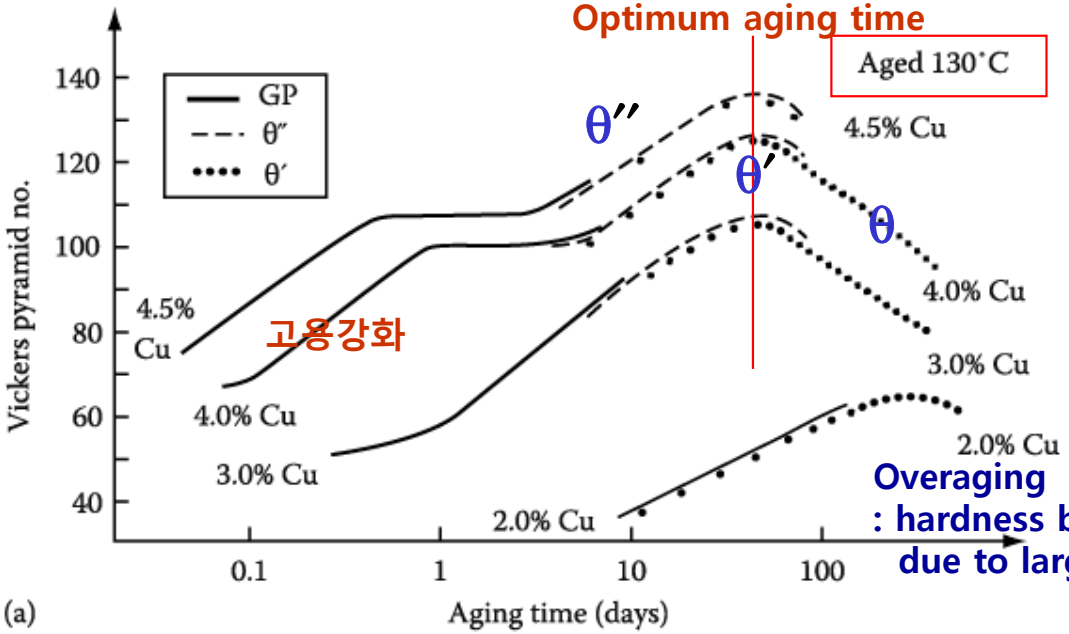

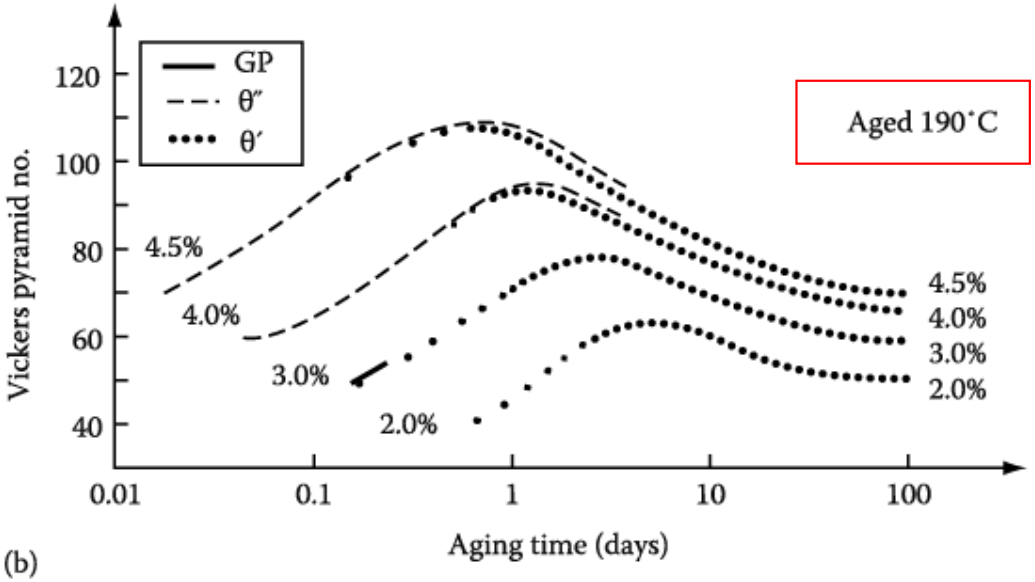

Maximum hardness~ largest fraction of θ″ (coherent precipitates)

Ageing at 130°C produces higher maximum hardness than ageing at 190°C.

At 130°C, however, it takes too a long time.

Overaging
: hardness begins to decrease due to large spacing between precipitates

How can you get the high hardness for the relatively short ageing time?

Double aging treatment
first below the GP zone solvus → fine dispersion of GP zones then ageing at higher T.

Finer precipitate distribution

Fig. 5.37 Hardness vs. time for various Al-Cu alloys at (a) 130 ℃ (b) 190 ℃

Precipitates on Grain Boundaries

Formation of a second-phase particle at the interfaces with two differently oriented grains

1) incoherent interfaces with both grains

2) a coherent or semi-coherent interface with one grain and an incoherent interface with the other,

3) coherent or semi-coherent interface with both grains

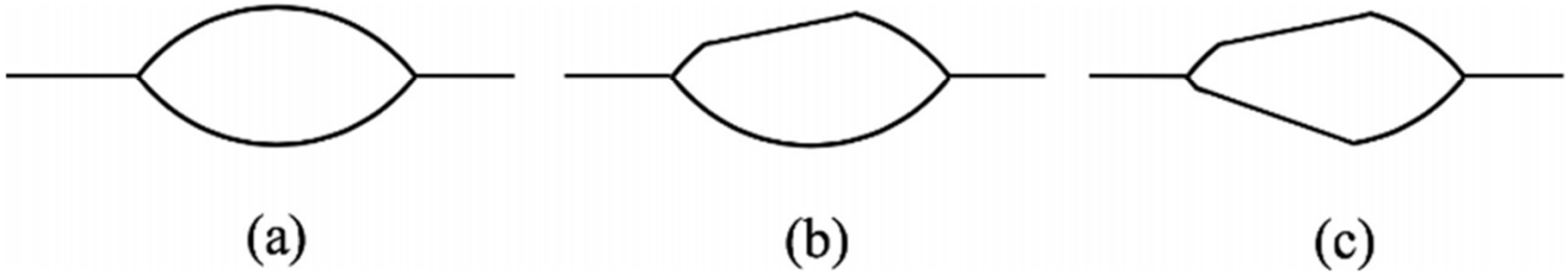

Fig. 3. 66 Possible morphologies for grain boundary precipitates. The different orientation relationship each side of the grain boundary can lead to different combinations of coherent, partly coherent and incoherent interfaces. A flat interface often indicates orientation relationship and coherence, but not always. Curved interfaces are often an indication of incoherence, but not always.

Precipitates on Grain Boundaries

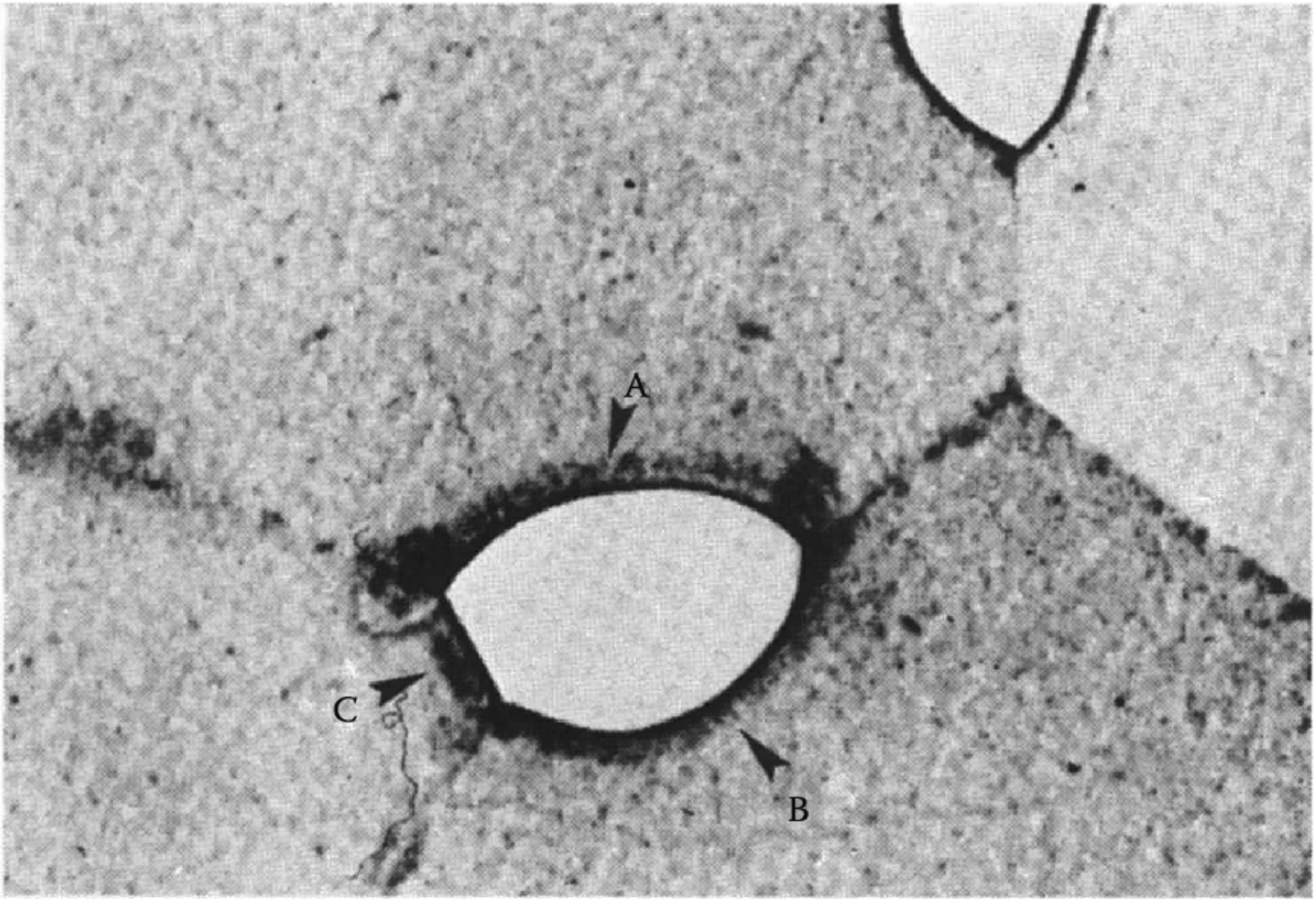

Fig. An α precipitate at a grain boundary triple point in an α – β Cu-In alloy. Interfaces A and B are incoherent while C is semicoherent (x 310).

A, B; Incoherent, C; Semi-coherent or coherent

3.4 Interphase Interfaces in Solids (α/β)

$$\sum A_i \gamma_i + \Delta G_s = minimum$$

1) Interphase boundary - different two phases : different crystal structure or different composition

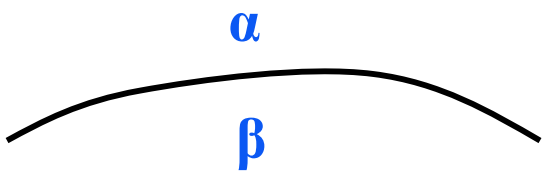

- Coherent/ Semicoherent/ Incoherent
- Complex Semicoherent

Fully coherent precipitates

γ_{ch} ⇨ γ_{ch} + *Lattice misfit* ⇨ γ_{ch} + $Volume\ Misfit \quad \Delta = \frac{\Delta V}{V}$

different composition — Coherency strain energy — **Incoherent inclusions**: Chemical and structural interfacial E

2) Second-Phase Shape: precipitate from solid solution in Al-Cu alloys

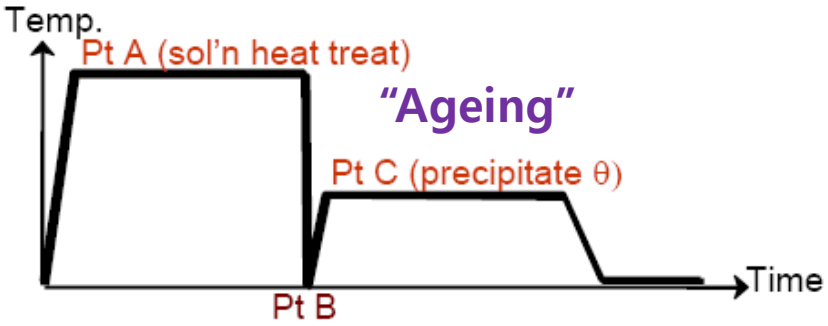

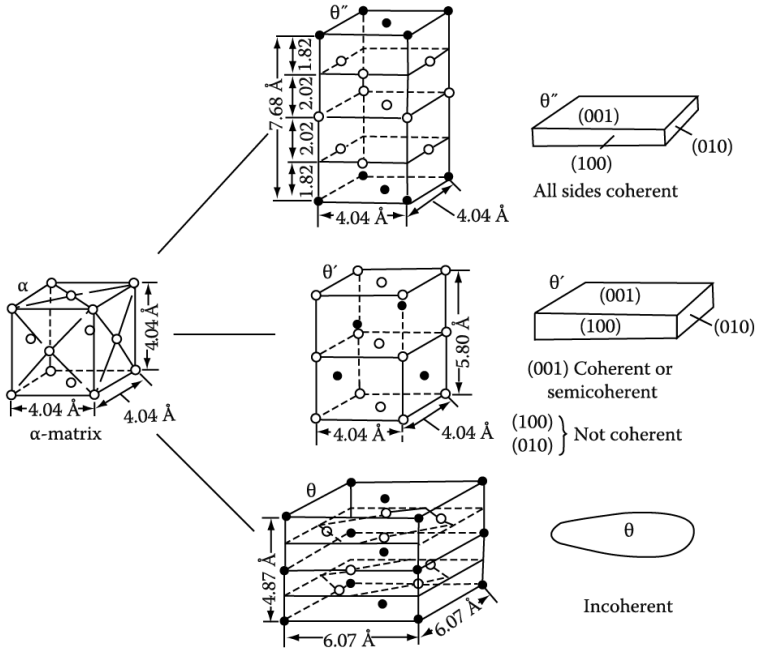

- **G.P. Zone**
- **θ″, all coherent**
- **θ', partially coherent**
- **θ, incoherent**